The Structure of the Nuclear Pore Complex (An Update)

Daniel H. Lin and **André Hoelz**

California Institute of Technology, Division of Chemistry and Chemical Engineering, Pasadena, California, 91125, USA

Abstract

The nuclear pore complex (NPC) serves as the sole bidirectional gateway of macromolecules in and out of the nucleus. Owing to its size and complexity (~1,000 protein subunits, ~110 MDa in humans), the NPC has remained one of the foremost challenges for structure determination. Structural studies have now provided atomic-resolution crystal structures of most nucleoporins. The acquisition of these structures, combined with biochemical reconstitution experiments, cross-linking mass spectrometry, and cryo–electron tomography, has facilitated the determination of the near-atomic overall architecture of the symmetric core of the human, fungal, and algal NPCs. Here, we discuss the insights gained from these new advances and outstanding issues regarding NPC structure and function. The powerful combination of bottom-up and top-down approaches toward determining the structure of the NPC offers a paradigm for uncovering the architectures of other complex biological machines to near-atomic resolution.

Keywords

Nuclear pore complex; nucleocytoplasmic transport; mRNA export; integrative structural biology; X-ray crystallography; electron microscopy

INTRODUCTION

The presence of membrane-enclosed organelles such as the nucleus is a hallmark feature of eukaryotic cells (1). The nucleus encloses genomic DNA within a double lipid bilayer termed the nuclear envelope, which separates genomic DNA from the rest of the cell. This architecture serves not only to isolate the genome from sources of damage but also to provide opportunities for gene regulation. At the same time, macromolecules such as messenger RNAs (mRNAs) or transcription factors must be able to traffic between the nucleus and cytoplasm. Nucleocytoplasmic transport, the trafficking of macromolecules in and out of the nucleus, occurs through nuclear pore complexes (NPCs), which are massive, proteinaceous macromolecular machines (Figure 1a). In humans, each NPC consists of ~1,000 protein subunits, termed nucleoporins, and totals to a molecular mass of ~110 MDa —making the NPC one of the largest macromolecular assemblies in cells. NPCs maintain

the integrity of the nuclear compartment by preventing macromolecules from freely diffusing in or out of the nucleus, but in contrast to most other membrane transporters, NPCs conduct cargoes in their native folded state (Figure 1b). This property allows for macromolecules to act immediately after transport, such as during signal transduction to activate a transcriptional program.

Each NPC resides in and stabilizes an ~800-Å-wide nuclear envelope pore that is generated by the fusion between the inner and outer nuclear membranes (2). The NPC generates a passive diffusion barrier comprising intrinsically disordered sequences termed FG repeats, a name reflecting their enrichment for phenylalanine and glycine residues (3–6). Macromolecules smaller than ~40 kDa can passively diffuse through the diffusion barrier, whereas larger macromolecules generally do not efficiently cross by themselves (7, 8) (**Supplemental Movie 1**). Instead, they must be ferried through by specialized transport factors, collectively known as nuclear transport factors. This form of facilitated transport through NPCs is rapid, with individual events occurring in a fraction of a second and total fluxes through individual NPCs totaling up to hundreds to thousands of macromolecules per second (4, 9). The size-exclusion limit of the diffusion barrier is not a hard cutoff but rather a rapidly increasing energetic barrier to the passive diffusion of macromolecules larger than ~40 kDa (6). Moreover, the surface properties of cargo proteins can dramatically change their permeability, and the introduction of hydrophobic surface residues can enable proteins larger than the size limit to cross the diffusion barrier passively (10, 11).

Nucleocytoplasmic transport of most proteins and some cellular RNAs occurs in a Ran-dependent manner. The mechanistic details of nucleocytoplasmic transport have been reviewed in great detail elsewhere (12–16). Briefly, the protein Ran is a small GTPase (Enzyme Commission (EC) number 3.6.5.2) that adopts different conformations in its GDP- and GTP-bound states. Localization of the Ran GTPase-activating protein RanGAP is restricted to the cytoplasm, whereas the Ran guanine exchange factor RCC1 is present only in the nucleus. Upon its formation in the cytoplasm, RanGDP is rapidly transported into the nucleus by its dedicated transporter Ntf2 (17, 18). Thus, a gradient of Ran is actively maintained in the cell, with an ~200-fold higher RanGTP level in the nucleus than in the cytoplasm (19). Cargoes usually possess nuclear localization signals (NLSs) or nuclear export signals (NESs) that are recognized by members of the karyopherin-β family of nuclear transport factors, although some cargoes are also recognized by their three-dimensional (3D) fold or through adaptor proteins, such as karyopherin-α (12–16). During nuclear import, karyopherin–cargo complexes can cross the diffusion barrier and are disassembled upon encountering nuclear RanGTP. In contrast, during nuclear export, RanGTP is an obligate component of export-competent karyopherin–cargo–RanGTP complexes. Upon their arrival in the cytoplasm, export complexes are disassembled when they encounter cytoplasm-specific Ran-binding proteins and RanGAP, which cooperate to activate Ran's GTPase activity (**Supplemental Movie 2**) (13).

A complete understanding of how the NPC is able to conduct selective nucleocytoplasmic transport requires a detailed understanding of its molecular architecture. The structure of the NPC has been the subject of intense study since NPCs were first discovered in the 1950s (2). Because of its size and complexity, elucidating the atomic structure of the NPC has

remained a frontier in structural biology. Previously, we and others have discussed the early electron microscopic and X-ray crystallographic characterization of the NPC (1, 20, 21). In this review, we describe our current understanding of the structure and function of the NPC and highlight recent advances that have revealed the overall architecture of the NPC at near-atomic resolution.

The Overall Architecture of the NPC Revealed by Electron Microscopy

Much of our understanding of the overall shape and architecture of the NPC comes from studies performed with electron microscopy (EM). The development of EM to study the NPC has recently been reviewed and is only briefly discussed here (1, 20). Pores in the nuclear envelope were first described in 1950 when EM was applied to examine the nuclear envelope (22). Subsequently, the embedded NPCs were discovered (23). Early studies revealed that the NPC approximates a hollow cylindrical shape with eight-fold rotational symmetry along the axis perpendicular to the nuclear envelope (24). EM studies of the NPC have since been refined using a variety of technical strategies, including heavy metal staining, isolation of NPCs from membranes, spreading purified nuclear envelopes on grids, and imaging natively within vitrified cells (25–28). A similarly large assortment of model systems has been used, including the Baker's yeast *Saccharomyces cerevisiae*, the slime mold *Dictyostelium discoideum*, oocytes of the African clawed frog *Xenopus laevis*, the unicellular algal species *Chlamydomonas reinhardtii*, and cultured human cells (26, 29–33). In aggregate, these studies have found that the overall shape and architecture of the NPC is evolutionarily conserved, but lineage- or species-specific differences have also emerged (for details, see 1).

More recently, cryo–electron tomography (cryo-ET) and subtomogram averaging have been utilized to generate 3D reconstructions of intact NPCs (Figure 2). Cryo-ET was first applied to *X. laevis* NPCs in 2003 (34). Subsequent cryo-ET studies yielded reconstructions of the *D. discoideum* NPC up to ~83-Å and ~58-Å resolution and the first reconstruction of a human NPC up to ~66-Å resolution (31, 32, 35). Rapid technical breakthroughs have now generated reconstructions of intact NPCs approaching up to ~20-Å resolution, providing sufficient resolution and quality for docking high-resolution crystal structures in a quantitative manner (36–39). Future technological advances have the potential to further improve the resolution of reconstructions to the point that secondary structure elements can be resolved, which would be necessary to enable flexible fitting of crystal structures into reconstructions. In addition, the ability to combine cryo-ET reconstructions with perturbation studies (e.g., acquiring NPC reconstructions from cells that have been depleted of specific nucleoporins) can enable direct comparisons between NPC structure and function (37, 38). High-resolution reconstructions of NPCs from a diverse collection of species are expected to further illuminate NPC evolution and the range of architectural diversity (33, 40).

The overall architecture emerging from current cryo-ET studies is one in which the most central NPC proteins typically form a symmetric core, which possesses not only eight-fold rotational symmetry but also two-fold rotational symmetry along an axis parallel to the nuclear envelope (Figure 1a). This symmetric core surrounds the central transport channel

and serves as the scaffold onto which asymmetric nucleoporins attach on the cytoplasmic and nuclear faces to form structures known as the cytoplasmic filaments and nuclear basket, respectively. The symmetric core itself is generated by three rings: one inner ring that is embedded within the nuclear envelope, and two outer rings that reside on the inner or outer nuclear membrane. Although these organizational principles appear to be evolutionarily conserved, they can yield substantially differently sized NPCs (see Conservation of Nuclear Pore Complex Architecture section below). In humans, the NPC has an outer diameter of ~1,200 Å, an inner diameter of ~425-Å for the central transport channel, a height of ~800 Å, and a molecular mass of ~110 MDa (36, 41). The *S. cerevisiae* NPC has similar dimensions but a shorter height of ~600 Å and a molecular mass of ~52 MDa (40). The *C. reinhardtii* NPC has a more dilated inner diameter, yielding a central transport channel that is ~650 Å in diameter, despite having approximately the same outer diameter as the human NPC (33).

Identification of Nucleoporins

Despite their large size, NPCs comprise multiple copies of only ~34 unique proteins with the exact number depending on the species (3, 42–44) (Figures 3 and 4). The majority of nucleoporins are conserved throughout eukaryotes, with recent surveys of eukaryotic genomes consistent with ancestral NPCs being present in the last eukaryotic common ancestor (45). However, nucleoporins generally display poor sequence conservation despite strong structural conservation, which prevents robust identification of nucleoporins in distantly related genomes. Early efforts identified the majority of yeast and vertebrate nucleoporins by employing genetic, biochemical, or computational approaches, for example, through screens for genetic interactions with known nucleoporins, pull-down experiments to identify physical complexes, or searches for proteins with homology to known nucleoporins (reviewed in 46, 47). The sets of nucleoporins in yeast and humans were most comprehensively defined later by systematic proteomics-based approaches, which involved isolation of highly purified NPC samples, exhaustive mass spectrometry identification of polypeptides, and validation of NPC localization (3, 42). Various proteomics approaches have since been fruitfully applied to characterize the nucleoporins, for example, in identification of protein–protein interactions, cross-linking and mass spectrometry mapping of the physical contacts within subcomplexes or entire NPCs, and quantitative mass spectrometry approaches to determine the stoichiometry of nucleoporins in the NPC (36–38, 40, 48–51).

A key question regarding the architecture of the NPC has been the stoichiometry of its subunits. Because of the eight-fold rotational symmetry of the NPC, nucleoporins are incorporated in multiples of eight. Absolute quantitation of human NPCs through a combination of super-resolution microscopy experiments and quantitative mass spectrometry arrived at a stoichiometry of 32 for most human symmetric core nucleoporins but also found that many other nucleoporins are present in higher or lower stoichiometries (50). Interestingly, different cell types display altered stoichiometries for some nucleoporins, especially those in the periphery, suggesting that different cellular contexts may tune NPC composition and function (50). The stoichiometry of some *S. cerevisiae* nucleoporins is reduced compared with the human NPC (40, 52) (see detailed discussion in Conservation of Nuclear Pore Complex Architecture section below).

Nucleoporins and Their Properties

Nucleoporins range in size from a few hundred to several thousand residues and possess molecular masses of ~30–358 kDa. A unifying nucleoporin nomenclature does not exist, and proteins are most often named with nucleoporin (nup) followed by a number that refers to their molecular mass (Figure 3). We generally refer to the nucleoporins using the human nomenclature throughout the text, but when discussing results obtained in a specific species, we denote homologs by their species (e.g., *sc*Nsp1, the *S. cerevisiae* homolog of human Nup62).

Many nucleoporins were first isolated using the mAb414 antibody, which recognizes glycosylated FG repeats (53). Almost half of the nucleoporins in any given species possess FG repeats, including nucleoporins in the symmetric core, the cytoplasmic filaments, and the nuclear basket. These unique and critical sequences not only form the NPC's diffusion barrier but also serve as specific binding sites for nuclear transport factors. FG-repeat regions are intrinsically disordered, typically span hundreds of residues, and are often enriched in polar amino acids and depleted of charged amino acids (54). The exact composition and specific sequence motifs of FG repeats varies between nucleoporins and species.

Besides FG-repeat regions, nucleoporins comprise a relatively small set of folds (55). Most of the large structured domains are built out of tandem repeats of secondary structure elements. For example, several nucleoporins consist solely of tandem repeats of β-strands that fold into a domain known as the β-propeller (Figure 4). β-propellers are formed by multiple wedge-shaped structural units termed blades, each of which consists of four antiparallel β-strands. The wedge-shaped blades pack together in a circular fashion to yield compact, disk-shaped domains that are ~70 Å in diameter and ~40 Å in height. The β-strands within a β-propeller domain are connected by surface-exposed loops, and these loops often contain insertions that mediate protein–protein interactions. Similarly, several families of nucleoporins are comprised primarily of antiparallel α-helical repeats, which pack into domains termed α-helical solenoids. α-Helical solenoids are elongated or rod-shaped domains that are generally larger than β-propellers, and among the nucleoporins, they approach up to ~200 Å in length along the longest axis (Figure 4). Different types of α-helical repeats pack in characteristic ways to form different overall shapes, which in the NPC have yielded "S"-shaped, "U"-shaped, as well as irregular topologies. A few nucleoporins contain both β-propellers and α-helical solenoids. A small set of nucleoporins contain long coiled-coil domains (CCDs), typically hundreds of residues in length, which mediate nucleoporin–nucleoporin interactions within the NPC. In addition, several nucleoporins primarily consist of either disordered sequences or several folded domains connected by flexible linkers. Despite the fact that NPCs are embedded in nuclear envelope pores, very few nucleoporins—only three or four in any given species—possess transmembrane domains.

Modular Architecture of the Nuclear Pore Complex

Investigations on the structure of the NPC have been greatly aided by its modular architecture. Nucleoporins form large, stable subcomplexes, and early studies capitalized on

this property to isolate complexes from cells and eventually reconstitute subcomplexes in vitro from purified proteins (56–59). The modularity of the NPC extends to multiple levels: These large subcomplexes are often also modular in architecture, and the major subcomplexes are themselves modules of the protomers that are related by the eight-fold rotational symmetry of the NPC. We consider four major subcomplexes: the coat nucleoporin complex (CNC), which is the primary constituent of the outer rings; the inner ring nucleoporins; and lastly, the cytoplasmic filaments and nuclear basket nucleoporins. Although most nucleoporins are only present in a single subcomplex, two nucleoporins—Nup98 and Nup62—are components of multiple subcomplexes, either owing to their presence in different complexes or because they bridge multiple subcomplexes.

In the following sections, we summarize advances in the biochemical reconstitution and X-ray crystallographic characterization of nucleoporin subcomplexes that form the symmetric core. We then describe how this knowledge was combined with recent breakthroughs in the cryo-ET characterization of intact NPCs, leading to the elucidation of near-atomic architectures of the NPCs from three diverse species. We discuss the evolutionary conservation of NPC design principles as well as species-specific differences revealed by these recent advances. Lastly, we summarize our current understanding of the structure and function of the asymmetric nucleoporins, the participation of the NPC in nucleocytoplasmic transport, and briefly overview the insights into diseases associated with nucleoporins.

STRUCTURE AND BIOCHEMISTRY OF SYMMETRIC CORE NUCLEOPORINS AND COMPLEXES

Coat Nucleoporin Complex

The CNC (also referred to as the Y-complex, Nup84 complex in yeast, or Nup107–Nup160 complex in metazoans) is the major constituent of the outer rings in the NPC, serving as a structural scaffold and docking site for other nucleoporins. It is also the best structurally characterized NPC subcomplex (60–76). The composition of the CNC can vary between species, with the human CNC containing 10 distinct proteins: Sec13, Seh1, Nup96, Nup75, Nup107, Nup160, Nup133, Nup37, Nup43, and ELYS (42, 77–81) (Figure 3). Of these 10 nucleoporins, 7 core components are also present in *S. cerevisiae* (*sc*Sec13, and *sc*Seh1, *sc*Nup145C, *sc*Nup85, *sc*Nup84, *sc*Nup120, and *sc*Nup133) (58, 59). Nup37 and ELYS are also present in some fungi, whereas Nup43 appears to be specific to metazoans (45). Sec13 is always a component of CNCs, but the Sec13 homolog Seh1 is not a component of CNCs in some fungi, such as *Chaetomium thermophilum* and *Myceliophthora thermophila*(75, 82). Moreover, Sec13 is also an essential component of the COP-II vesicle coat, and both Sec13 and Seh1 are also components of the GATOR2 complex, which is a multiprotein complex that regulates mammalian target of rapamycin (mTOR) signaling (83–86).

Early studies on the architecture of intact yeast CNCs by negative-stain EM revealed an elongated shape reminiscent of the letter Y, an arrangement later found to be conserved in the human complex (38, 59, 87). Owing to the modular assembly of the CNC, the relative positions of the subunits in the "Y" shape could be approximately assigned in a two-dimensional (2D) reconstruction: The *S. cerevisiae* homologs of Nup160 and Nup75

(*sc*Nup120 and *sc*Nup85) each formed one arm of the "Y" shape, and the longer bottom stalk was generated by the homologs of Nup96, Nup107, and Nup133 (*sc*Nup145C, *sc*Nup84, and *sc*Nup133) (59). As described in detail below, the 3D molecular architecture of the CNC has more recently been pieced together with high-resolution crystal structures of the individual components (60–73, 75, 76, 88). These advances have yielded valuable insights not only into the interactions that mediate CNC assembly but also about the evolution of the nucleoporins and their functions in the NPC.

Among the smallest nucleoporins, Sec13 and Seh1 are ~30-kDa proteins containing six blades of a seven-bladed β-propeller. However, their structures are incomplete in the absence of their specific binding partners, which contribute the missing seventh blade in the form of a domain invasion motif (DIM) (Figure 5). In the NPC, the Sec13 and Seh1 DIMs are embedded within the primarily unstructured N-terminal extensions of Nup96 and Nup75, respectively (61, 63, 64). In addition to their N-terminal extensions, Nup96 and Nup75 primarily consist of a domain possessing a unique α-helical architecture termed a U-bend solenoid (also known as ancestral coatomer element 1) (63). In U-bend solenoids, the α-helices stack to form a rod-shaped molecule like many other solenoids, but the N-terminal helices of the solenoid reside in the middle of the rod rather than at an end. To form a rod shape, the helices stack from the N terminus to the C terminus toward one end of the rod before making a U-bend turn to form the second end of the rod (61, 63, 64). Several crystal structures of Sec13–Nup96 heterodimers (*sc*Sec13–*sc*Nup145C and a chimeric *hs*Sec13–*sc*Nup145C complex) and the Seh1–Nup75 heterodimer (*sc*Seh1–*sc*Nup85) have revealed very similar mechanisms of interaction: The Nup96 and Nup75 DIMs complement the incomplete β-propellers of Sec13 and Seh1, and this primary interaction is supplemented by contacts between the U-bend solenoids and the bottom faces of the Sec13 and Seh1 β-propellers (61, 63–65, 68) (Figure 5). The U-bend solenoid architecture is also found in the COP-II vesicle coat binding partners of Sec13, Sec16, and Sec31; the CNC component Nup107; and the NPC inner ring complex (IRC) component Nup93, leading to the proposal of a common ancestral origin for these scaffolding proteins (62, 83, 84, 89–91). In the CNC, the U-bend architecture is used repeatedly in a structural role to mediate major interactions. For example, in the stalk of the "Y" shape, Nup107 bridges Nup96 and Nup133 by interacting with one partner on each end of its U-bend solenoid. Crystal structures of the *S. cerevisiae* Sec13–Nup96–Nup107 heterotrimer (*sc*Sec13–*sc*Nup145C–*sc*Nup84) revealed that Nup96 and Nup107 interact through large hydrophobic surfaces at the U-bend ends of each nucleoporin (65, 68) (Figure 5). Similarly, in the structures of the Nup107–Nup133 heterodimer, the C-terminal helices of the Nup107 solenoid pack against the side of the Nup133 solenoid in another large hydrophobic interface (62, 70) (Figure 5).

Similar to the U-bend solenoid nucleoporins, the core CNC nucleoporins Nup160 and Nup133, together with the IRC nucleoporin Nup155, may also be derived from a common ancestral protein (41, 70, 92). All three of these nucleoporins consist of N-terminal β-propellers followed by large C-terminal α-helical solenoids but are otherwise structurally distinct (41, 60, 62, 67, 69, 70, 88, 93). Based on the crystal structures of the fungal homologs *sc*Nup120 and *sp*Nup120, the Nup160 β-propeller is rigidly integrated into a C-terminal α-helical solenoid that is largely formed by a regular zigzag array of helices (Figure 5). This integration is accomplished in part through an insertion of 4–6 α-helices in the

*sc*Nup120/*sp*Nup120 β-propellers that pack against the C-terminal α-helical solenoid (67, 69, 71). In contrast, the Nup133 β-propeller appears to be flexibly connected to its C-terminal α-helical solenoid, which is formed by a more irregular arrangement of α-helices (60, 70, 74) (Figure 5). The β-propellers of Nup160 and Nup133 both harbor a loop that contains highly conserved amphipathic lipid packing sensor (ALPS) motifs, which are amphipathic helices characterized by an absence of charged residues on their polar faces and that specifically bind curved lipid membranes (60, 67, 69, 76, 94).

The final three nucleoporins found in the human CNC—Nup37, Nup43, and ELYS—are not present in all species. Although homologs of Nup37 and ELYS do exist in some fungi, these homologs often possess dramatically altered domain architectures (71, 82, 95). For example, whereas fungal ELYS homologs (~300 residues) consist solely of an evolutionarily conserved α-helical domain, the human protein (~2,200 residues) additionally possesses an N-terminal β-propeller and a large C-terminal region required for chromatin association (73, 82) (Figure 4). In metazoans, which undergo a completely open mitosis, ELYS is believed to recruit CNCs to chromatin to initiate postmitotic NPC assembly, a functionality that may be dispensable in fungal species that undergo a closed or semiopen mitosis (79, 80, 96). The fungal homologs of Nup160, Nup37, and ELYS from *Schizosaccharomyces pombe* (*sp*Nup120, *sp*Nup37, and *sp*Elys) and *C. thermophilum* (*ct*Nup120, *ct*Nup37, and *ct*Elys) cooperatively assemble into a stable heterotrimer (71, 82). Although the α-helical domain of ELYS is sufficient for interaction with Nup160 and Nup37 in fungi, the N-terminal β-propeller of ELYS also contributes to Nup160 binding in humans (73). In *S. pombe*, *sp*Nup37 binds *sp*Nup120 at an L-shaped groove formed by α-helices from both the solenoid domain and the α-helical insertion of the β-propeller, without directly contacting the *sp*Nup120 β-propeller (71, 72) (Figure 5). This interaction is primarily mediated by loops on the top face of the *sp*Nup37 β-propeller (71, 82). These structural data, combined with cross-linking mass spectrometry data, indicate that ELYS and Nup37 decorate the Nup160 arm of the Y-shaped CNC, whereas the metazoan-specific nucleoporin Nup43 binds to the other arm of the "Y" shape formed by Seh1–Nup75 (38, 97). Crystal structures of the murine ELYS and human Nup43 β-propeller domains have shown that they also possess a seven-bladed β-propeller architecture, but a detailed molecular understanding of their association with the CNC awaits high-resolution structural characterization (73, 97) (Figure 5). In mammalian cells, ELYS is not symmetrically distributed but rather is asymmetrically localized to the nuclear face of the NPC, consistent with its interaction with chromatin (79, 80, 96). Indeed, extra density on the Nup160 arm of the CNC attributable to ELYS is present only on the nuclear outer rings in the intact human NPC (38). This asymmetry is also supported by the reduced, half-fold stoichiometry of ELYS compared with other CNC components measured by quantitative mass spectrometry approaches (50). As fungal ELYS homologs do not possess chromatin-binding domains, characterization of other fungal NPCs are necessary to determine whether ELYS is asymmetrically localized in those species as well (95).

As summarized above, high-resolution structures of most CNC components and their interactions have now been determined. Negative-stain EM reconstructions of the *S. cerevisiae* and *H. sapiens* CNC have provided envelopes into which these crystal structures can be docked but have been of insufficient resolution to allow for de novo modeling of

missing pieces; most importantly, the central interaction hub at the center of the "Y" shape, where the upper arms and stalk meet (also known as the central triskelion) (38, 66, 68). Two crystal structures of CNC assemblies have recently provided the molecular details of this central hub: a 7.4-Å resolution crystal structure of a heterohexamer from *S. cerevisiae* (*sc*Sec13–*sc*Nup145C–*sc*Nup84–*sc*Nup120–*sc*Seh1–*sc*Nup85) and a 4.1-Å resolution crystal structure of a heterotetramer from *M. thermophila* (*mt*Sec13–*mt*Nup145C–*mt*Nup120–*mt*Nup85) (75, 76) (Figure 6a). In both structures, the C-terminal helices of *sc*Nup120/*mt*Nup120 serve as the lynchpin of the central triskelion and are sandwiched between the C-terminal helices of *sc*Nup85/*mt*Nup85 and *sc*Nup145C/*mt*Nup145C. Additional contacts that may be specific to these species were also observed in both structures. In the *M. thermophila* structure, these contacts are made by *mt*Sec13 with *mt*Nup120 and *mt*Nup85 as well as a helical insertion in the C-terminal region of *mt*Nup120 that wraps around the side of *mt*Nup145C (75). Furthermore, *mt*Nup85 does not possess a DIM, providing a molecular explanation for why Seh1 is not a member of the *M. thermophila* CNC (75). In the *S. cerevisiae* structure, a small helix in the flexible N-terminal extension of *sc*Nup145C is bound to a distal site on *sc*Nup85 (76).

A notable difference between the two structures is the angle of the Nup75 solenoid relative to the rest of the central triskelion (75, 76) (Figure 6a). This difference could be the result of species-specific differences in conformation, the overall conformational flexibility of the complex, or a combination of both factors. A large degree of flexibility has also been observed in the stalk formed by Nup107 and Nup133 in EM reconstructions of both the yeast and the human CNCs (38, 66, 68). An important difference between the yeast heterohexameric crystal structure and the negative-stain EM reconstructions of the human and yeast CNCs is the curvature of the arms of the "Y" shape, which may be the result of EM sample preparation (76). However, despite the flatness of both EM reconstructions, the heterohexameric *S. cerevisiae* structure readily fits into the EM envelopes of the yeast and human CNCs and can even be docked into cryo-ET reconstructions of the intact human NPC, highlighting the evolutionary conservation of the CNC architecture (76) (Figure 6b). Indeed, docking of either the *S. cerevisiae* CNC crystal structure or the negative-stain EM reconstruction of the human CNC resulted in the same arrangement of CNCs in the intact human NPC (38, 76).

In summary, atomic-resolution structural information is now available for the vast majority of the CNC, albeit predominantly from fungal species. Although fungal and human CNCs appear to have the same overall topology and shape, architectural differences between different species have also been found. High-resolution structural characterization of the CNCs from multiple species is necessary to appreciate the extent of evolutionary divergence in this essential NPC subcomplex.

Inner Ring Nucleoporins

Analysis of the symmetric core nucleoporins that reside in the inner ring, Nup53, Nup93, Nup155, Nup205, Nup188, Nup98, and the channel nucleoporin heterotrimer (CNT) nucleoporins Nup54, Nup58, and Nup62, had long been hindered by the difficulty of reconstituting these proteins in vitro. Deciphering the interaction network within the inner

ring nucleoporins in *S. cerevisiae* was further confounded by the presence of *S. cerevisiae*–specific gene duplications that encode paralogs with partially overlapping functions not found in humans or other model organisms (Nup155, *sc*Nup157/*sc*Nup170; Nup53, *sc*Nup53/*sc*Nup59; Nup98, *sc*Nup100/*sc*Nup116/*sc*Nup145N). Recent progress in their biochemical and structural characterization has predominantly come from the study of inner ring nucleoporins from the thermophilic fungus *C. thermophilum*, which are both more biochemically robust than their mesophilic counterparts and lack the *S. cerevisiae*–specific paralogs (41, 98–101).

In contrast to the defined Y-shaped architecture of the CNC, inner ring subcomplexes observed by negative-stain EM are highly heterogeneous in conformation (36, 100). This is because, unlike the CNC, in which nucleoporin binding is mediated by large interfaces between folded domains, the interactions within the inner ring are predominantly mediated by short sequence motifs connected by flexible linkers that tether the large structured domains together (41, 98–101) (Figure 7). These motifs have been mapped to high biochemical resolution primarily in *C. thermophilum*, where they reside in the *ct*Nic96 N-terminal extension and in the primarily unstructured proteins *ct*Nup53 and *ct*Nup145N. Unlike the highly modular CNC architecture, each nucleoporin in the inner ring binds multiple other nucleoporins, yielding an intricate interaction network: The *ct*Nic96 N-terminal extension contains short sequence motifs that bind *ct*Nup192, *ct*Nup188, and the *ct*CNT; *ct*Nup53 contains binding sites for *ct*Nup192, *ct*Nic96, and *ct*Nup170; and *ct*Nup145N contains binding sites for *ct*Nup192, *ct*Nup188, and *ct*Nup170 (41, 98–101) (Figure 7). In addition to these inner ring nucleoporin binding sites, *ct*Nup145N uniquely spans multiple subcomplexes, as it also harbors binding sites for the coat nucleoporin *ct*Nup145C and the cytoplasmic filament nucleoporins *ct*Nup82 and *ct*Gle2 (see the section below titled Nup98 Spans the Nuclear Pore Complex Subcomplexes). Furthermore, these short motifs are often adjacent or overlapping. For example, *ct*Nup188 binding to *ct*Nup145N is mutually exclusive with *ct*Nup192 and *ct*Nup170 binding because the binding sites are overlapping, whereas *ct*Nup192 and *ct*Nup170 binding to *ct*Nup145N can occur simultaneously despite their binding sites being adjacent (41, 100) (Figure 7). Structures of nearly all of the inner ring nucleoporins and some of their interactions are now available, revealing the molecular details of how the NPC's inner ring is assembled (41, 70, 89, 90, 93, 98, 99, 102–107).

Nup53 comprises a conserved central domain possessing an RNA-recognition motif (RRM)–like fold flanked on either side by unstructured regions (*S. cerevisiae* possesses two paralogs, *sc*Nup53 and *sc*Nup59). In *C. thermophilum,* these unstructured regions contain short, ~30-residue sequence motifs that mediate interactions with *ct*Nic96, *ct*Nup192, and *ct*Nup170 (41, 98, 100, 101) (Figure 7). Additionally, a widely conserved C-terminal amphipathic α-helix in Nup53 has been shown to bind lipid membranes, possibly in conjunction with the transmembrane nucleoporin Ndc1 (108–111). Despite its name, the Nup53 RRM-like domain does not bind RNA but instead facilitates homodimerization in several species, an interaction that yields NPC assembly defects when disrupted (103, 112). Crystal structures of the Nup53 RRM-like domain from mouse, human, and the fungus *Meyerozyma guilliermondii* all contained a homodimer whose formation was mediated by the same conserved interface (103). Interestingly, this interface is not conserved in structures

of the Nup53 RRM-like domain from *C. thermophilum*, where the domain is a monomer in solution (41) (Figure 8a).

Nup93 (Nic96 in fungi) comprises a large N-terminal extension containing binding sites for other inner ring nucleoporins followed by a C-terminal U-bend solenoid (89, 90). Within the Nup93 N-terminal extension there are two conserved α-helical regions, which mediate interactions with the CNT and Nup205/Nup188, respectively (discussed below (98, 100, 101, 113). In *C. thermophilum*, the *ct*Nic96 U-bend solenoid contains a binding site for a short motif from *ct*Nup53 (41, 100). This interaction was visualized in a crystal structure of the *ct*Nic96–*ct*Nup53 heterodimer, wherein *ct*Nup53 forms an ~20-residue amphipathic α-helix that packs its hydrophobic face into a hydrophobic cleft on the *ct*Nic96 surface (41) (Figure 8).

Nup155 (Nup170 in fungi; an additional paralog termed Nup157 is also present in *S. cerevisiae*) is an extended, ~175-Å-long molecule formed by an N-terminal β-propeller that is integrated into a C-terminal α-helical solenoid. Thus, despite possessing a C-terminal α-helical solenoid that is structurally homologous to the C-terminal α-helical solenoid found in the CNC component Nup133, the Nup155 β-propeller is not flexibly anchored (41, 70, 93) (Figure 8a). A series of crystal structures of the *ct*Nup170 solenoid revealed considerable conformational flexibility α-helical solenoid mediated by rotations along several hinge regions in the solenoid, a phenomenon also observed for Nup133 (41, 70). The Nup155 β-propeller is also predicted to contain an ALPS motif at the same position as Nup133 (41, 94). In *C. thermophilum*, *ct*Nup170 binds to *ct*Nup53 via its N-terminal β-propeller and to *ct*Nup145N via its C-terminal α-helical solenoid (41) (Figure 8a). Crystal structures of the *ct*Nup170–*ct*Nup53 and *ct*Nup170–*ct*Nup145N heterodimers showed that *ct*Nup53 and *ct*Nup145N both bind as short extended peptides to conserved hydrophobic surfaces on opposite ends of the *ct*Nup170 molecule, producing an architecture in which these interaction surfaces are spatially separated by more than ~100 Å (41) (Figure 8b). Interestingly, the *ct*Nup53 binding site on *ct*Nup170 is adjacent to the *ct*Nup170 ALPS motif and a highly conserved tryptophan-phenylalanine (WF) motif residing in a surface-exposed loop (41) (Figure 8b). Because the *ct*Nup53 region that *ct*Nup170 recognizes is immediately upstream in sequence of the C-terminal amphipathic helix, this arrangement has been proposed to spatially cluster several membrane-binding motifs (41).

Nup205 and Nup188 are evolutionarily related nucleoporins comprised almost entirely by α-helices. With the exception of the middle portion of Nup188, the fungal homologs of Nup205 and Nup188 (Nup192 and Nup188) have been visualized at high resolution in their entirety by X-ray crystallography (41, 98, 99, 106, 107) (Figure 8a). Nup205 and Nup188 are predominantly built of tandem armadillo (ARM)– and HEAT [Huntingtin, elongation factor 3 (EF3), protein phosphatase 2A (PP2A), and TOR1]–like repeats, which stack into solenoids with a superhelical twist (114). Altogether, this architecture generates ~160-Å-long α-helical solenoids that are roughly "S"– or question mark–shaped (41, 100, 106, 115). The karyopherin-α and karyopherin-β families of nuclear transport factors also consist of ARM or HEAT repeats, respectively, which has led to the proposal that the karyopherins and Nup205/Nup188 are derived from common ancestral proteins (41, 55, 99, 100, 106, 115). Consistent with this hypothesis, the fungal homologs of Nup205 and Nup188 possess some

karyopherin-like biochemical properties, as *ct*Nup192 recognizes an NLS-like sequence in *ct*Nup53 and the fungal homologs of Nup205 and Nup188 can bind FG repeats (99, 106). Because *ct*Nup192 and *ct*Nup188 bind competitively to overlapping motifs in both *ct*Nic96 and *ct*Nup145N, they exist in mutually exclusive subcomplexes, comprising *ct*Nic96, *ct*Nup145N, *ct*Nup53, *ct*Nup170, the three CNT nucleoporins *ct*Nup49, *ct*Nup57, and *ct*Nsp1, and either *ct*Nup192 or *ct*Nup188 (41, 98, 100, 101, 116). No structural information is yet available for these interactions, but biochemical and site-directed mutagenesis studies in *S. cerevisiae* and *C. thermophilum* have mapped the *ct*Nic96 binding sites to the C-terminal tails of *ct*Nup192 and *ct*Nup188, whereas the binding site for *ct*Nup53 was mapped to the opposite end of the *ct*Nup192 molecule (98, 99) (Figures 7 and 8a).

In summary, the inner ring nucleoporins are assembled via a different mechanism than the CNC. Whereas large hydrophobic interfaces between structured domains mediate CNC assembly, the structured domains of the inner ring nucleoporins are linked by short sequence motifs separated by flexible linkers. The binding sites for these short sequence motifs are often at opposing ends of the structured domains. This architecture provides greater potential for flexibility than in the CNC. Future studies are necessary to resolve the atomic details of these interactions to understand how they facilitate assembly of the inner ring.

Nup98 Spans the Nuclear Pore Complex Subcomplexes

Among the nucleoporins, Nup98 is unique in both its biogenesis and its interaction with multiple subcomplexes. Nup98 arises from the autoproteolytic cleavage of an evolutionarily conserved precursor protein encoded by a single gene (EC number 3.4.21.-) (77, 117, 118). The Nup98-Nup96 precursor (Nup145 in fungi) is cleaved by an autoproteolytic domain (APD) located in the middle of the polypeptide chain. Cleavage yields an N-terminal product, Nup98 (Nup145N in fungi), which is part of both the NPC's inner ring and the cytoplasmic filaments, and a C-terminal product, Nup96 (Nup145C in fungi), a component of the CNC (discussed above) (77, 118–120). Nup98 possesses a modular architecture that can be divided into three regions: (*a*) an N-terminal FG-repeat region that also harbors the highly conserved Gle2-binding sequence (GLEBS), which binds the mRNA export factor Rae1 (Gle2 in fungi; see discussion on cytoplasmic filament nucleoporins below); (*b*) a largely unstructured middle section containing motifs that mediate interactions with inner ring nucleoporins Nup155, Nup205, and Nup188; and (*c*) the C-terminal APD, which can bind to not only the cytoplasmic filament nucleoporin Nup88 but also the CNC component Nup96 (121, 122). The Nup98 APD possesses a β-sandwich fold and binds the C-terminal residues of the domain within the active site to specifically strain the polypeptide chain for nucleophilic attack by a serine residue in an intein-like mechanism (102, 104, 117, 123). There are only minor structural rearrangements upon proteolytic cleavage, and Nup96 can still bind the APD after cleavage (41, 102, 104, 122) (Figure 8a).

Mitotic phosphorylation of Nup98 is necessary for NPC disassembly during mitosis, reflecting its critical role in NPC architecture (124). Interestingly, Nup98 is one of the few nucleoporins with a stoichiometry of 48 copies rather than 32 copies in the human NPC (50). In addition to the Nup98 homolog *sc*Nup145N, *S. cerevisiae* possesses two additional Nup145N paralogs, termed *sc*Nup116 and *sc*Nup100, but despite possessing C-terminal

domains that adopt the APD fold, they lack autoproteolytic cleavage activity (105, 125, 126). Furthermore, the three *S. cerevisiae* paralogs are asymmetrically distributed, with *sc*Nup116 and *sc*Nup100 primarily residing on the cytoplasmic side and *sc*Nup145N residing on the nuclear side (40). Given its stoichiometry, it is likely that biochemically distinct Nup98 molecules also exist in the human NPC. The paralogs found in *S. cerevisiae* may have specialized for these distinct biochemical roles.

Channel Nucleoporin Heterotrimer

In addition to Nup98, the FG repeats within the central transport channel are primarily contributed by the channel nucleoporin heterotrimer (CNT), a subcomplex comprising Nup54, Nup58, and Nup62 (Nup57, Nup49, and Nsp1 in fungi, respectively) (56, 57, 127, 128). Each channel nucleoporin contains a large N-terminal FG-repeat region followed by an extensive conserved coiled-coil region (Figure 4). Depending on the species, additional FG-repeat regions are sometimes also present in the C-terminal region, as is the case for human Nup58. Estimates of the relative stoichiometry of channel nucleoporins in the context of the NPC have varied considerably (3, 50, 56, 128–132). This is largely because early models for both the structure and stoichiometry of the channel nucleoporins were informed by early reconstitution efforts that excluded subunits or utilized incomplete fragments of the extensive coiled-coil regions (130–132). Independent efforts to reconstitute the intact coiled-coil regions of the three channel nucleoporins from *S. cerevisiae*, *C. thermophilum*, *Rattus norvegicus*, and *X. laevis* have revealed a conserved 1:1:1 stoichiometry, consistent with early biochemical characterizations of the natively purified *R. norvegicus* complex (98, 101, 113, 129, 133). Importantly, only an intact CNT containing all three constituent nucleoporins can be recognized by Nup93 and therefore recruited to the NPC (98, 101, 113). The crystal structure of the complete *C. thermophilum* CNT bound to *ct*Nic96 (*ct*Nsp1–*ct*Nup49–*ct*Nup57–*ct*Nic96) revealed that each channel nucleoporin contains three coiled-coil segments connected by short linkers (98) (Figure 9a). These coiled-coil segments assemble into parallel heterotrimeric coiled-coil domains (CCDs 1–3), with the short linkers mediating sharp bends between the CCDs and ultimately generating a "4"-shaped complex (98). *ct*Nic96 forms a small, ~40-residue helical hairpin that binds in the opening of the "4," thereby contacting all three CCDs (98). A critical consequence of this mode of interaction is that *ct*Nic96 recognition of the *ct*CNT requires the proper assembly of the CCDs of all three channel nucleoporins, providing a molecular explanation for why only an intact and properly assembled CNT containing all three constituent nucleoporins can interact with Nup93 and be recruited into the NPC (98). A crystal structure of a fragment of the *X. laevis* CNT (*xl*Nup62–*xl*Nup54–*xl*Nup58) containing CCD1 and CCD2 revealed an identical arrangement, highlighting the evolutionary conservation of this architecture (113) (Figure 9a). Both crystal structures also revealed an insertion in the first coiled-coil segment of Nup54 that forms a small folded domain, which is expanded in metazoans to also include an additional ferredoxin-like domain, but the functional role of these insertions remain unknown (98, 113).

In conclusion, the CNT is recruited to the NPC via an interaction with Nup93 that requires a highly specific conformation of an equimolar stoichiometric complex of the three channel nucleoporins (98, 101, 113). Confirming the importance of this interaction mechanism, its

disruption results in the loss of the CNT from the nuclear envelope in *S. cerevisiae* (98). The above described stoichiometry and structural arrangement of the CNT have been observed in diverse species ranging from fungi to human, suggesting that this could be a conserved NPC design principle shared by all eukaryotes. The crystal structures also provide an explanation for why earlier reconstitution attempts yielded promiscuous or dynamic complexes (130–132, 134). Specifically, N-terminal sequences critical for the proper parallel assembly of the three coiled-coil strands were omitted in earlier studies, including the conserved domain insertion in Nup54. Indeed, deletion of these residues converts the stable, monodisperse *C. thermophilum* CNT complex into a polydisperse mixture (98). Thus, models based on the solution behavior and crystal structures of artificial complexes assembled from truncated channel nucleoporin fragments that invoke variations in CNT arrangement or stoichiometry as a mechanism to dilate the central transport channel are implausible (130–132, 134–136).

Transmembrane Nucleoporins

Of all nucleoporins, the transmembrane nucleoporins, also known as the pore membrane proteins (POMs), are the least conserved and structurally characterized (Figure 4). The roles of the various POMs have been difficult to decipher in part owing to their apparent functional redundancy (95). The only universally conserved member is Ndc1, but Ndc1 also functions in cell division and is a component of the spindle pole body in fungi (108, 137, 138). *S. cerevisiae* possess three additional POMs, *sc*POM152, *sc*POM34, and *sc*POM33, whereas humans possess two additional POMs, POM210 and POM121, which are not direct homologs of the fungal POMs (3, 42, 108, 138–143). Most POMs possess large regions that either face the nuclear envelope lumen (POM152 and POM210) or project toward the pore side (Ndc1, POM121, POM33, and POM34), the latter of which could facilitate interactions with the soluble nucleoporins (Figure 4). Although most of these regions are predicted to be unstructured, the pore-facing region of Ndc1 is predicted to contain several α-helices in both fungi and humans. Pull-down experiments suggest that the transmembrane POMs can also associate with each other (110).

POM210 (also known as GP210) homologs can be found in most eukaryotes except fungi, which instead possess the nucleoporin POM152 (45). Both proteins contain at least eight immunoglobulin (Ig)–like domains in their lumenal regions, but in POM210 the lumenal region is N-terminal to its sole transmembrane helix, whereas in POM152 the lumenal region is C-terminal to its three transmembrane helices (144, 145). This similarity has led to speculation that these proteins may have similar functions. An NMR structure of a single Ig-like domain from *sc*POM152 revealed that it forms a C3-subtype Ig-like fold that does not utilize a canonical intramolecular disulfide bridge to stabilize its fold (145). Negative-stain EM analysis of *sc*POM152 has led to a flexible string-of-pearls model, in which the Ig-like domains are arranged linearly and flexibly connected to each other (145). A recent cryo-EM analysis of *ct*POM152 is consistent with this model and further suggests that full-length molecules are capable of oligomerization, possibly with a head-to-tail arrangement (144). Future studies are needed to illuminate the structure and function of the POMs in stabilizing the nuclear envelope curvature and anchoring the symmetric core in nuclear envelope pores.

THE ARCHITECTURE OF THE NUCLEAR PORE COMPLEX SYMMETRIC CORE

Recent studies have reported near-atomic resolution architectures of the symmetric core for NPCs from humans, *S. cerevisiae*, and the unicellular algal species *C. reinhardtii* (33, 36, 40, 41). These advances have been made possible by the acquisition of improved cryo-ET reconstructions of intact NPCs, determination of crystal structures of most symmetric core nucleoporins, detailed biochemical characterization of their interactions, and high-quality cross-linking and mass spectrometry experiments. Importantly, the NPCs from this diverse set of species share the same overall architecture, underscoring the evolutionary conservation of the organizational principles of the NPC. However, within this conserved architecture, the NPCs also display examples of divergence, including differences in the stoichiometry of subunits, the overall dimensions of the NPC, and the presence of specific architectural features. Most notably, the stoichiometry of the CNC is different in the three species, with the human, algal, and fungal NPCs possessing 32, 24, or 16 copies of the CNC, respectively (33, 36, 40, 41).

Although all of these studies fundamentally fitted crystal structures of nucleoporins into cryo-ET reconstructions of intact NPCs, they employed a diverse set of approaches. The first reported composite structures were for the human NPC symmetric core and were obtained through docking of either high-resolution fungal crystal structures (Hoelz group) (41) or human homology models derived from fungal crystal structures (Beck group) (36) into an ~20-Å resolution cryo-ET reconstruction of the intact human NPC acquired by the Beck group, methods that led to agreeing composite structures. In both studies, nucleoporins were docked by computationally searching through large numbers of randomly generated positions and orientations for each structure to identify the best-fitting positions. The composite structures of the human NPC symmetric core were consistent with high-resolution biochemical nucleoporin–nucleoporin interaction mapping of fungal nucleoporins (41) and with cross-linking mass spectrometry analysis of human and fungal nucleoporin interactomes (36, 37). For the algal NPC, cryo-ET combined with ion beam milling yielded a reconstruction with a resolution approaching ~30 Å. Owing to the lower resolution of this reconstruction, entire subcomplexes from the human NPC rather than individual crystal structures were fitted. Lastly, a study led by the Rout group (40) employed an integrative modeling approach to obtain the architecture of the *S. cerevisiae* NPC. This approach combined quantitative mass spectrometry, chemical cross-linking, models and restraints generated primarily from fungal nucleoporin crystal structures, small-angle X-ray scattering, and a newly acquired ~28-Å cryo-ET reconstruction of the *S. cerevisiae* NPC with computational modeling. Ultimately, all of these approaches yielded near-atomic composite structures for each NPC and revealed the position, orientation, and stoichiometry of each nucleoporin (Figure 10). We first discuss the architecture of the human NPC and then use it as a reference to discuss the differences between the three NPCs.

The human NPC symmetric core is formed by three rings: an inner ring that resides in the plane of the nuclear envelope and lines the central transport channel and two outer rings, each of which resides above the nuclear envelope on either the nuclear or cytoplasmic side

(36, 41) (Figure 10). The inner ring and outer rings are sparsely connected. The symmetric core comprises eight distinct spokes, which are the units related by the NPC's eight-fold rotational symmetry. Each spoke also possesses two-fold rotational symmetry relating its cytoplasmic and nuclear halves (Figure 11). The outer rings primarily, but not entirely, consist of CNCs. There are 4 CNCs per spoke, with 2 CNCs on either side of the nuclear envelope, for a total of 32 CNCs in each human NPC. The Y-shaped CNCs are oriented horizontally such that the Nup160 arm and Nup133 end of the stalk point toward the membrane, whereas the Nup75 arm points away from the nuclear envelope. In each of the cytoplasmic and nuclear halves of a spoke, the two CNCs are parallel but slightly offset to each other. On the basis of their distance from the center of the nuclear pore, we refer to them as inner or outer CNCs. The CNCs in adjacent spokes connect in a head-to-tail fashion, thereby generating continuous rings formed from the outer or inner CNCs. Because the outer and inner CNC rings are slightly offset in position, this arrangement yields a reticulated double-ring architecture. The head-to-tail interaction of horizontally arranged CNCs in the intact NPC is primarily mediated by Nup133–Nup160 interactions occurring between adjacent CNCs at the inter-spoke interfaces in the intact human NPC. A similar interaction was previously discovered between the *sc*Nup133 N-terminal extension and *sc*Nup120, consistent with the evolutionary conservation of this head-to-tail arrangement (69).

The inner and outer CNC rings have slightly different diameters (38, 76). This heterogeneity is facilitated by the flexibility of the Nup133 stalk, especially the flexibly attached Nup133 β-propeller domain, consistent with the conformational heterogeneity observed in negative-stain EM reconstructions of isolated CNCs (38, 66, 68). In addition to the CNCs, a question mark–shaped density consistent with an unanticipated copy of either Nup205 or Nup188 is present in both the nuclear and cytoplasmic outer rings, intercalated between the CNCs (37, 41). The identity of this nucleoporin remains ambiguous because the Nup205 and Nup188 molecules possess similar shapes and cannot be distinguished at the current resolutions of EM reconstructions. This surprising finding is consistent with the total stoichiometry of Nup205/Nup188 molecules in the NPC (48 total), of which only 32 are localized in the inner ring (36, 41, 50). The presence of Nup205/Nup188 molecules in the outer ring is conserved in the *C. reinhardtii* NPC but does not appear to be in the *S. cerevisiae* NPC (33, 40). Additional densities are present on both outer rings. These densities are unique to either the cytoplasmic or the nuclear outer ring, suggesting they contain the asymmetric cytoplasmic filament and nuclear basket nucleoporins, but assignment of these densities has not yet been possible owing to a lack of high-resolution crystal structures of these nucleoporins and the inability to obtain unambiguous placements of the available crystal structures during quantitative docking (see the section below titled Organization of the Asymmetric Nucleoporins) (36, 41).

Early working models for the arrangement of the coat nucleoporins captured specific aspects of this observed architecture, but no individual model fully predicted this arrangement. Specifically, the lattice model proposed an architecture similar to vesicle coats in which vertexes comprising β-propellers were spanned by edges comprising the α-helical solenoids (63). Although several α-helical solenoids are used as edges, vertexes similar to those in vesicle coats are not found in the NPC, with the exception of the Nup160–Nup133 interaction. In contrast, the fence model correctly proposed the formation of four head-to-tail

CNC rings; however, based on biochemical and structural observations of oligomerization of isolated CNC components, the model incorrectly proposed that the four CNC rings would be stacked with alternating directionality to form a continuous coat that would span the entire height of the NPC (64). Lastly, an early integrative structural model of the yeast NPC correctly captured the separation of CNCs into outer rings and a circumferential arrangement, albeit with a limited resolution of the arrangement of subunits (49).

Similar to the outer rings, the cytoplasmic and nuclear halves of the inner ring spoke each contain two IRCs per half-spoke, for a total of 4 IRCs per spoke and 32 per NPC (36, 41). This stoichiometry and arrangement is evolutionarily conserved in the *S. cerevisiae* and *C. reinhardtii* NPCs (33, 40). Within the nuclear and cytoplasmic pairs, one IRC is more equatorially positioned, whereas the other is more peripherally positioned (Figure 11). Therefore, the IRCs in each spoke can be uniquely identified as the nuclear peripheral IRC, nuclear equatorial IRC, cytoplasmic peripheral IRC, or cytoplasmic equatorial IRC (Figure 11c). The subunits within the peripheral and equatorial IRCs occupy the same positions but with slightly different orientations of the subunits relative to each other. This variability can conceivably be accommodated by the IRCs because the large structural nucleoporins are held together by short motifs connected by flexible linker sequences. The IRCs extend from the nuclear envelope to the central transport channel, but the scaffold nucleoporins are aligned circumferentially around the pore, resulting in each nucleoporin forming a distinct layer in the inner ring (Figure 12). Nup155 molecules form the outermost layer and compose the major structured scaffold immediately proximal to the nuclear envelope. Nup93 molecules form the next layer by intercalating between adjacent peripheral and equatorial Nup155 molecules. Lastly, Nup205/Nup188 and CNT molecules generate the innermost two layers, respectively. In contrast to the circumferential orientation of the scaffold nucleoporins, the path of the primarily unstructured regions of Nup53, Nup98, and Nup93 must extend radially from the nuclear envelope to the central transport channel to bridge the layers. In the human NPC, additional Nup155 molecules form structural bridges between the inner ring and the cytoplasmic and nuclear outer rings by inserting their N-terminal β-propellers into the inner ring and contacting the Nup160 arm of the CNCs with their C-terminal α-helical solenoids (36, 41). However, this feature appears to be poorly conserved, as it is not found in the *S. cerevisiae* NPC, and is present only in the nuclear half of the *C. reinhardtii* NPC (33, 40).

Conservation of Nuclear Pore Complex Architecture

Although the human, fungal, and algal NPCs have the same overall architectures, there are notable differences between the three NPCs as well (Figures 11 and 12). One very clear difference between the human and *S. cerevisiae* NPC is in size and mass. The human NPC has a mass of ~110 MDa, whereas the *S. cerevisiae* NPC has a mass of ~52 MDa owing to a reduced stoichiometry of several nucleoporins (40, 50) (Figure 3). Three differences account for the vast majority of this difference. First, *S. cerevisiae* does not possess direct or functional homologs of several nucleoporins, including the CNC components Nup37, Nup43, and ELYS and the cytoplasmic filament nucleoporin Nup358 (3). Second, the *S. cerevisiae* NPC possesses only 16 copies of the CNC, most nuclear basket nucleoporins, and transmembrane nucleoporins, rather than the 32 copies found in the human NPC (40, 50,

52). And third, *S. cerevisiae* possesses 32 copies of Nup155, Nup93, and Nup205/Nup188 homologs, rather than the 48 of each found in the human NPC (40, 50, 52).

The relative arrangements of nucleoporins within a CNC and in the inner ring are essentially identical between the *S. cerevisiae* and the human NPCs. In contrast, the *S. cerevisiae* nuclear and cytoplasmic outer rings possess only a single ring, as opposed to the reticulated double-ring architecture found in the human NPC. This single ring architecture is consistent with a reduced stoichiometry of only 16 CNC copies in *S. cerevisiae* compared with 32 copies in the human NPC (40, 52). An additional difference is the absence of a scaffold protein bridging the inner and outer rings, a role fulfilled by Nup155 molecules in the human NPC. These differences all contribute to the reduced overall height of the *S. cerevisiae* NPCs compared with human NPCs (~600 Å in yeast compared with ~800 Å in humans) (37, 40, 76). Moreover, the *S. cerevisiae* Nup155 paralogs, *sc*Nup170 and *sc*Nup157, are specifically localized to the equatorial and peripheral IRCs, respectively (40). Lastly, there are no Nup205/Nup188 molecules in the outer ring of the *S. cerevisiae* NPC, in contrast to the additional copies interdigitated between CNCs in the outer rings of the human NPC (Figure 11). In the inner ring, the *S. cerevisiae* homologs of Nup205 and Nup188 (*sc*Nup192 and *sc*Nup188) are localized to the equatorial and peripheral IRCs, respectively (40). Future work needs to establish whether this Nup188 placement is evolutionarily conserved in species that also possess Nup205/Nup188 molecules in the outer rings, as that would suggest that the ambiguous molecules in the outer ring are Nup205 molecules.

The *C. reinhardtii* NPC also exhibits general conservation of the architecture and arrangement of its subunits with some alterations in overall NPC dimensions. Specifically, although the outer diameter of the outer ring is approximately the same as in the human NPC, the inner ring is dilated compared with the yeast and human NPCs, increasing the diameter of the central transport channel by at least 200 Å (33) (Figure 12). The most notable other difference between the *C. reinhardtii* NPC and the human NPC is a breakdown of the two-fold symmetry across the plane of the nuclear envelope, resulting from the presence of only a single ring of CNCs on the cytoplasmic face, whereas a reticulated double CNC ring architecture similar to the human NPC is present on the nuclear face (33). This asymmetric reduction results in a stoichiometry of 24 copies of the CNC in the *C. reinhardtii* NPC. A cryo-ET reconstruction of the human NPC obtained from Nup358-depleted HeLa cells yielded human NPCs with a single outer cytoplasmic CNC ring (37). This observation has led to the proposal that Nup358 stabilizes the reticulated double CNC ring architecture in humans, a functional link consistent with the observation that both *S. cerevisiae* and *C. reinhardtii* do not possess Nup358 homologs (see Nup358 Is a Unique Multifunctional Component of Animal Nuclear Pore Complexes section below) (33, 40). Furthermore, in *C. reinhardtii* the presence of a single cytoplasmic outer CNC ring is concomitant with the loss of the structural bridge between the inner and outer CNC ring mediated by the Nup155 homolog solely on the cytoplasmic side (33). Thus, in the three known examples, bridging Nup155 molecules that connect the inner and outer rings are only observed in conjunction with double CNC rings. Intriguingly, despite possessing a larger central transport channel, the three *C. reinhardtii* channel nucleoporins, Nup54, Nup58, Nup62, do not possess larger FG-repeat regions, suggesting that its diffusion barrier functions with a lower density of FG repeats (33).

Organization of the Diffusion Barrier Scaffold

The physical nature and mechanism for the formation of the diffusion barrier itself continue to be debated. FG repeats constitute the diffusion barrier, but FG-repeat sequences from various nucleoporins display a range of sequence compositions and biophysical properties (54). In *S. cerevisiae*, most FG repeats are dispensable for viability, with the exception of those contributed by the CNT and two of the *S. cerevisiae* Nup98 homologs, *sc*Nup100 and *sc*Nup116 (127). Furthermore, genetic studies, biochemical reconstitution experiments, and in vivo measurements of the diffusion barrier strongly indicate that FG repeats from Nup98, or its homologs, make the most important contribution to the diffusion barrier, with the second-largest contribution made by the CNT (6, 127, 146). Indeed, Nup98 is sufficient to reconstitute a diffusion barrier in reconstitution experiments (146). Several models for how FG repeats function in a selective barrier have been proposed: the virtual gate model, which invokes the intrinsically disordered nature of the FG repeats to generate an entropic barrier to passage; a reversible collapse model based on the observation of karyopherin binding causing an extended FG filament to collapse in size; and a selective phase model wherein FG repeats self-assemble into a phase that nuclear transport factors can selectively partition in and out of because of their ability to interact with FG repeats (reviewed in 147–149). Purified FG repeats undergo phase transitions in vitro ranging from liquid–liquid phase separation to hydrogels to amyloid-like species that can replicate many properties of the diffusion barrier including selective permeability to transport factors (150). Resolution of the molecular nature of the diffusion barrier requires knowledge of the molecular architecture of the FG repeats in vivo.

Because FG repeats are intrinsically disordered, they do not adopt a single conformation that can be resolved at high resolution in crystal structures or EM reconstructions. However, the organization of the nucleoporins lining the central transport channel provides some insight into the organization of the diffusion barrier (33, 36, 40, 41, 98, 113). As all three components of the CNT possess N-terminal FG-repeat regions, the N termini of the CNT coiled-coil regions define the FG origins for these nucleoporins (Figure 9b). One consequence of the organization of the CNT into a coiled-coil structure is that the FG origins from each CNT are tightly clustered (98, 113). The overall arrangement of the four CNTs positions all of their origins at evenly spaced intervals around the central transport channel but within ~35 Å of the equator of the central transport channel. Therefore, although the entire human symmetric core encompasses ~800 Å in height and the inner ring itself is ~240 Å in height, these FG repeats only originate from an ~70-Å-thin zone (36, 41).

The location of Nup98 FG repeats is more poorly defined, but biochemical mapping of the interactions between Nup98 and Nup205/Nup188 homologs in *C. thermophilum* indicates that the sequences in *ct*Nup145N that mediate binding to *ct*Nup192 and *ct*Nup188 are immediately adjacent in sequence to the *ct*Nup145N FG repeats (41, 101). Thus, the binding sites for *ct*Nup145N on *ct*Nup192 and *ct*Nup188 would define the origins of the *ct*Nup145N FG repeats. Further structural and biochemical characterization are necessary to precisely map these origins and determine whether they are conserved. Based on cross-linking and modeling, the FG origins of the *S. cerevisiae* Nup98 homologs are predicted to project from a position adjacent to the inner ring (40). However, because Nup116 and Nup100 are

localized to the cytoplasmic half of the *S. cerevisiae* NPC, this localization suggests that the critical region of the diffusion barrier for the *S. cerevisiae* NPC resides at the cytoplasmic entrance to the central channel (40).

Future studies mapping the locations of all the FG-repeat origins in multiple species and their biophysical behavior in situ are necessary to definitively understand the nature of the diffusion barrier. Further high-resolution delineation of the roles of each FG-repeat sequence will be aided by accurate maps of their locations. Development of alternative techniques to measure the structure and dynamics of the FG repeats in situ also holds great potential for revealing the nature of the diffusion barrier, for example, through high-speed atomic force microscopy experiments (151). In addition to contributing to the diffusion barrier, FG-repeat sequences have other roles, most importantly as specific binding sites for karyopherins (discussed in the section below titled Interactions Between FG Repeats and Transport Factors) (127, 152–154). Many nucleoporin–FG repeat interactions have now also been identified, leading to the proposal that an additional layer of architectural nucleoporin–FG repeat interactions promotes NPC stability (106, 155).

Contacts Between the Symmetric Core and the Nuclear Envelope

Because the NPC resides at the site of fusion between the inner and outer nuclear membranes, it must stabilize the unfavorable extreme membrane curvature in nuclear pores. This function is similar to those of membrane vesicle coats, but the NPC is unique compared with vesicle coats owing to the presence of both negative and positive membrane curvature. However, the mechanisms by which membrane bending is achieved remain poorly understood. Only a few nucleoporins in the symmetric core of the human NPC directly contact the nuclear envelope (36, 41). Nucleoporins possessing transmembrane domains necessarily reside in the nuclear envelope, but their structures and localization within the NPC remain unresolved. Within the composite structures, the only contacts observed between the CNC and the nuclear envelope are mediated by the ALPS motif–containing Nup160 and Nup133 β-propellers (33, 36, 40, 41). Nup155 molecules integrated within the inner ring form the closest layer of scaffold proteins to the nuclear envelope in the inner ring, and they also contact the nuclear envelope via their ALPS motif–containing β-propellers. The inner and outer rings in humans and C. *reinhardtii* are connected by an additional set of bridging Nup155 molecules. These bridging Nup155 molecules also interface with the membrane with their ALPS motif–containing β-propellers within the inner ring, but then they extend out of the inner ring to contact the Nup160 arms of the inner CNCs with the C-terminal helices of their α-helical solenoids (36, 41). In this arrangement, the outer ring coats formed by CNCs are directly connected to the inner ring coat formed primarily by Nup155 and Nup93 in the human NPC. This connection of the outer and inner ring coats is similar on the nuclear half of the *C. reinhardtii* NPC, but on the cytoplasmic side the outer ring–inner ring contact is mediated by the outer ring Nup205/Nup188 molecule (33). Furthermore, no ordered structural contacts have been observed in the *S. cerevisiae* NPC, although the orientation of the CNCs remains ambiguous (40). An interaction between *sc*Nup157 and *sc*Nup120 was previously identified, which is consistent with orientation of the C-terminal end of Nup157 adjacent to the outer rings (156). Higher-

resolution reconstructions of the *S. cerevisiae* outer rings are necessary to definitively characterize the connection between the inner and outer rings in *S. cerevisiae*.

In contrast to the evenly spaced distribution of FG-repeat origins in the central transport channel, the sites of contact between the inner and outer ring coats and the membrane are highly clustered. This architecture is strongly reminiscent of other membrane-bending coats, which also consist of a scaffold of structural proteins surrounding highly clustered membrane contacts (157). Additional membrane contacts have been mapped to a C-terminal amphipathic helix in Nup53, amphipathic helices in the human nuclear basket protein Nup153, and fungal nuclear basket proteins Nup1 and Nup60 (109, 112, 158, 159). The localization of these helices in relation to other membrane contacts can only be inferred, but intriguingly, both the Nup53 and Nup153 amphipathic helices are constrained to be near ALPS-motif binding sites owing to interactions with either Nup155 or the CNCs, respectively (41, 158). Indeed, based on the crystal structure of the *ct*Nup170–*ct*Nup53 heterodimer, the Nup53 amphipathic helix and both of the proposed Nup170 membrane-binding motifs are clustered next to each other (41). Thus, multiple membrane-binding motifs may be utilized simultaneously at each membrane contact site.

Further work is necessary to gain mechanistic insight into how all of these membrane interactions combine to mediate NPC biogenesis. Evidence has also been found that a number of other membrane-associated proteins, including reticulons and the ESCRT-III (endosomal sorting complexes required for transport) machinery, contribute to NPC biogenesis, even if they are not present in mature NPCs (160–164). Further study is also needed to uncover the structures of the transmembrane nucleoporins and clarify their roles in stabilizing the sharp curvature of the nuclear envelope at nuclear pores and in recruiting the symmetric core of the NPC. Incorporating the transmembrane nucleoporins into in vitro reconstitutions of the *C. thermophilum* symmetric core nucleoporin complexes could potentially uncover the biochemical determinants of these functions in the near future.

Limitations of Current Near-Atomic Composite Structures

The composite structures of the human, *S. cerevisiae*, and *C. reinhardtii* NPCs have provided unprecedented insight into their near-atomic architectures. However, there are a few considerations to acknowledge when interpreting the currently available composite structures of NPCs. The foremost constraint is the low and often asymmetric resolution limit of the cryo-ET reconstructions from which composite structures are derived. How reliably individual subunits can be localized in the reconstructions depends on not only the resolution of the cryo-ET map but also the size of the subunit and whether features are apparent at low resolution. The precise orientations of individual subunits that are partially symmetric (e.g., disk-shaped β-propellers or rod-like α-helical solenoids) remain ambiguous even at the highest of the currently available resolutions. Even within the same cryo-ET reconstructions, the resolution can vary tremendously. For example, in the *S. cerevisiae* NPC, the inner ring is resolved to ~20 Å, whereas the outer rings are only resolved to ~45 Å. Consequently, the exact orientations of the *S. cerevisiae* CNCs and associated cytoplasmic filament and nuclear basket nucleoporins are ambiguous (see the section below titled Organization of the Asymmetric Nucleoporins) (40). Importantly, the incorporation of

additional spatial constraints for subunits, for example, from cross-linking and mass spectrometry, can only partially ameliorate this ambiguity.

Another key limitation is that the vast majority of crystal structures of nucleoporins and nucleoporin complexes are usually available only from fungal species, often contain only a fragment rather than a complete nucleoporin, and typically capture only a single conformation of the subunit. Thus, the current composite structures employ large numbers of homology models (36, 40) or otherwise make the assumption that the overall shapes and conformations of the subunits are conserved between species (41). However, generating accurate homology models for the human nucleoporins and their complexes is challenging owing to the poor sequence conservation of most nucleoporins, despite an overall structural conservation, and the fact that the β-propeller and α-helical solenoid folds of most nucleoporins are able to accommodate large loops or insertions between their secondary structure elements. As a result, the localizations of specific residues within the overall structure, such as those that are linked to human disease, possess some ambiguity in the currently available composite structures. Lastly, a related consideration is that, owing to the extensive averaging needed to acquire cryo-ET reconstructions, the current composite structures largely provide insight into only the structurally ordered and symmetric components of the NPC. Notably, additional densities attributed to transport factors in the central transport channel have been observed in several reconstructions, but the details of these interactions are averaged out (30, 40, 49). Similarly, regions of nucleoporins that can adopt different conformations, such as FG repeats or flexibly attached domains, are currently not resolved either. Thus, further advances in cryo-ET that enable the capture of specific functional states are needed to shed light on how the NPC directly participates in nucleocytoplasmic transport. Further acquisition of high-resolution crystal structures of subunits from multiple species are necessary to validate the current near-atomic composite structures and perform structure-guided functional studies.

ORGANIZATION OF THE ASYMMETRIC NUCLEOPORINS

Although the symmetric core accounts for a major portion of the NPC, decorations specific to the cytoplasmic or nuclear side formed by the asymmetric cytoplasmic filament and nuclear basket nucleoporins provide much of the functionality associated with the NPC. In some cases, these nucleoporins are much more flexible, and parts or all of the proteins may not be visible in EM reconstructions owing to the averaging necessary to acquire high-resolution reconstructions. On both the cytoplasmic and nuclear sides, these nucleoporins contain FG repeats and binding sites for transport factor–cargo complexes as well as other cellular machinery. In addition to their structural flexibility, these asymmetric subcomplexes also display substantial divergence in composition and domain organization between humans and *S. cerevisiae*.

The Organization of the Cytoplasmic Filaments

The asymmetric nucleoporins at the cytoplasmic face of the NPC are often referred to as the cytoplasmic filament nucleoporins owing to the observation of long, flexible extensions into the cytoplasm in early micrographs of human NPCs (165). The evolutionarily conserved set

of cytoplasmic filament nucleoporins includes Nup214, Nup88, Nup62, Gle1, Nup42 (also known as CG1), Rae1, and Nup98. Homologs in *S. cerevisiae* are known as *sc*Nup159, *sc*Nup82, *sc*Nsp1, *sc*Gle1, *sc*Nup42, *sc*Gle2, and *sc*Nup145N/*sc*Nup100/*sc*Nup116. Nup358 (also known as RanBP2) is a metazoan-specific nucleoporin, and conversely, the cytoplasmic filament complex in *S. cerevisiae* also constitutively incorporates *sc*Dyn2. In addition, the mRNA export factor DDX19 (*sc*Dbp5 in *S. cerevisiae*) rapidly associates and disassociates from the NPC (166). Nup62 and Nup98 are both also components of the symmetric core (see the section above titled Structure and Biochemistry of Symmetric Core Nucleoporins and Complexes).

Immunogold-labeling experiments identified the metazoan-specific nucleoporin Nup358 as the primary constituent of the originally observed EM-visible filaments, a finding consistent with the fact that similar extensive filamentous extensions are not found in the *S. cerevisiae* NPC by EM (167, 168). In contrast, cross-linking studies on both human and yeast NPC are consistent with an architecture in which the structured domains of most cytoplasmic-specific nucleoporins are integrated into or decorate the outer CNC ring (38, 40). Consistent with this model, considerable amounts of cytoplasmic face-specific density present in the cytoplasmic outer ring in recent EM reconstructions of intact human NPCs are not explained by the docking of symmetric core nucleoporin crystal structures (36, 41). The cytoplasmic filaments play critical roles in nucleocytoplasmic transport, as they not only contain several FG repeat nucleoporins and other binding sites for nucleocytoplasmic transport factors but also position and regulate the activity of the ATP-dependent RNA helicase DDX19 (EC number 3.6.4.13), which terminates mRNA export.

The cytoplasmic filaments possess an intricate biochemical architecture, with structured domains within Nup214, Nup88, and Gle1 serving as major hubs for interactions with other nucleoporins in the complex. Different domains within each of the nucleoporins are members of different hubs. However, these structured interaction domains are typically separated by flexible linkers that can extend for up to hundreds of residues (Figure 4). Thus, some domains or even entire nucleoporins, for example, the Nup214 N-terminal β-propeller domain and Rae1, are flexibly tethered to the core of the complex (169–171). Although a substantial amount of high-resolution structural detail is available for some interaction hubs (98, 105, 122, 126, 169–177), an integrative structural model of the *S. cerevisiae* complex is the only model for the overall assembly of the cytoplasmic filament nucleoporins (51). In this section, we consider four major interaction hubs: (*a*) a coiled-coil hub comprising the coiled-coil regions of Nup214, Nup88, and Nup62; (*b*) the Nup88 β-propeller domain hub built around the Nup88 β-propeller domain, the Nup98 APD, and a Nup214 α-helical motif; (*c*) the Rae1 hub, comprising the Nup98 GLEBS and Rae1; and (*d*) the Gle1 hub, comprising Gle1, Nup42, DDX19, and the Nup214 N-terminal β-propeller domain (Figure 13a).

A molecular keystone of the cytoplasmic filaments is the heterotrimeric hub that is formed by the coiled-coil regions of Nup214, Nup88, and Nup62. Current structural models predict that the coiled-coil regions of the three proteins assemble into a heterotrimeric parallel CCD with an architecture akin to the CNT (see above) (51, 98, 178). This prediction is supported

by the observation that the same coiled-coil region of Nup62 is present in both complexes and by cross-linking studies performed in *S. cerevisiae* (51, 179–181).

Another major interaction hub forms on the Nup88 N-terminal β-propeller domain, which possesses binding sites for an α-helical motif in Nup214 and the Nup98 APD (122, 126). The human Nup98 APD can bind the *sc*Nup82–*sc*Nup159 complex, suggesting the mechanism of interaction is conserved between the two species (122). Indeed, crystal structures of the chimeric complex between the human Nup98 APD and the *sc*Nup82–*sc*Nup159 heterodimer revealed the same architecture as observed for cognate complexes between the *S. cerevisiae* and *C. thermophilum* nucleoporins (98, 122, 126) (Figure 13b). In all three structures, the APD binds to a large loop in the *sc*Nup82/*ct*Nup82 β-propeller domain by utilizing residues adjacent to and within the APD active site, which is also the binding site for Nup96 (*sc*Nup145C/*ct*Nup145C) (98, 102, 122, 126). At a separate surface on *sc*Nup82/*ct*Nup82, α-helical insertions in the β-propeller domain form the binding site for a C-terminal α-helix from the fungal homologs of Nup214 (*ct*Nup159/*sc*Nup159). In this arrangement, Nup214 and Nup98 would not form direct contacts, providing a molecular explanation for their independent and noncooperative binding to Nup88 (98, 122, 126). It remains unclear whether Nup96 (*sc*Nup145C/*ct*Nup145C) can bind to the APD in this complex.

Although all three *S. cerevisiae* paralogs of Nup98 (*sc*Nup100, *sc*Nup116, and *sc*Nup145N) can form analogous interactions with the *S. cerevisiae* homolog of Nup88 (*sc*Nup82), *sc*Nup116 appears to be the preferred interaction partner (122, 126, 182). Nup98 also contains a highly conserved GLEBS motif that mediates NPC recruitment of the mRNA export factor Rae1 (known as Gle2 in *S. cerevisiae*) (183). This heterodimeric complex appears to be one of several hubs flexibly tethered to the remainder of the NPC because the GLEBS motif is embedded in the N-terminal Nup98 FG-repeat region (Figure 4). Of the three *S. cerevisiae* paralogs of Nup98, only the cytoplasmic-specific paralog *sc*Nup116 possesses a GLEBS motif, suggesting that the GLEBS motif may function to localize Rae1 near the rest of the cytoplasmic mRNA export machinery (184). The crystal structure of the Nup98–Rae1 heterodimer has revealed that the Nup98 GLEBS motif forms an extended hairpin fold that forms extensive interactions with large loop insertions at the top of the seven-bladed Rae1 β-propeller (171) (Figure 13c). Together, the proteins form a composite, positively charged surface that mediates binding to single-stranded RNA (171, 176). Disruption of the interaction between Rae1 and Nup98 yields mRNA export defects, but the precise function of Rae1 in mRNA export remains unclear (171, 176, 183, 185, 186).

The final major interaction hub includes Nup42, Nup214, and DDX19 and is anchored by Gle1, which possesses an unstructured N-terminal region, a large central coiled-coil region, and a C-terminal α-helical domain that forms a MIF4G (middle of eIF4G) fold (187–190). This fold is found in several other factors involved in RNA biology (e.g., eIF4G, CNOT1, and UPF2) and mediates binding and regulation of their respective RNA helicase partners (191). In humans, all three domains of Gle1 are required for proper Gle1 localization (192–194). Cross-linking data from *S. cerevisiae* suggest that its coiled-coil region may bind the Nup214–Nup88–Nup62 coiled-coil hub, but the paucity of other cross-links between Gle1 and the remainder of the NPC has led to the proposal that it is also flexibly tethered to the

remainder of the NPC (40). A direct interaction between an N-terminal region of human Gle1 and Nup155 has also been identified (192). These interactions are consistent with a localization of the Gle1 interaction hub above the central transport channel, where it would be poised to regulate DDX19 activity on nascent exported mRNAs. The Gle1 C-terminal domain serves as the interaction platform for both Nup42 and DDX19 (174, 177, 189, 190, 195–197). DDX19 can in turn simultaneously bind to the Nup214 β-propeller domain, which is connected by an extended unstructured linker to the Nup214–Nup88–Nup62 CCD interaction hub (172, 189, 198). Genetic analyses and biochemical mapping identified a C-terminal fragment in Nup42 that binds to the Gle1 C-terminal domain (177, 187, 189, 190, 193, 197). Crystal structures of the Gle1–Nup42 complex from *C. thermophilum*, *S. cerevisiae*, and *H. sapiens* revealed that, in all three species, the C-terminal fragment of Nup42 adopts the same compact fold, which has a hydrophobic core that buries surface-exposed hydrophobic residues on a highly conserved Gle1 surface located on the opposite side from the DDX19 binding site (177) (Figure 13e). The regulation of DDX19 activity and its role in mRNA export are discussed below.

Despite substantial progress in characterizing the individual interaction hubs, how the individual hubs assemble together and integrate into the NPC remains less clear. Much greater progress has been made in determining the overall architecture of the *S. cerevisiae* holo complex than the human complex through application of the same integrative structural approach that was later used to determine the composite structure of the yeast NPC (51). In *S. cerevisiae*, the coiled-coil hub and *sc*Nup82 β-propeller domain hub form an ordered complex, whereas the *sc*Gle2 and *sc*Gle1 hubs are more flexibly attached (51). The ordered portion of the holo complex forms a "P"-shaped architecture built of an asymmetric arrangement of two *sc*Nup159–*sc*Nup82–*sc*Nsp1 complexes (51, 179). In this arrangement, two Nup82 β-propeller interaction platforms form a central core around which the two CCDs assemble in two distinct, elongated conformations (51).

Whether this assembly mechanism is conserved in humans remains unclear, owing to a key difference between the structure of human Nup214 and the *S. cerevisiae* homolog, wherein *sc*Nup159 contains a unique ~100-residue dynein interaction domain (DID) consisting of five tandem motifs that can each bind a molecule of the dynein light-chain protein *sc*Dyn2. *sc*Dyn2 forms a constitutive homodimer, and the *sc*Nup159 DID motif forms a β-strand that extends *sc*Dyn2's β-sheet core (175) (Figure 13d). In *S. cerevisiae*, the *sc*Dyn2–*sc*Nup159 DID interaction occurs constitutively, with up to 25% of the cellular pool of Dyn2 associated with NPCs, and functionally homodimerizes the *sc*Nup159–*sc*Nup82–*sc*Nsp1 assembly (51, 175, 179, 199). The overall shape and oligomerization state of the intact human heterotrimeric complex remain unclear, as the Dyn2–DID interaction is not widely conserved.

Another example of divergence of the interaction network within the cytoplasmic filament complex is found in *C. thermophilum*, where an interaction has been identified between the *ct*Nup159–*ct*Nup82–*ct*Nsp1 complex and a sequence motif in the *ct*Nup145C N-terminal extension that may be analogous to the interaction between the Nup93 assembly sensor and the CNT, but this interaction does not appear to be conserved to *S. cerevisiae* (98, 101, 178). Interactions between the Nup214–Nup88–Nup62 complex and the CNCs have been

observed in both fungi and humans, consistent with the integration of the cytoplasmic filament nucleoporins into the cytoplasmic outer ring (38, 51, 98, 200, 201). In *S. cerevisiae*, the complex is anchored to the NPC via the Nup85 arm of the CNC, an orientation that is supported by the observation that disruption of the Nup85 arm yields the most dramatic defects in mRNA export and Nup82 localization (40, 51). This architecture would position both the FG repeats and more flexibly tethered nucleoporins involved in mRNA export to project into the central transport channel.

Regulation of mRNA Export at the Cytoplasmic Face of the Nuclear Pore Complex

One critical role for the cytoplasmic filament nucleoporins is spatially restricted activation of DDX19 (Dbp5 in fungi) in the final step of mRNA export (195, 196). The bulk of mRNAs are transported through the diffusion barrier by the conserved, heterodimeric transport factor Nxf1–Nxt1 (previously termed p15–TAP in humans, and Mex67–Mtr2 in *S. cerevisiae*) in a mechanism that is Ran-independent (202). Instead, the ATPase activity of DDX19 facilitates the removal of Nxf1–Nxt1 from mRNAs, which leads to their release into the cytoplasm (203) (Figure 14). The NPC ensures that DDX19 acts only on mRNAs that have reached the cytoplasm by recruiting and activating DDX19 via nucleoporins (Nup214 and Gle1) that exclusively reside on the cytoplasmic face of the NPC. Extensive studies on the interplay between these nucleoporins and DDX19 in yeast and humans have provided a clearer picture of the mechanistic details of the DDX19 activation cycle.

DDX19 is a member of a family of proteins known as the DEAD-box RNA helicases, which couple ATP hydrolysis to binding or remodeling RNA (204) (Figure 13f). DDX19 is a slow ATPase and possesses weak RNA unwinding activity (196). Gle1 and RNA binding to DDX19 synergistically stimulates DDX19's ATPase activity (174, 177, 195, 196). In *S. cerevisiae*, this activity requires the small-molecule inositol hexaphosphate (IP_6), which bridges the interaction between *sc*Gle1 and the *S. cerevisiae* homolog of DDX19, *sc*Dbp5 (195, 196) (Figure 13g). There are conflicting reports on whether IP_6 plays a similar role in humans (177, 197). Nup214 is required for steady-state localization of DDX19 to the NPC and binds DDX19 via its N-terminal β-propeller domain, which is flexibly tethered to the NPC through an unstructured linker (172, 173, 189, 198) (Figure 13g,h). Although this interaction is required for localization to the NPC, DDX19 binding to RNA and the Nup214 β-propeller domain are mutually exclusive, and DDX19 associates dynamically with NPCs (166, 169, 170, 173) (Figure 13f,h).

Similar to other DEAD-box helicases, DDX19 possesses two RecA-like domains, referred to as the N-terminal domain (NTD) and C-terminal domain (CTD), and binds ATP and single-stranded RNA at distinct sites at the interface between the NTD and CTD (173, 205). When bound to RNA, DDX19 forms a closed conformation, wherein its catalytic residues are positioned to catalyze ATP hydrolysis, explaining RNA's stimulatory effect on DDX19 activity (173, 205). Nup214 binds to the DDX19 NTD, whereas the major Gle1-binding surface is on the DDX19 CTD (173, 174, 177). Because a covalent phosphate moiety is attached to each position of its inositol ring, IP_6 is a highly negatively charged molecule. As revealed by crystal structures of the *S. cerevisiae* complex, IP_6 simultaneously binds to positively charged residues in both *sc*Gle1 and the *sc*Dbp5 CTD, effectively acting as a

small-molecule tether between the two proteins (174) (Figure 13g). In contrast, the Nup214-binding interface on DDX19 partially overlaps with its RNA-binding surface, explaining the mutually exclusive nature of their interaction (169, 173) (Figure 13f,h). Because Nup214 and RNA binding are mutually exclusive, Nup214 inhibits RNA-dependent DDX19 activation. However, in in vitro assays, Gle1 alleviates Nup214 inhibition (174, 177).

One difference between the human and *S. cerevisiae* systems appears to be the presence of an autoinhibitory α-helix within the N-terminal region of human DDX19, which can bind between the NTD and CTD to trap DDX19 in an autoinhibited state (205) (Figure 13f). This α-helix does not appear to be present in *sc*Dbp5, but the N-terminal region of *sc*Dbp5 also possesses autoinhibitory activity (174). This difference may explain why, in the crystal structures of the *sc*Gle1–*sc*Dbp5 complex, the two DEAD-box domains of *sc*Dbp5 were partially separated through additional contacts between the *sc*Dbp5 NTD and *sc*Gle1, whereas in the crystal structure of the human complex, DDX19 remains in a partially autoinhibited state (174, 177) (Figure 13e,g). Gle1 binding induces conformational rearrangements in the DDX19 CTD that destabilize interactions with the autoinhibitory α-helix, in part explaining its ability to stimulate DDX19's ATPase activity (177). However, mutation of the Gle1 residues that form contacts in the partially open state suppress DDX19 and Dbp5 activity, indicating that the separation of the NTD and CTD is also a critical step in DDX19 activation (174, 177) (Figure 14).

A recent study reported that human DDX19 activation did not require IP_6 (177). This report was supported by structural analysis of human Gle1, which revealed a loss of electrostatic potential at the homologous pocket to the fungal IP_6-binding pocket, an absence of detectable IP_6 binding by human Gle1, and biochemical characterization of the Gle1–DDX19 interaction. In contrast, a separate study found a stimulatory role for IP_6 in vitro and observed mRNA export defects in human cells when putative IP_6-binding residues in Gle1 were disrupted (197). Future studies are necessary to conclusively define the role of IP_6 in humans in DDX19 activation.

The precise order of molecular events in DDX19 activation remains debated, although proposed models agree on the overall principles of activation (174, 177, 206). One working model is that Gle1 binding to DDX19 triggers conformational changes that favor RNA binding, in part by relieving autoinhibition (174, 177) (Figure 14). RNA binding promotes ATP hydrolysis by favoring a closed, catalytically competent conformation of DDX19. In addition to its clear role in DDX19 localization to the NPC, Nup214 has several proposed functions, including promoting an open conformation of DDX19, as an ADP exchange factor, or accelerating DDX19 release from Gle1 (174, 207, 208). Detailed kinetic analyses are necessary to completely describe the molecular details of DDX19 activation (207, 209). Furthermore, major questions remain unanswered, including the spatial organization of these factors in relationship to each other and the rest of the NPC during the dynamic DDX19 activation cycle. Perhaps most importantly, how ATPase activity is coupled to mRNA remodeling and the displacement of specific proteins from mRNAs remains poorly understood.

Nup358 Is a Unique Multifunctional Component of Animal Nuclear Pore Complexes

Metazoans possess an additional cytoplasmic filament nucleoporin, Nup358 (also known as RanBP2), which comprises several modular domains connected by flexible linkers or FG repeats (210, 211) (Figure 4). The domain structure of Nup358 varies from species to species, but in humans, Nup358 contains an N-terminal α-helical domain, four Ran-binding domains (RanBDs) distributed throughout the protein, a tandem array of eight Ran-binding zinc-finger domains, a small region that serves as a binding site for SUMOylated RanGAP and the SUMO E3 ligase Ubc9, and a catalytically active C-terminal cyclophilin domain (EC number 5.2.1.8) (Figure 4). Nearly all of these domains have now been structurally characterized, with the important exception of most of the N-terminal α-helical domain (212–215). As shown with immunogold labeling, the C-terminal end of Nup358 can project upward of ~50 nm into the cytoplasm, suggesting that Nup358 is anchored to the NPC via its N-terminal end (167). This arrangement is supported by fluorescence microscopy experiments that mapped the NPC binding site to the N-terminal α-helical region (216). Based on a cryo-ET reconstruction of human NPCs from Nup358-depleted cells, Nup358 molecules were proposed to dock onto the cytoplasmic outer CNC rings (38). However, the precise mechanisms of Nup358 recruitment to the NPC remain poorly understood, as it also depends on the presence of Nup88 and Nup214 (217). Besides a structural role in the organization of the outer CNC ring on the cytoplasmic side of the NPC (see Conservation of Nuclear Pore Complex Architecture section above) and providing binding sites for Ran in its GDP- and GTP-bound states, Nup358 also has important roles in protein import and export as well as regulating mRNA export (218–222).

Nuclear Basket Nucleoporins

Basket-like structures were first observed by EM decorating the nuclear face of NPCs (165). The nuclear basket nucleoporins directly interact with the nucleocytoplasmic transport machinery, provide anchoring sites for mRNA export and quality control factors, and link the NPC to the transcriptional regulatory machinery (223). In humans, the nuclear basket consists of the nucleoporins Nup50, Nup153, and Tpr. *S. cerevisiae* possesses homologs of Tpr (*sc*Mlp1/*sc*Mlp2) and Nup50 (*sc*Nup2) and additionally possesses the nucleoporins *sc*Nup1 and *sc*Nup60, which both appear to be functionally similar to Nup153, if not directly homologous (Figure 3). Nup153 contains a C-terminal FG-repeat region as well as a tandem array of four Ran-binding zinc-finger domains that are homologous to those found in Nup358 (see below) (224). Tpr consists of a massive coiled-coil region spanning more than 1,500 residues, which can homo-oligomerize, followed by a highly acidic C-terminal region that is presumed to be mostly disordered, with the NPC-targeting region located within the N-terminal coiled-coil region (225). Lastly, Nup50 contains an N-terminal region that mediates interactions with both Nup153 and karyopherin-α, a middle FG-repeat region, and a C-terminal Ran-binding domain (226).

Nup153 is required for the localization of Tpr and Nup50 in the human NPC, suggesting that Nup153 anchors the other nuclear basket components to the NPC (227, 228). Interaction mapping studies and cross-linking studies have consistently found that the nuclear basket components interact with components of the CNC (40, 201, 229–231). This organization is consistent with immunogold labeling experiments that found Nup153 localized proximal to

the outer ring, whereas the C-terminal end of Tpr extends into the nucleus and is the primary constituent of the fibrillar extensions originally observed by EM (232). Thus, the nuclear basket displays a similar organizing principle to the cytoplasmic filaments, in which a subset of components localizes to the NPC via interactions with the CNC, anchoring the projection of large, flexible domains into the nucleus or cytoplasm. Further highlighting these similar architectural principles, in *S. cerevisiae*, the nuclear basket components appear to be anchored to the *sc*Nup85 arm of the CNC, analogous to the cytoplasmic filament complex (40).

INTERACTIONS BETWEEN NUCLEOPORINS AND TRANSPORT FACTORS

Interactions Between FG Repeats and Transport Factors

In addition to forming the diffusion barrier, one of the most important functions of FG repeats is specifically binding to transport factor–cargo complexes, which facilitates rapid, selective transport through the diffusion barrier. Although the diffusion barrier has not been visualized by high-resolution structure determination methods, the interactions between FG repeats and transport factors have been visualized in X-ray crystal structures.

Crystal structures of individual FG repeats bound to karyopherins have shown that the karyopherin-β family members contain hydrophobic pockets on their convex surfaces in the grooves between HEAT repeats that serve as the binding sites for FG repeats (233–237). FG repeats bind by inserting a phenylalanine residue into a hydrophobic pocket, which usually necessitates a sharp backbone turn enabled by the following glycine residue, explaining the specificity for the FG motif. Although the interactions between individual FG repeats and karyopherin-β family members are weak, multiple FG repeat binding sites are on the surface of each karyopherin-β that can be engaged simultaneously by multiple FG repeats from the same nucleoporin (235–237) (Figure 15a–c). These interactions can therefore exhibit the fast binding kinetics necessary for rapid transport while remaining highly specific through the avidity of multivalent interactions with FG repeats (238, 239). Different types of FG repeats bind to the same pockets on karyopherin-β family members, but nucleoporins display vastly different binding affinities to karyopherins. Multiple mechanisms appear to be at play in tuning the preference of the karyopherins for different FG nucleoporins, including the spacing of FG repeats, additional interactions in the sequences connecting FG repeats, and even specialized sequences that confer additional affinity (233, 235, 237, 240).

The other major family of FG repeat–binding proteins includes the RanGDP nuclear import factor Ntf2 and the heterodimeric mRNA export factor Nxf1–Nxt1, which are characterized by the presence of Ntf2-like domains. Ntf2 facilitates nuclear import of Ran and forms a homodimer that recognizes FG repeats at symmetrical binding sites (241, 242). Nxf1 is a multidomain protein containing two FG repeat–binding domains: (*a*) a ubiquitin-associated (UBA) domain and (*b*) an Ntf2-like domain that also facilitates heterodimerization with Nxt1, which itself consists of a sole Ntf2-like domain. The UBA domain recognizes a single FG repeat via a hydrophobic surface (243) (Figure 15d). The Ntf2 homodimer possesses symmetric binding sites for FG repeat motifs (241) (Figure 15e). In contrast, the heterodimeric assembly of Ntf2-like domains in the Nxf1–Nxt1 complex only contains one FG binding site on the Nxf1 surface (244) (Figure 15f). Despite their drastically different

folds, Ntf2-like and karyopherin-β family members recognize similar conformations of the FG motif and display similar rapid binding properties (238).

Nuclear Localization Signal–Like Interactions

Some interactions between karyopherins and nucleoporins mimic the interactions between karyopherins and their cargoes. NLS-like sequences have been identified in many nucleoporins, some of which may facilitate their nuclear import. One example is *sc*Nup53, which possesses an NLS near its C terminus that is recognized by *sc*Kap121 via its NLS binding site (245) (Figure 15g). In contrast, *ct*Nup53 contains a karyopherin-α binding motif that overlaps with its *ct*Nup192 binding site, which is near its N terminus (99). Similarly, POM121 is recognized by karyopherin-α via both the major and minor NLS binding sites in a manner similar to canonical NLS recognition (246) (Figure 15h). Some of these interactions may not be critical to NPC function itself but may be related to targeting the nucleoporins to the nucleus or to mitotic structures during cell division (247).

In contrast, a highly conserved interaction between karyopherin-α and the nuclear basket offers another paradigm for NLS-like interactions between nucleoporins and nuclear transport factors. Nup50 and its homologs contain an NLS-like sequence that binds to karyopherin-α with a higher affinity than canonical NLS sequences (226). Crystal structures of mammalian and yeast karyopherin-α bound to their cognate Nup50 homologs reveal that their NLS-like sequences all bind with the same mechanism via an extensive interface that overlaps with the major and minor NLS binding sites on karyopherin-α and also bind to a surface not used for NLS recognition (226, 248) (Figure 15i). As Nup50 resides at the nucleus-facing nuclear basket, this interaction is believed to displace import cargoes and prepare karyopherin-α for export back into the cytoplasm.

Interactions with Ran

In the human nuclear basket, a Ran-binding domain (RanBD) in Nup50 and a tandem array of four zinc-finger domains in Nup153 serve as binding sites for the small GTPase Ran. In the human cytoplasmic filaments, Nup358 contains four additional RanBDs as well as a tandem array of eight zinc-finger domains homologous to those in Nup153. Together, these nucleoporins potentially provide up to ~500 Ran binding sites per NPC. RanBDs have a strong preference for binding to RanGTP, whereas the zinc-finger domains have a weaker preference for RanGDP (249). Crystal structures have revealed the molecular basis for these preferences wherein the two domains recognize features of Ran, particularly the switch I region, which adopt dramatically different conformations in the presence of GDP or GTP (214, 224, 250) (Figure 15j,k). Altogether, these binding sites are thought to increase the local concentration of Ran at NPCs to increase the efficiency of nucleocytoplasmic transport.

In animals, Nup358 also provides an anchoring site for RanGAP, the GTPase-activating protein for Ran. This interaction is mediated by the posttranslational SUMOylation of RanGAP with SUMO-1, leading to the formation of a complex between RanGAP*SUMO-1 (where the * denotes a covalent linkage), Nup358, and the SUMO E3 ligase Ubc9 (215, 251). As revealed by a crystal structure of this heterotrimeric complex, the specificity for

RanGAP*SUMO-1 is mediated in part by direct recognition of the isopeptide bond between RanGAP and SUMO-1 (215) (Figure 15l). Although a soluble fraction of RanGAP also exists in the cytoplasm, the Nup358 binding site is stoichiometrically occupied by RanGAP*SUMO-1 (252, 253). This subcomplex, which is flanked by FG repeats and RanBDs in Nup358, can act as a disassembly factor for nuclear export complexes (222).

Links to Transcriptional Regulation and mRNA Processing

At the nuclear basket, the NPC also serves as a hub for organizing nuclear architecture and coordinating gene transcription, mRNA processing, and mRNA export. These functions are fulfilled through interactions with nuclear transcription and processing factors as well as potential direct interactions between nucleoporins and genomic loci (223, 254, 255). The interaction between the nuclear basket and the evolutionarily conserved transcription elongation and RNA export (TREX-2) complex links the NPC to transcriptional regulation, mRNA processing, and mRNA export (256, 257). In *S. cerevisiae*, the heterotrimeric *sc*Sac3–*sc*Sus1–*sc*Cdc31 module of the TREX-2 complex mediates localization of the TREX-2 complex at the NPC by binding to a flexible N-terminal motif in *sc*Nup1 that vaguely resembles an FxFG motif (258). However, a crystal structure has revealed a distinct interaction mechanism (258) (Figure 15m). Furthermore, this *sc*Nup1 motif does not bind to canonical FG repeat-binding proteins, and the TREX-2 complex does not bind to canonical FG repeats (258). Thus, the TREX-2 anchoring mechanism at the NPC is similar to but distinct from other FG-repeat interactions. TREX-2 also localizes to the NPC in humans, but the exact molecular determinants appear to be different (259, 260). As a whole, these results show how the TREX-2 complex links fundamental nuclear processes, including the regulation of gene expression and mRNA export, to the NPC. Furthermore, the similarity of the Nup1 motif to canonical FG motifs raises the possibility that other FG-like sequences in nucleoporins may have been adapted to bind other cellular machinery. Future work is expected to illuminate how the nuclear basket coordinates these complex processes.

NUCLEOPORIN STRUCTURE AND DISEASE

Perturbations in NPC function are associated with a wide array of diseases including cancer, neurodegenerative diseases, developmental diseases, and viral infection. Some of the earliest discovered associations between the NPC and disease were chromosomal rearrangements resulting in fusions of a transcription factor or kinase to a nucleoporin, such as Tpr, Nup98, Nup214, and Nup358 (223, 261). More recently, links have been reported between neurodegenerative diseases and nucleocytoplasmic transport defects, including mislocalization of transport factors and nucleoporins in amyotrophic lateral sclerosis (ALS) and Huntington's disease (HD) (262–265). These connections between age-related neurodegenerative diseases and the NPC are particularly striking because nucleoporins are some of the longest-living proteins in nondividing cells such as neurons (266).

Role of Nucleoporin Mutations in Disease

With the increasing number of sequenced human genomes, a growing number of mutations in nucleoporins have now been linked to diseases, including acute myeloid leukemia and various other cancers, triple A syndrome, lethal congenital contracture syndrome (LCCS),

ALS, atrial fibrillation, gonadal dysgenesis, steroid-resistant nephrotic syndrome (SRNS), acute necrotizing encephalopathy (ANE), and infantile bilateral striatal necrosis (IBSN) (223, 261, 267–273). As structures of the nucleoporins involved in many of these diseases are now available, there are opportunities to map the mutations onto the structures and to generate testable hypotheses for how they could contribute to disease. However, many structures are only available for fungal homologs, which often possess poor sequence homology despite strong structural conservation, and predictions for the functional consequences of mutations based on homology models may be inaccurate. Thus, structural and functional characterization of the human nucleoporins are necessary to accurately define the mechanisms of dysfunction.

The effect of mutations on the cytoplasmic filament nucleoporin Gle1 offers a paradigm for how some mutations may affect nucleoporin function, as one of the few disease-linked nucleoporins for which mutations can be mapped directly onto a crystal structure. Missense mutations in Gle1 linked to LCCS were found to affect residues involved in intramolecular hydrogen bonds or within the hydrophobic core (177). Several of these mutations reduced Gle1 stability in vitro and led to mislocalization of the mutant protein in cultured human cells (177, 274). Mutations in other nucleoporins including Nup62, Nup155, Nup205, Nup107, and Nup93 are also predicted to affect nucleoporin–nucleoporin interactions or intramolecular interactions that could similarly be important for protein stability (177, 269, 271, 273, 275, 276).

A number of gene fusions involving nucleoporins, often resulting from chromosomal rearrangements, have been identified in cancers, particularly in leukemias. Fusions have been shown to occur with Nup98, Nup214, Nup358, and Tpr, but it has not been established whether all of these fusion products are drivers of oncogenesis or progression (reviewed in 223, 261). For some, specific mechanisms have been uncovered that could promote oncogenesis. For example, in the Tpr-MET kinase fusion, residues 2–142 of Tpr replace the regulatory domains of the MET kinase to yield a constitutively active kinase (277). This isolated fragment of Tpr homodimerizes and further oligomerizes, and although these oligomerization states may not occur in the context of the full-length protein and within the NPC, they are certainly important for oncogenic MET activation (278). In this example, fusion with a nucleoporin seems to be coincidental. However, other cases such as the wide array of cancer-associated Nup98 fusion proteins, for which the direct mechanisms are not as clear, raise the question whether concomitant loss of a functional nucleoporin also promotes oncogenesis (279). As further data becomes available, it is likely that more diseases will be linked to nucleoporins. Future structural and mechanistic studies of nucleoporins in both functional and dysfunctional contexts may lead to new avenues for therapeutics.

Interactions Between Nucleoporins and Viral Factors

Many viruses have developed mechanisms for subverting the NPC to gain access to the nucleus, export viral RNAs from the nucleus, or inhibit host nucleocytoplasmic transport. Viral hijacking of nuclear transport factors is a common strategy (280–282). Here, we

briefly highlight insights gained from the structural characterization of interactions between nucleoporins and viruses.

Vesicular stomatitis virus (VSV) is a zoonotic virus that encodes a protein, the VSV matrix protein, which directly binds to the Rae1–Nup98 heterodimer. This interaction occurs competitively with RNA, and VSV matrix protein binding to Rae1–Nup98 leads to severe mRNA export defects (283, 284). A crystal structure of the VSV matrix protein–Rae1–Nup98 complex not only revealed how an acidic motif in the VSV matrix protein was bound on the side of the Rae1–Nup98 heterodimer but also simultaneously facilitated the identification of the physiological nucleic acid binding surface on Rae1–Nup98 (171, 176) (Figure 16). Thus, characterization of viral–nucleoporin interactions has yielded insights not only into viral virulence but also into normal NPC function.

Many interactions between HIV proteins and nucleoporins have been identified, and they occur throughout the HIV life cycle. During nuclear import of the HIV genome, intact HIV capsids have been observed docking at NPCs in an interaction mediated by Nup358 (285, 286). HIV capsid protein (CA) binds to the Nup358 cyclophilin domain (212, 287), and a crystal structure of the Nup358 cyclophilin domain bound to the HIV CA protein revealed that Nup358 binds a proline-rich loop in HIV CA with its cyclophilin domain active site (288) (Figure 16). Although the Nup358 cyclophilin domain catalyzes peptidyl-prolyl isomerization of a model cyclophilin A substrate very inefficiently, it catalyzes the isomerization of HIV CA more rapidly, indicating that the domain is catalytically active and may have a substrate preference distinct from cyclophilin A (212, 288). Thus, HIV may use isomerization by the NPC to trigger capsid disassembly or rearrangement immediately before nuclear entry (288). Within the nucleus, the HIV CA can bind to the FG-repeat region of Nup153 (289). A crystal structure of this interaction revealed that the FG motif in Nup153 binds to an oligomeric interface between two monomers in the HIV CA hexamer (290) (Figure 16). Interactions between Nup153 and other viral capsid proteins have also been observed, and they may serve as a subsequent signal to release the genome after nuclear entry (289, 291). Future studies on the interaction between viral factors and nucleoporins hold the potential for new insights into not only the mechanisms of viral infection but also the physiological roles of nucleoporins in healthy cells.

ACKNOWLEDGMENTS

LITERATURE CITED

1. Hoelz A, Debler EW, Blobel G. 2011 The structure of the nuclear pore complex. Annu. Rev. Biochem. 80:613–43 [PubMed: 21495847]

2. Watson ML. 1959 Further observations on the nuclear envelope of the animal cell. J. Biophys. Biochem. Cytol. 6:147–56 [PubMed: 13843146]

3. Rout MP, Aitchison JD, Suprapto A, Hjertaas K, Zhao Y, Chait BT. 2000 The yeast nuclear pore complex: composition, architecture, and transport mechanism. J. Cell Biol. 148:635–51 [PubMed: 10684247]

4. Ribbeck K, Görlich D. 2001 Kinetic analysis of translocation through nuclear pore complexes. EMBO J. 20:1320–30 [PubMed: 11250898]

5. Denning DP, Patel SS, Uversky V, Fink AL, Rexach M. 2003 Disorder in the nuclear pore complex: The FG repeat regions of nucleoporins are natively unfolded. PNAS 100:2450–55 [PubMed: 12604785]

6. Timney BL, Raveh B, Mironska R, Trivedi JM, Kim SJ, et al. 2016 Simple rules for passive diffusion through the nuclear pore complex. J. Cell Biol. 215:57–76 [PubMed: 27697925]

7. Bonner WM. 1975 Protein migration into nuclei. I. Frog oocyte nuclei in vivo accumulate microinjected histones, allow entry to small proteins, and exclude large proteins. J. Cell Biol. 64:421–30 [PubMed: 46868]

8. Paine PL, Moore LC, Horowitz SB. 1975 Nuclear envelope permeability. Nature 254:109–14 [PubMed: 1117994]

9. Yang W, Gelles J, Musser SM. 2004 Imaging of single-molecule translocation through nuclear pore complexes. PNAS 101:12887–92 [PubMed: 15306682]

10. Naim B, Zbaida D, Dagan S, Kapon R, Reich Z. 2009 Cargo surface hydrophobicity is sufficient to overcome the nuclear pore complex selectivity barrier. EMBO J. 28:2697–705 [PubMed: 19680225]

11. Frey S, Rees R, Schünemann J, Ng SC, Fünfgeld K, et al. 2018 Surface properties determining passage rates of proteins through nuclear pores. Cell 174:202–17.e9 [PubMed: 29958108]

12. Christie M, Chang CW, Róna G, Smith KM, Stewart AG, et al. 2016 Structural biology and regulation of protein import into the nucleus. J. Mol. Biol. 428:2060–90 [PubMed: 26523678]

13. Matsuura Y 2016 Mechanistic insights from structural analyses of Ran-GTPase-driven nuclear export of proteins and RNAs. J. Mol. Biol. 428:2025–39 [PubMed: 26519791]

14. Soniat M, Chook YM. 2015 Nuclear localization signals for four distinct karyopherin-β nuclear import systems. Biochem. J. 468:353–62 [PubMed: 26173234]

15. Cook A, Bono F, Jinek M, Conti E. 2007 Structural biology of nucleocytoplasmic transport. Annu. Rev. Biochem. 76:647–71 [PubMed: 17506639]

16. Pumroy RA, Cingolani G. 2015 Diversification of importin-α isoforms in cellular trafficking and disease states. Biochem. J. 466:13–28 [PubMed: 25656054]

17. Smith A, Brownawell A, Macara IG. 1998 Nuclear import of Ran is mediated by the transport factor NTF2. Curr. Biol. 8:1403–6 [PubMed: 9889103]

18. Ribbeck K, Lipowsky G, Kent HM, Stewart M, Görlich D. 1998 NTF2 mediates nuclear import of Ran. EMBO J. 17:6587–98 [PubMed: 9822603]

19. Kalab P, Weis K, Heald R. 2002 Visualization of a Ran-GTP gradient in interphase and mitotic Xenopus egg extracts. Science 295:2452–56 [PubMed: 11923538]

20. von Appen A, Beck M. 2016 Structure determination of the nuclear pore complex with three-dimensional cryo electron microscopy. J. Mol. Biol. 428:2001–10 [PubMed: 26791760]

21. Schwartz TU. 2016 The structure inventory of the nuclear pore complex. J. Mol. Biol. 428:1986–2000 [PubMed: 27016207]

22. Callan HG, Tomlin SG, Waddington CH. 1950 Experimental studies on amphibian oocyte nuclei. I. Investigation of the structure of the nuclear membrane by means of the electron microscope. Proc. R. Soc. B Biol. Sci. 137:367–78 [PubMed: 14786306]

23. Watson ML. 1955 The nuclear envelope: its structure and relation to cytoplasmic membranes. J. Biophys. Biochem. Cytol. 1:257–70 [PubMed: 13242591]

24. Gall JG. 1967 Octagonal nuclear pores. J. Cell Biol. 32:391–99 [PubMed: 10976230]

25. Hinshaw JE, Carragher BO, Milligan RA. 1992 Architecture and design of the nuclear pore complex. Cell 69:1133–41 [PubMed: 1617726]

26. Akey CW, Radermacher M. 1993 Architecture of the Xenopus nuclear pore complex revealed by three-dimensional cryo-electron microscopy. J. Cell Biol. 122:1–19 [PubMed: 8314837]

27. Akey CW. 1995 Structural plasticity of the nuclear pore complex. J. Mol. Biol. 248:273–93 [PubMed: 7739040]

28. Fahrenkrog B, Hurt EC, Aebi U, Panté N. 1998 Molecular architecture of the yeast nuclear pore complex: localization of Nsp1p subcomplexes. J. Cell Biol. 143:577–88 [PubMed: 9813081]

29. Kiseleva E, Goldberg MW, Allen TD, Akey CW. 1998 Active nuclear pore complexes in Chironomus: visualization of transporter configurations related to mRNP export. J. Cell Sci. 111:223–36 [PubMed: 9405308]

30. Yang Q, Rout MP, Akey CW. 1998 Three-dimensional architecture of the isolated yeast nuclear pore complex: functional and evolutionary implications. Mol. Cell 1:223–34 [PubMed: 9659919]

31. Beck M, Forster F, Ecke M, Plitzko JM, Melchior F, et al. 2004 Nuclear pore complex structure and dynamics revealed by cryoelectron tomography. Science 306:1387–90 [PubMed: 15514115]

32. Maimon T, Elad N, Dahan I, Medalia O. 2012 The human nuclear pore complex as revealed by cryo-electron tomography. Structure 20:998–1006 [PubMed: 22632834]

33. Mosalaganti S, Kosinski J, Albert S, Schaffer M, Strenkert D, et al. 2018 In situ architecture of the algal nuclear pore complex. Nat. Commun. 9:2361 [PubMed: 29915221]

34. Stoffler D, Feja B, Fahrenkrog B, Walz J, Typke D, Aebi U. 2003 Cryo-electron tomography provides novel insights into nuclear pore architecture: implications for nucleocytoplasmic transport. J. Mol. Biol. 328:119–30 [PubMed: 12684002]

35. Beck M, Lucic V, Forster F, Baumeister W, Medalia O. 2007 Snapshots of nuclear pore complexes in action captured by cryo-electron tomography. Nature 449:611–15 [PubMed: 17851530]

36. Kosinski J, Mosalaganti S, von Appen A, Teimer R, DiGuilio AL, et al. 2016 Molecular architecture of the inner ring scaffold of the human nuclear pore complex. Science 352:363–65 [PubMed: 27081072]

37. von Appen A, Kosinski J, Sparks L, Ori A, DiGuilio AL, et al. 2015 In situ structural analysis of the human nuclear pore complex. Nature 526:140–43 [PubMed: 26416747]

38. Bui KH, von Appen A, DiGuilio AL, Ori A, Sparks L, et al. 2013 Integrated structural analysis of the human nuclear pore complex scaffold. Cell 155:1233–43 [PubMed: 24315095]

39. Eibauer M, Pellanda M, Turgay Y, Dubrovsky A, Wild A, Medalia O. 2015 Structure and gating of the nuclear pore complex. Nat. Commun. 6:7532 [PubMed: 26112706]

40. Kim SJ, Fernandez-Martinez J, Nudelman I, Shi Y, Zhang W, et al. 2018 Integrative structure and functional anatomy of a nuclear pore complex. Nature 555:475–82 [PubMed: 29539637]

41. Lin DH, Stuwe T, Schilbach S, Rundlet EJ, Perriches T, et al. 2016 Architecture of the symmetric core of the nuclear pore. Science 352:aaf1015

42. Cronshaw JM, Krutchinsky AN, Zhang W, Chait BT, Matunis MJ. 2002 Proteomic analysis of the mammalian nuclear pore complex. J. Cell Biol. 158:915–27 [PubMed: 12196509]

43. DeGrasse JA, DuBois KN, Devos D, Siegel TN, Sali A, et al. 2009 Evidence for a shared nuclear pore complex architecture that is conserved from the last common eukaryotic ancestor. Mol. Cell. Proteom. 8:2119–30

44. Tamura K, Fukao Y, Iwamoto M, Haraguchi T, Hara-Nishimura I. 2010 Identification and characterization of nuclear pore complex components in Arabidopsis thaliana. Plant Cell 22:4084–97 [PubMed: 21189294]

45. Neumann N, Lundin D, Poole AM. 2010 Comparative genomic evidence for a complete nuclear pore complex in the last eukaryotic common ancestor. PLOS ONE 5:e13241

46. Doye V, Hurt E. 1997 From nucleoporins to nuclear pore complexes. Curr. Opin. Cell Biol. 9:401–11 [PubMed: 9159086]

47. Vasu SK, Forbes DJ. 2001 Nuclear pores and nuclear assembly. Curr. Opin. Cell Biol. 13:363–75 [PubMed: 11343909]

48. Alber F, Dokudovskaya S, Veenhoff LM, Zhang W, Kipper J, et al. 2007 Determining the architectures of macromolecular assemblies. Nature 450:683–94 [PubMed: 18046405]

49. Alber F, Dokudovskaya S, Veenhoff LM, Zhang W, Kipper J, et al. 2007 The molecular architecture of the nuclear pore complex. Nature 450:695–701 [PubMed: 18046406]

Author Manuscript

Author Manuscript

Author Manuscript

Author Manuscript

50. Ori A, Banterle N, Iskar M, Andrés-Pons A, Escher C, et al. 2013 Cell type-specific nuclear pores: a case in point for context-dependent stoichiometry of molecular machines. Mol. Syst. Biol. 9:648 [PubMed: 23511206]

51. Fernandez-Martinez J, Kim SJ, Shi Y, Upla P, Pellarin R, et al. 2016 Structure and function of the nuclear pore complex cytoplasmic mRNA export platform. Cell 167:1215–28.e25 [PubMed: 27839866]

52. Rajoo S, Vallotton P, Onischenko E, Weis K. 2018 Stoichiometry and compositional plasticity of the yeast nuclear pore complex revealed by quantitative fluorescence microscopy. PNAS 115:E3969–77

53. Davis LI, Blobel G. 1986 Identification and characterization of a nuclear pore complex protein. Cell 45:699–709 [PubMed: 3518946]

54. Rout MP, Wente SR. 1994 Pores for thought: nuclear pore complex proteins. Trends Cell Biol. 4:357–65 [PubMed: 14731624]

55. Devos D, Dokudovskaya S, Williams R, Alber F, Eswar N, et al. 2006 Simple fold composition and modular architecture of the nuclear pore complex. PNAS 103:2172–77 [PubMed: 16461911]

56. Finlay DR, Meier E, Bradley P, Horecka J, Forbes DJ. 1991 A complex of nuclear pore proteins required for pore function. J. Cell Biol. 114:169–83 [PubMed: 2050741]

57. Grandi P, Doye V, Hurt EC. 1993 Purification of NSP1 reveals complex formation with 'GLFG' nucleoporins and a novel nuclear pore protein NIC96. EMBO J. 12:3061–71 [PubMed: 7688296]

58. Siniossoglou S, Wimmer C, Rieger M, Doye V, Tekotte H, et al. 1996 A novel complex of nucleoporins, which includes Sec13p and a Sec13p homolog, is essential for normal nuclear pores. Cell 84:265–75 [PubMed: 8565072]

59. Lutzmann M, Kunze R, Buerer A, Aebi U, Hurt E. 2002 Modular self-assembly of a Y-shaped multiprotein complex from seven nucleoporins. EMBO J. 21:387–97 [PubMed: 11823431]

60. Berke IC, Boehmer T, Blobel G, Schwartz TU. 2004 Structural and functional analysis of Nup133 domains reveals modular building blocks of the nuclear pore complex. J. Cell Biol. 167:591–97 [PubMed: 15557116]

61. Hsia KC, Stavropoulos P, Blobel G, Hoelz A. 2007 Architecture of a coat for the nuclear pore membrane. Cell 131:1313–26 [PubMed: 18160040]

62. Boehmer T, Jeudy S, Berke IC, Schwartz TU. 2008 Structural and functional studies of Nup107/ Nup133 interaction and its implications for the architecture of the nuclear pore complex. Mol. Cell 30:721–31 [PubMed: 18570875]

63. Brohawn SG, Leksa NC, Spear ED, Rajashankar KR, Schwartz TU. 2008 Structural evidence for common ancestry of the nuclear pore complex and vesicle coats. Science 322:1369–73 [PubMed: 18974315]

64. Debler EW, Ma Y, Seo HS, Hsia KC, Noriega TR, et al. 2008 A fence-like coat for the nuclear pore membrane. Mol. Cell 32:815–26 [PubMed: 19111661]

65. Brohawn SG, Schwartz TU. 2009 Molecular architecture of the Nup84–Nup145C–Sec13 edge element in the nuclear pore complex lattice. Nat. Struct. Mol. Biol. 16:1173–77 [PubMed: 19855394]

66. Kampmann M, Blobel G. 2009 Three-dimensional structure and flexibility of a membrane-coating module of the nuclear pore complex. Nat. Struct. Mol. Biol. 16:782–88 [PubMed: 19503077]

67. Leksa NC, Brohawn SG, Schwartz TU. 2009 The structure of the scaffold nucleoporin Nup120 reveals a new and unexpected domain architecture. Structure 17:1082–91 [PubMed: 19576787]

68. Nagy V, Hsia KC, Debler EW, Kampmann M, Davenport AM, et al. 2009 Structure of a trimeric nucleoporin complex reveals alternate oligomerization states. PNAS 106:17693–98 [PubMed: 19805193]

69. Seo HS, Ma Y, Debler EW, Wacker D, Kutik S, et al. 2009 Structural and functional analysis of Nup120 suggests ring formation of the Nup84 complex. PNAS 106:14281–86 [PubMed: 19706512]

70. Whittle JRR, Schwartz TU. 2009 Architectural nucleoporins Nup157/170 and Nup133 are structurally related and descend from a second ancestral element. J. Biol. Chem. 284:28442–52 [PubMed: 19674973]

71. Bilokapic S, Schwartz TU. 2012 Molecular basis for Nup37 and ELY5/ELYS recruitment to the nuclear pore complex. PNAS 109:15241–46 [PubMed: 22955883]

72. Liu X, Mitchell JM, Wozniak RW, Blobel G, Fan J. 2012 Structural evolution of the membrane-coating module of the nuclear pore complex. PNAS 109:16498–503 [PubMed: 23019579]

73. Bilokapic S, Schwartz TU. 2013 Structural and functional studies of the 252 kDa nucleoporin ELYS reveal distinct roles for its three tethered domains. Structure 21:572–80 [PubMed: 23499022]

74. Kim SJ, Fernandez-Martinez J, Sampathkumar P, Martel A, Matsui T, et al. 2014 Integrative structure-function mapping of the nucleoporin Nup133 suggests a conserved mechanism for membrane anchoring of the nuclear pore complex. Mol. Cell. Proteom. 13:2911–26

75. Kelley K, Knockenhauer KE, Kabachinski G, Schwartz TU. 2015 Atomic structure of the Y complex of the nuclear pore. Nat. Struct. Mol. Biol. 22:425–31 [PubMed: 25822992]

76. Stuwe T, Correia AR, Lin DH, Paduch M, Lu VT, et al. 2015 Architecture of the nuclear pore complex coat. Science 347:1148–52 [PubMed: 25745173]

77. Fontoura BMA, Blobel G, Matunis MJ. 1999 A conserved biogenesis pathway for nucleoporins: Proteolytic processing of a 186-kilodalton precursor generates Nup98 and the novel nucleoporin, Nup96. J. Cell Biol. 144:1097–112 [PubMed: 10087256]

78. Belgareh N, Rabut G, Bai SW, van Overbeek M, Beaudouin J, et al. 2001 An evolutionarily conserved NPC subcomplex, which redistributes in part to kinetochores in mammalian cells. J. Cell Biol. 154:1147–60 [PubMed: 11564755]

79. Franz C, Wázak R, Yavuz S, Santarella R, Gentzel M, et al. 2007 MEL-28/ELYS is required for the recruitment of nucleoporins to chromatin and postmitotic nuclear pore complex assembly. EMBO Rep. 8:165–72 [PubMed: 17235358]

80. Rasala BA, Orjalo AV, Shen Z, Briggs S, Forbes DJ. 2006 ELYS is a dual nucleoporin/kinetochore protein required for nuclear pore assembly and proper cell division. PNAS 103:17801–6 [PubMed: 17098863]

81. Loiodice I, Alves A, Rabut G, Van Overbeek M, Ellenberg J, et al. 2004 The entire Nup107–160 complex, including three new members, is targeted as one entity to kinetochores in mitosis. Mol. Biol. Cell 15:3333–44 [PubMed: 15146057]

82. Thierbach K, von Appen A, Thoms M, Beck M, Flemming D, Hurt E. 2013 Protein interfaces of the conserved Nup84 complex from Chaetomium thermophilum shown by crosslinking mass spectrometry and electron microscopy. Structure 21:1672–82 [PubMed: 23954503]

83. Stagg SM, LaPointe P, Balch WE. 2007 Structural design of cage and coat scaffolds that direct membrane traffic. Curr. Opin. Struct. Biol. 17:221–28 [PubMed: 17395454]

84. Whittle JRR, Schwartz TU. 2010 Structure of the Sec13–Sec16 edge element, a template for assembly of the COPII vesicle coat. J. Cell Biol. 190:347–61 [PubMed: 20696705]

85. Bar-Peled L, Chantranupong L, Cherniack AD, Chen WW, Ottina KA, et al. 2013 A tumor suppressor complex with GAP activity for the Rag GTPases that signal amino acid sufficiency to mTORC1. Science 340:1100–6 [PubMed: 23723238]

86. Dokudovskaya S, Waharte F, Schlessinger A, Pieper U, Devos DP, et al. 2011 A conserved coatomer-related complex containing Sec13 and Seh1 dynamically associates with the vacuole in Saccharomyces cerevisiae. Mol. Cell. Proteom. 10:mcp.M110.006478

87. Siniossoglou S, Lutzmann M, Santos-Rosa H, Leonard K, Mueller S, et al. 2000 Structure and assembly of the Nup84p complex. J. Cell Biol. 149:41–54 [PubMed: 10747086]

88. Sampathkumar P, Gheyi T, Miller SA, Bain KT, Dickey M, et al. 2011 Structure of the C-terminal domain of Saccharomyces cerevisiae Nup133, a component of the nuclear pore complex. Proteins 79:1672–77 [PubMed: 21365675]

89. Jeudy S, Schwartz TU. 2007 Crystal structure of nucleoporin Nic96 reveals a novel, intricate helical domain architecture. J. Biol. Chem. 282:34904–12 [PubMed: 17897938]

90. Schrader N, Stelter P, Flemming D, Kunze R, Hurt E, Vetter IR. 2008 Structural basis of the nic96 subcomplex organization in the nuclear pore channel. Mol. Cell 29:46–55 [PubMed: 18206968]

91. Debler EW, Hsia KC, Nagy V, Seo HS, Hoelz A. 2010 Characterization of the membrane-coating Nup84 complex: paradigm for the nuclear pore complex structure. Nucleus 1:150–57 [PubMed: 21326946]

92. Devos D, Dokudovskaya S, Alber F, Williams R, Chait BT, et al. 2004 Components of coated vesicles and nuclear pore complexes share a common molecular architecture. PLOS Biol. 2:e380

93. Seo HS, Blus BJ, Jankovic NZ, Blobel G. 2013 Structure and nucleic acid binding activity of the nucleoporin Nup157. PNAS 110:16450–55 [PubMed: 24062435]

94. Drin G, Casella JF, Gautier R, Boehmer T, Schwartz TU, Antonny B. 2007 A general amphipathic α-helical motif for sensing membrane curvature. Nat. Struct. Mol. Biol. 14:138–46 [PubMed: 17220896]

95. Liu HL, De Souza CPC, Osmani AH, Osmani SA. 2009 The three fungal transmembrane nuclear pore complex proteins of Aspergillus nidulans are dispensable in the presence of an intact An-Nup84–120 complex. Mol. Biol. Cell 20:616–30 [PubMed: 19019988]

96. Rasala BA, Ramos C, Harel A, Forbes DJ. 2008 Capture of AT-rich chromatin by ELYS recruits POM121 and NDC1 to initiate nuclear pore assembly. Mol. Biol. Cell 19:3982–96 [PubMed: 18596237]

97. Xu C, Li Z, He H, Wernimont A, Li Y, et al. 2015 Crystal structure of human nuclear pore complex component NUP43. FEBS Lett. 589:3247–53 [PubMed: 26391640]

98. Stuwe T, Bley CJ, Thierbach K, Petrovic S, Schilbach S, et al. 2015 Architecture of the fungal nuclear pore inner ring complex. Science 350:56–64 [PubMed: 26316600]

99. Stuwe T, Lin DH, Collins LN, Hurt E, Hoelz A. 2014 Evidence for an evolutionary relationship between the large adaptor nucleoporin Nup192 and karyopherins. PNAS 111:2530–35 [PubMed: 24505056]

100. Amlacher S, Sarges P, Flemming D, van Noort V, Kunze R, et al. 2011 Insight into structure and assembly of the nuclear pore complex by utilizing the genome of a eukaryotic thermophile. Cell 146:277–89 [PubMed: 21784248]

101. Fischer J, Teimer R, Amlacher S, Kunze R, Hurt E. 2015 Linker Nups connect the nuclear pore complex inner ring with the outer ring and transport channel. Nat. Struct. Mol. Biol. 22:774–81 [PubMed: 26344569]

102. Hodel AE, Hodel MR, Griffis ER, Hennig KA, Ratner GA, et al. 2002 The three-dimensional structure of the autoproteolytic, nuclear pore-targeting domain of the human nucleoporin Nup98. Mol. Cell 10:347–58 [PubMed: 12191480]

103. Handa N, Kukimoto-Niino M, Akasaka R, Kishishita S, Murayama K, et al. 2006 The crystal structure of mouse Nup35 reveals atypical RNP motifs and novel homodimerization of the RRM domain. J. Mol. Biol. 363:114–24 [PubMed: 16962612]

104. Sun Y, Guo HC. 2008 Structural constraints on autoprocessing of the human nucleoporin Nup98. Protein Sci. 17:494–505 [PubMed: 18287282]

105. Sampathkumar P, Kim SJ, Manglicmot D, Bain KT, Gilmore J, et al. 2012 Atomic structure of the nuclear pore complex targeting domain of a Nup116 homologue from the yeast, Candida glabrata. Proteins 80:2110–16 [PubMed: 22544723]

106. Andersen KR, Onischenko E, Tang JH, Kumar P, Chen JZ, et al. 2013 Scaffold nucleoporins Nup188 and Nup192 share structural and functional properties with nuclear transport receptors. eLife 2:e00745

107. Sampathkumar P, Kim SJ, Upla P, Rice WJ, Phillips J, et al. 2013 Structure, dynamics, evolution, and function of a major scaffold component in the nuclear pore complex. Structure 21:560–71 [PubMed: 23499021]

108. Mansfeld J, Guttinger S, Hawryluk-Gara LA, Panté N, Mall M, et al. 2006 The conserved transmembrane nucleoporin NDC1 is required for nuclear pore complex assembly in vertebrate cells. Mol. Cell 22:93–103 [PubMed: 16600873]

109. Hawryluk-Gara LA, Platani M, Santarella R, Wozniak RW, Mattaj IW. 2008 Nup53 is required for nuclear envelope and nuclear pore complex assembly. Mol. Biol. Cell 19:1753–62 [PubMed: 18256286]

110. Onischenko E, Stanton LH, Madrid AS, Kieselbach T, Weis K. 2009 Role of the Ndc1 interaction network in yeast nuclear pore complex assembly and maintenance. J. Cell Biol. 185:475–91 [PubMed: 19414609]

111. Eisenhardt N, Redolfi J, Antonin W. 2014 Interaction of Nup53 with Ndc1 and Nup155 is required for nuclear pore complex assembly. J. Cell Sci. 127:908–21 [PubMed: 24363447]

112. Vollmer B, Schooley A, Sachdev R, Eisenhardt N, Schneider AM, et al. 2012 Dimerization and direct membrane interaction of Nup53 contribute to nuclear pore complex assembly. EMBO J. 31:4072–84 [PubMed: 22960634]

113. Chug H, Trakhanov S, Hülsmann BB, Pleiner T, Görlich D. 2015 Crystal structure of the metazoan Nup62·Nup58·Nup54 nucleoporin complex. Science 350:106–10 [PubMed: 26292704]

114. Andrade MA, Petosa C, O'Donoghue SI, Muller CW, Bork P. 2001 Comparison of ARM and HEAT protein repeats. J. Mol. Biol. 309:1–18 [PubMed: 11491282]

115. Flemming D, Devos DP, Schwarz J, Amlacher S, Lutzmann M, Hurt E. 2012 Analysis of the yeast nucleoporin Nup188 reveals a conserved S-like structure with similarity to karyopherins. J. Struct. Biol. 177:99–105 [PubMed: 22138091]

116. Theerthagiri G, Eisenhardt N, Schwarz H, Antonin W. 2010 The nucleoporin Nup188 controls passage of membrane proteins across the nuclear pore complex. J. Cell Biol. 189:1129–42 [PubMed: 20566687]

117. Rosenblum JS, Blobel G. 1999 Autoproteolysis in nucleoporin biogenesis. PNAS 96:11370–75 [PubMed: 10500183]

118. Teixeira MT, Fabre E, Dujon B. 1999 Self-catalyzed cleavage of the yeast nucleoporin Nup145p precursor. J. Biol. Chem. 274:32439–44 [PubMed: 10542288]

119. Emtage JL, Bucci M, Watkins JL, Wente SR. 1997 Defining the essential functional regions of the nucleoporin Nup145p. J. Cell Sci. 110:911–25 [PubMed: 9133678]

120. Teixeira MT, Siniossoglou S, Podtelejnikov S, Bénichou JC, Mann M, et al. 1997 Two functionally distinct domains generated by in vivo cleavage of Nup145p: a novel biogenesis pathway for nucleoporins. EMBO J. 16:5086–97 [PubMed: 9305650]

121. Griffis ER, Xu S, Powers MA. 2003 Nup98 localizes to both nuclear and cytoplasmic sides of the nuclear pore and binds to two distinct nucleoporin subcomplexes. Mol. Biol. Cell 14:600–10 [PubMed: 12589057]

122. Stuwe T, von Borzyskowski LS, Davenport AM, Hoelz A. 2012 Molecular basis for the anchoring of proto-oncoprotein Nup98 to the cytoplasmic face of the nuclear pore complex. J. Mol. Biol. 419:330–46 [PubMed: 22480613]

123. Sampathkumar P, Ozyurt SA, Do J, Bain KT, Dickey M, et al. 2010 Structures of the autoproteolytic domain from the Saccharomyces cerevisiae nuclear pore complex component, Nup145. Proteins 78:1992–98 [PubMed: 20310066]

124. Laurell E, Beck K, Krupina K, Theerthagiri G, Bodenmiller B, et al. 2011 Phosphorylation of Nup98 by multiple kinases is crucial for NPC disassembly during mitotic entry. Cell 144:539–50 [PubMed: 21335236]

125. Wente SR, Rout MP, Blobel G. 1992 A new family of yeast nuclear pore complex proteins. J. Cell Biol. 119:705–23 [PubMed: 1385442]

126. Yoshida K, Seo HS, Debler EW, Blobel G, Hoelz A. 2011 Structural and functional analysis of an essential nucleoporin heterotrimer on the cytoplasmic face of the nuclear pore complex. PNAS 108:16571–76 [PubMed: 21930948]

127. Strawn LA, Shen T, Shulga N, Goldfarb DS, Wente SR. 2004 Minimal nuclear pore complexes define FG repeat domains essential for transport. Nat. Cell Biol. 6:197–206 [PubMed: 15039779]

128. Kita K, Omata S, Horigome T. 1993 Purification and characterization of a nuclear pore glycoprotein complex containing p62. J. Biochem. 113:377–82 [PubMed: 8486610]

129. Guan T, Muller S, Klier G, Panté N, Blevitt JM, et al. 1995 Structural analysis of the p62 complex, an assembly of O-linked glycoproteins that localizes near the central gated channel of the nuclear pore complex. Mol. Biol. Cell 6:1591–603 [PubMed: 8589458]

130. Solmaz SR, Blobel G, Melcak I. 2013 Ring cycle for dilating and constricting the nuclear pore. PNAS 110:5858–63 [PubMed: 23479651]

131. Solmaz SR, Chauhan R, Blobel G, Melcak I. 2011 Molecular architecture of the transport channel of the nuclear pore complex. Cell 147:590–602 [PubMed: 22036567]

132. Melcak I, Hoelz A, Blobel G. 2007 Structure of Nup58/45 suggests flexible nuclear pore diameter by intermolecular sliding. Science 315:1729–32 [PubMed: 17379812]

133. Ulrich A, Partridge JR, Schwartz TU. 2014 The stoichiometry of the nucleoporin 62 subcomplex of the nuclear pore in solution. Mol. Biol. Cell 25:1484–92 [PubMed: 24574455]

134. Sharma A, Solmaz SR, Blobel G, Melcak I. 2015 Ordered regions of channel nucleoporins Nup62, Nup54, and Nup58 form dynamic complexes in solution. J. Biol. Chem. 290:18370–78 [PubMed: 26025361]

135. Koh J, Blobel G. 2015 Allosteric regulation in gating the central channel of the nuclear pore complex. Cell 161:1361–73 [PubMed: 26046439]

136. Dewangan PS, Sonawane PJ, Chouksey AR, Chauhan R. 2017 The Nup62 coiled-coil motif provides plasticity for triple-helix bundle formation. Biochemistry 56:2803–11 [PubMed: 28406021]

137. Stavru F, Hülsmann BB, Spang A, Hartmann E, Cordes VC, Görlich D. 2006 NDC1: a crucial membrane-integral nucleoporin of metazoan nuclear pore complexes. J. Cell Biol. 173:509–19 [PubMed: 16702233]

138. Chial HJ, Rout MP, Giddings TH, Winey M. 1998 Saccharomyces cerevisiae Ndc1p is a shared component of nuclear pore complexes and spindle pole bodies. J. Cell Biol. 143:1789–800 [PubMed: 9864355]

139. Chadrin A, Hess B, San Roman M, Gatti X, Lombard B, et al. 2010 Pom33, a novel transmembrane nucleoporin required for proper nuclear pore complex distribution. J. Cell Biol. 189:795–811 [PubMed: 20498018]

140. Gerace L, Ottaviano Y, Kondor-Koch C. 1982 Identification of a major polypeptide of the nuclear pore complex. J. Cell Biol. 95:826–37 [PubMed: 7153248]

141. Hallberg E, Wozniak RW, Blobel G. 1993 An integral membrane protein of the pore membrane domain of the nuclear envelope contains a nucleoporin-like region. J. Cell Biol. 122:513–21 [PubMed: 8335683]

142. Wozniak RW, Bartnik E, Blobel G. 1989 Primary structure analysis of an integral membrane glycoprotein of the nuclear pore. J. Cell Biol. 108:2083–92 [PubMed: 2738089]

143. Wozniak RW, Blobel G, Rout MP. 1994 POM152 is an integral protein of the pore membrane domain of the yeast nuclear envelope. J. Cell Biol. 125:31–42 [PubMed: 8138573]

144. Hao Q, Zhang B, Yuan K, Shi H, Blobel G. 2018 Electron microscopy of Chaetomium pom152 shows the assembly of ten-bead string. Cell Discov. 4:56 [PubMed: 30245846]

145. Upla P, Kim SJ, Sampathkumar P, Dutta K, Cahill SM, et al. 2017 Molecular architecture of the major membrane ring component of the nuclear pore complex. Structure 25:434–45 [PubMed: 28162953]

146. Hülsmann BB, Labokha AA, Görlich D. 2012 The permeability of reconstituted nuclear pores provides direct evidence for the selective phase model. Cell 150:738–51 [PubMed: 22901806]

147. Walde S, Kehlenbach RH. 2010 The part and the whole: functions of nucleoporins in nucleocytoplasmic transport. Trends Cell Biol. 20:461–69 [PubMed: 20627572]

148. Schmidt HB, Görlich D. 2016 Transport selectivity of nuclear pores, phase separation, and membraneless organelles. Trends Biochem. Sci. 41:46–61 [PubMed: 26705895]

149. Lim RYH, Huang B, Kapinos LE. 2015 How to operate a nuclear pore complex by Kap-centric control. Nucleus 6:366–72 [PubMed: 26338152]

150. Frey S, Görlich D. 2007 A saturated FG-repeat hydrogel can reproduce the permeability properties of nuclear pore complexes. Cell 130:512–23 [PubMed: 17693259]

151. Sakiyama Y, Mazur A, Kapinos LE, Lim RYH. 2016 Spatiotemporal dynamics of the nuclear pore complex transport barrier resolved by high-speed atomic force microscopy. Nat. Nanotechnol 11:719–23 [PubMed: 27136131]

152. Adams RL, Terry LJ, Wente SR. 2015 A novel Saccharomyces cerevisiae FG nucleoporin mutant collection for use in nuclear pore complex functional experiments. G3 Genes Genomes Genet. 6:51–58

153. Fiserova J, Richards SA, Wente SR, Goldberg MW. 2010 Facilitated transport and diffusion take distinct spatial routes through the nuclear pore complex. J. Cell Sci. 123:2773–80 [PubMed: 20647373]

154. Terry LJ, Wente SR. 2009 Flexible gates: dynamic topologies and functions for FG nucleoporins in nucleocytoplasmic transport. Eukaryot. Cell 8:1814–27 [PubMed: 19801417]

155. Onischenko E, Tang JH, Andersen KR, Knockenhauer KE, Vallotton P, et al. 2017 Natively unfolded FG repeats stabilize the structure of the nuclear pore complex. Cell 171:904–17.e19 [PubMed: 29033133]

156. Lutzmann M, Kunze R, Stangl K, Stelter P, Toth KF, et al. 2005 Reconstitution of Nup157 and Nup145N into the Nup84 complex. J. Biol. Chem. 280:18442–51 [PubMed: 15741174]

157. Faini M, Beck R, Wieland FT, Briggs JA. 2013 Vesicle coats: structure, function, and general principles of assembly. Trends Cell Biol. 23:279–88 [PubMed: 23414967]

158. Vollmer B, Lorenz M, Moreno-Andrés D, Bodenhöfer M, De Magistris P, et al. 2015 Nup153 recruits the Nup107–160 complex to the inner nuclear membrane for interphasic nuclear pore complex assembly. Dev. Cell 33:717–28 [PubMed: 26051542]

159. Meszaros N, Cibulka J, Mendiburo MJ, Romanauska A, Schneider M, Köhler A. 2015 Nuclear pore basket proteins are tethered to the nuclear envelope and can regulate membrane curvature. Dev. Cell 33:285–98 [PubMed: 25942622]

160. Dawson TR, Lazarus MD, Hetzer MW, Wente SR. 2009 ER membrane–bending proteins are necessary for de novo nuclear pore formation. J. Cell Biol. 184:659–75 [PubMed: 19273614]

161. Yewdell WT, Colombi P, Makhnevych T, Lusk CP. 2011 Lumenal interactions in nuclear pore complex assembly and stability. Mol. Biol. Cell 22:1375–88 [PubMed: 21346187]

162. Webster BM, Colombi P, Jäger J, Lusk CP. 2014 Surveillance of nuclear pore complex assembly by ESCRT-III/Vps4. Cell 159:388–401 [PubMed: 25303532]

163. Casey AK, Chen S, Novick P, Ferro-Novick S, Wente SR. 2015 Nuclear pore complex integrity requires Lnp1, a regulator of cortical endoplasmic reticulum. Mol. Biol. Cell 26:2833–44 [PubMed: 26041935]

164. Webster BM, Thaller DJ, Jäger J, Ochmann SE, Borah S, Lusk CP. 2016 Chm7 and Heh1 collaborate to link nuclear pore complex quality control with nuclear envelope sealing. EMBO J. 35:2447–67 [PubMed: 27733427]

165. Jarnik M, Aebi U. 1991 Toward a more complete 3-D structure of the nuclear pore complex. J. Struct. Biol. 107:291–308 [PubMed: 1725493]

166. Hodge CA, Tran EJ, Noble KN, Alcázar-Román AR, Ben-Yishay R, et al. 2011 The Dbp5 cycle at the nuclear pore complex during mRNA export I: dbp5 mutants with defects in RNA binding and ATP hydrolysis define key steps for Nup159 and Gle1. Genes Dev. 25:1052–64 [PubMed: 21576265]

167. Walther TC, Pickersgill HS, Cordes VC, Goldberg MW, Allen TD, et al. 2002 The cytoplasmic filaments of the nuclear pore complex are dispensable for selective nuclear protein import. J. Cell. Biol. 158:63–77 [PubMed: 12105182]

168. Kiseleva E, Allen TD, Rutherford S, Bucci M, Wente SR, Goldberg MW. 2004 Yeast nuclear pore complexes have a cytoplasmic ring and internal filaments. J. Struct. Biol. 145:272–88 [PubMed: 14960378]

169. Napetschnig J, Kassube SA, Debler EW, Wong RW, Blobel G, Hoelz A. 2009 Structural and functional analysis of the interaction between the nucleoporin Nup214 and the DEAD-box helicase Ddx19. PNAS 106:3089–94 [PubMed: 19208808]

170. Napetschnig J, Blobel G, Hoelz A. 2007 Crystal structure of the N-terminal domain of the human protooncogene Nup214/CAN. PNAS 104:1783–88 [PubMed: 17264208]

171. Ren Y, Seo HS, Blobel G, Hoelz A. 2010 Structural and functional analysis of the interaction between the nucleoporin Nup98 and the mRNA export factor Rae1. PNAS 107:10406–11 [PubMed: 20498086]

172. Weirich CS, Erzberger JP, Berger JM, Weis K. 2004 The N-terminal domain of Nup159 forms a β-propeller that functions in mRNA export by tethering the helicase Dbp5 to the nuclear pore. Mol. Cell 16:749–60 [PubMed: 15574330]

173. von Moeller H, Basquin C, Conti E. 2009 The mRNA export protein DBP5 binds RNA and the cytoplasmic nucleoporin NUP214 in a mutually exclusive manner. Nat. Struct. Mol. Biol. 16:247–54 [PubMed: 19219046]

174. Montpetit B, Thomsen ND, Helmke KJ, Seeliger MA, Berger JM, Weis K. 2011 A conserved mechanism of DEAD-box ATPase activation by nucleoporins and InsP6 in mRNA export. Nature 472:238–42 [PubMed: 21441902]

175. Romes EM, Tripathy A, Slep KC. 2012 Structure of a yeast Dyn2-Nup159 complex and molecular basis for dynein light chain–nuclear pore interaction. J. Biol. Chem. 287:15862–73 [PubMed: 22411995]

176. Quan B, Seo HS, Blobel G, Ren Y. 2014 Vesiculoviral matrix (M) protein occupies nucleic acid binding site at nucleoporin pair (Rae1·Nup98). PNAS 111:9127–32 [PubMed: 24927547]

177. Lin DH, Correia AR, Cai SW, Huber FM, Jette CA, Hoelz A. 2018 Structural and functional analysis of mRNA export regulation by the nuclear pore complex. Nat. Commun. 9:2319 [PubMed: 29899397]

178. Teimer R, Kosinski J, von Appen A, Beck M, Hurt E. 2017 A short linear motif in scaffold Nup145C connects Y-complex with pre-assembled outer ring Nup82 complex. Nat. Commun. 8:1107 [PubMed: 29062044]

179. Gaik M, Flemming D, von Appen A, Kastritis P, Mucke N, et al. 2015 Structural basis for assembly and function of the Nup82 complex in the nuclear pore scaffold. J. Cell Biol. 208:283–97 [PubMed: 25646085]

180. Belgareh N, Snay-Hodge C, Pasteau F, Dagher S, Cole CN, Doye V. 1998 Functional characterization of a Nup159p-containing nuclear pore subcomplex. Mol. Biol. Cell 9:3475–92 [PubMed: 9843582]

181. Bailer SM, Balduf C, Hurt E. 2001 The Nsp1p carboxy-terminal domain is organized into functionally distinct coiled-coil regions required for assembly of nucleoporin subcomplexes and nucleocytoplasmic transport. Mol. Cell. Biol. 21:7944–55 [PubMed: 11689687]

182. Bailer SM, Balduf C, Katahira J, Podtelejnikov A, Rollenhagen C, et al. 2000 Nup116p associates with the Nup82p-Nsp1p-Nup159p nucleoporin complex. J. Biol. Chem. 275:23540–48 [PubMed: 10801828]

183. Pritchard CE, Fornerod M, Kasper LH, van Deursen JM. 1999 RAE1 is a shuttling mRNA export factor that binds to a GLEBS-like NUP98 motif at the nuclear pore complex through multiple domains. J. Cell Biol. 145:237–54 [PubMed: 10209021]

184. Bailer SM, Siniossoglou S, Podtelejnikov A, Hellwig A, Mann M, Hurt E. 1998 Nup116p and Nup100p are interchangeable through a conserved motif which constitutes a docking site for the mRNA transport factor Gle2p. EMBO J. 17:1107–19 [PubMed: 9463388]

185. Blevins MB, Smith AM, Phillips EM, Powers MA. 2003 Complex formation among the RNA export proteins Nup98, Rae1/Gle2, and TAP. J. Biol. Chem. 278:20979–88 [PubMed: 12637516]

186. Murphy R, Watkins JL, Wente SR. 1996 GLE2, a Saccharomyces cerevisiae homologue of the Schizosaccharomyces pombe export factor RAE1, is required for nuclear pore complex structure and function. Mol. Biol. Cell 7:1921–37 [PubMed: 8970155]

187. Stutz F, Neville M, Rosbash M. 1995 Identification of a novel nuclear pore–associated protein as a functional target of the HIV-1 Rev protein in yeast. Cell 82:495–506 [PubMed: 7634338]

188. Watkins JL, Murphy R, Emtage JL, Wente SR. 1998 The human homologue of Saccharomyces cerevisiae Gle1p is required for poly(A)+ RNA export. PNAS 95:6779–84 [PubMed: 9618489]

189. Hodge CA, Colot HV, Stafford P, Cole CN. 1999 Rat8p/Dbp5p is a shuttling transport factor that interacts with Rat7p/Nup159p and Gle1p and suppresses the mRNA export defect of xpo1–1 cells. EMBO J. 18:5778–88 [PubMed: 10523319]

190. Strahm Y, Fahrenkrog B, Zenklusen D, Rychner E, Kantor J, et al. 1999 The RNA export factor Gle1p is located on the cytoplasmic fibrils of the NPC and physically interacts with the FG-nucleoporin Rip1p, the DEAD-box protein Rat8p/Dbp5p and a new protein Ymr 255p. EMBO J. 18:5761–77 [PubMed: 10610322]

191. Sloan KE, Bohnsack MT. 2018 Unravelling the mechanisms of RNA helicase regulation. Trends Biochem. Sci. 43:237–50 [PubMed: 29486979]

192. Rayala HJ, Kendirgi F, Barry DM, Majerus PW, Wente SR. 2004 The mRNA export factor human Gle1 interacts with the nuclear pore complex protein Nup155. Mol. Cell. Proteom. 3:145–55

193. Kendirgi F, Rexer DJ, Alcázar-Román AR, Onishko HM, Wente SR. 2005 Interaction between the shuttling mRNA export factor Gle1 and the nucleoporin hCG1: a conserved mechanism in the export of Hsp70 mRNA. Mol. Biol. Cell 16:4304–15 [PubMed: 16000379]

194. Folkmann AW, Collier SE, Zhan X, Aditi, Ohi MD, Wente SR. 2013 Gle1 functions during mRNA export in an oligomeric complex that is altered in human disease. Cell 155:582–93 [PubMed: 24243016]

195. Alcázar-Román AR, Tran EJ, Guo S, Wente SR. 2006 Inositol hexakisphosphate and Gle1 activate the DEAD-box protein Dbp5 for nuclear mRNA export. Nat. Cell Biol. 8:711–16 [PubMed: 16783363]

196. Weirich CS, Erzberger JP, Flick JS, Berger JM, Thorner J, Weis K. 2006 Activation of the DExD/H-box protein Dbp5 by the nuclear-pore protein Gle1 and its coactivator InsP6 is required for mRNA export. Nat. Cell Biol. 8:668–76 [PubMed: 16783364]

197. Adams RL, Mason AC, Glass L, Aditi, Wente SR. 2017 Nup42 and IP6 coordinate Gle1 stimulation of Dbp5/DDX19B for mRNA export in yeast and human cells. Traffic 18:776–90 [PubMed: 28869701]

198. Schmitt C, von Kobbe C, Bachi A, Panté N, Rodrigues JP, et al. 1999 Dbp5, a DEAD-box protein required for mRNA export, is recruited to the cytoplasmic fibrils of nuclear pore complex via a conserved interaction with CAN/Nup159p. EMBO J. 18:4332–47 [PubMed: 10428971]

199. Stelter P, Kunze R, Flemming D, Hopfner D, Diepholz M, et al. 2007 Molecular basis for the functional interaction of dynein light chain with the nuclear-pore complex. Nat. Cell Biol. 9:788–96 [PubMed: 17546040]

200. Kellner N, Schwarz J, Sturm M, Fernandez-Martinez J, Griesel S, et al. 2016 Developing genetic tools to exploit Chaetomium thermophilum for biochemical analyses of eukaryotic macromolecular assemblies. Sci. Rep. 6:20937 [PubMed: 26864114]

201. Kim DI, Birendra KC, Zhu W, Motamedchaboki K, Doye V, Roux KJ. 2014 Probing nuclear pore complex architecture with proximity-dependent biotinylation. PNAS 111:E2453–61

202. Clouse KN, Luo MJ, Zhou Z, Reed R. 2001 A Ran-independent pathway for export of spliced mRNA. Nat. Cell Biol. 3:97–99 [PubMed: 11146633]

203. Lund MK, Guthrie C. 2005 The DEAD-box protein Dbp5p is required to dissociate Mex67p from exported mRNPs at the nuclear rim. Mol. Cell 20:645–51 [PubMed: 16307927]

204. Linder P, Jankowsky E. 2011 From unwinding to clamping—the DEAD box RNA helicase family. Nat. Rev. Mol. Cell Biol. 12:505–16 [PubMed: 21779027]

205. Collins R, Karlberg T, Lehtiö L, Schütz P, van den Berg S, et al. 2009 The DEXD/H-box RNA helicase DDX19 is regulated by an α-helical switch. J. Biol. Chem. 284:10296–300 [PubMed: 19244245]

206. Folkmann AW, Noble KN, Cole CN, Wente SR. 2011 Dbp5, Gle1-IP6 and Nup159: a working model for mRNP export. Nucleus 2:540–48 [PubMed: 22064466]

207. Wong EV, Gray S, Cao W, Montpetit R, Montpetit B, De La Cruz EM. 2018 Nup159 weakens Gle1 binding to Dbp5 but does not accelerate ADP release. J. Mol. Biol. 430:2080–95 [PubMed: 29782832]

208. Noble KN, Tran EJ, Alcázar-Román AR, Hodge CA, Cole CN, Wente SR. 2011 The Dbp5 cycle at the nuclear pore complex during mRNA export II: Nucleotide cycling and mRNP remodeling by Dbp5 are controlled by Nup159 and Gle1. Genes Dev. 25:1065–77 [PubMed: 21576266]

209. Wong EV, Cao W, Vörös J, Merchant M, Modis Y, et al. 2016 P_i release limits the intrinsic and RNA-stimulated ATPase cycles of DEAD-box protein 5 (Dbp5). J. Mol. Biol. 428:492–508 [PubMed: 26730886]

210. Wu J, Matunis MJ, Kraemer D, Blobel G, Coutavas E. 1995 Nup358, a cytoplasmically exposed nucleoporin with peptide repeats, Ran-GTP binding sites, zinc fingers, a cyclophilin A homologous domain, and a leucine-rich region. J. Biol. Chem. 270:14209–13 [PubMed: 7775481]

211. Yokoyama N, Hayashi N, Seki T, Panté N, Ohba T, et al. 1995 A giant nucleopore protein that binds Ran/TC4. Nature 376:184–88 [PubMed: 7603572]

212. Lin DH, Zimmermann S, Stuwe T, Stuwe E, Hoelz A. 2013 Structural and functional analysis of the C-terminal domain of Nup358/RanBP2. J. Mol. Biol. 425:1318–29 [PubMed: 23353830]

213. Kassube SA, Stuwe T, Lin DH, Antonuk CD, Napetschnig J, et al. 2012 Crystal structure of the N-terminal domain of Nup358/RanBP2. J. Mol. Biol. 423:752–65 [PubMed: 22959972]

214. Vetter IR, Nowak C, Nishimoto T, Kuhlmann J, Wittinghofer A. 1999 Structure of a Ran-binding domain complexed with Ran bound to a GTP analogue: implications for nuclear transport. Nature 398:39–46 [PubMed: 10078529]

215. Reverter D, Lima CD. 2005 Insights into E3 ligase activity revealed by a SUMO–RanGAP1–Ubc9–Nup358 complex. Nature 435:687–92 [PubMed: 15931224]

216. Joseph J, Dasso M. 2008 The nucleoporin Nup358 associates with and regulates interphase microtubules. FEBS Lett. 582:190–96 [PubMed: 18070602]

217. Bernad R, van der Velde H, Fornerod M, Pickersgill H. 2004 Nup358/RanBP2 attaches to the nuclear pore complex via association with Nup88 and Nup214/CAN and plays a supporting role in CRM1-mediated nuclear protein export. Mol. Cell. Biol. 24:2373–84 [PubMed: 14993277]

218. Mahadevan K, Zhang H, Akef A, Cui XA, Gueroussov S, et al. 2013 RanBP2/Nup358 potentiates the translation of a subset of mRNAs encoding secretory proteins. PLOS Biol. 11:e1001545

219. Hamada M, Haeger A, Jeganathan KB, van Ree JH, Malureanu L, et al. 2011 Ran-dependent docking of importin-β to RanBP2/Nup358 filaments is essential for protein import and cell viability. J. Cell Biol. 194:597–612 [PubMed: 21859863]

220. Hutten S, Walde S, Spillner C, Hauber J, Kehlenbach RH. 2009 The nuclear pore component Nup358 promotes transportin-dependent nuclear import. J. Cell Sci. 122:1100–10 [PubMed: 19299463]

221. Hutten S, Flotho A, Melchior F, Kehlenbach RH. 2008 The Nup358-RanGAP complex is required for efficient importin α/β-dependent nuclear import. Mol. Biol. Cell 19:2300–10 [PubMed: 18305100]

222. Ritterhoff T, Das H, Hofhaus G, Schroder RR, Flotho A, Melchior F. 2016 The RanBP2/RanGAP1*SUMO1/Ubc9 SUMO E3 ligase is a disassembly machine for Crm1-dependent nuclear export complexes. Nat. Commun. 7:11482 [PubMed: 27160050]

223. Köhler A, Hurt E. 2010 Gene regulation by nucleoporins and links to cancer. Mol. Cell 38:6–15 [PubMed: 20385085]

224. Partridge JR, Schwartz TU. 2009 Crystallographic and biochemical analysis of the Ran-binding zinc finger domain. J. Mol. Biol. 391:375–89 [PubMed: 19505478]

225. Hase ME, Kuznetsov NV, Cordes VC. 2001 Amino acid substitutions of coiled-coil protein Tpr abrogate anchorage to the nuclear pore complex but not parallel, in-register homodimerization. Mol. Biol. Cell 12:2433–52 [PubMed: 11514627]

226. Matsuura Y, Stewart M. 2005 Nup50/Npap60 function in nuclear protein import complex disassembly and importin recycling. EMBO J. 24:3681–89 [PubMed: 16222336]

227. Walther TC, Fornerod M, Pickersgill H, Goldberg M, Allen TD, Mattaj IW. 2001 The nucleoporin Nup153 is required for nuclear pore basket formation, nuclear pore complex anchoring and import of a subset of nuclear proteins. EMBO J. 20:5703–14 [PubMed: 11598013]

228. Hase ME, Cordes VC. 2003 Direct interaction with Nup153 mediates binding of Tpr to the periphery of the nuclear pore complex. Mol. Biol. Cell 14:1923–40 [PubMed: 12802065]

229. Galy V, Olivo-Marin JC, Scherthan H, Doye V, Rascalou N, Nehrbass U. 2000 Nuclear pore complexes in the organization of silent telomeric chromatin. Nature 403:108–12 [PubMed: 10638763]

230. Vasu S, Shah S, Orjalo A, Park M, Fischer WH, Forbes DJ. 2001 Novel vertebrate nucleoporins Nup133 and Nup160 play a role in mRNA export. J. Cell Biol. 155:339–54 [PubMed: 11684705]

231. Niño CA, Guet D, Gay A, Brutus S, Jourquin F, et al. 2016 Posttranslational marks control architectural and functional plasticity of the nuclear pore complex basket. J. Cell Biol. 212:167–80 [PubMed: 26783300]

232. Krull S, Thyberg J, Björkroth B, Rackwitz HR, Cordes VC. 2004 Nucleoporins as components of the nuclear pore complex core structure and Tpr as the architectural element of the nuclear basket. Mol. Biol. Cell 15:4261–77 [PubMed: 15229283]

233. Bayliss R, Littlewood T, Strawn LA, Wente SR, Stewart M. 2002 GLFG and FxFG nucleoporins bind to overlapping sites on importin-β. J. Biol. Chem. 277:50597–606 [PubMed: 12372823]

234. Bayliss R, Littlewood T, Stewart M. 2000 Structural basis for the interaction between FxFG nucleoporin repeats and importin-β in nuclear trafficking. Cell 102:99–108 [PubMed: 10929717]

235. Koyama M, Hirano H, Shirai N, Matsuura Y. 2017 Crystal structure of the Xpo1p nuclear export complex bound to the SxFG/PxFG repeats of the nucleoporin Nup42p. Genes Cells 22:861–75 [PubMed: 28791779]

236. Koyama M, Shirai N, Matsuura Y. 2014 Structural insights into how Yrb2p accelerates the assembly of the Xpo1p nuclear export complex. Cell Rep. 9:983–95 [PubMed: 25437554]

237. Port SA, Monecke T, Dickmanns A, Spillner C, Hofele R, et al. 2015 Structural and functional characterization of CRM1-Nup214 interactions reveals multiple FG-binding sites involved in nuclear export. Cell Rep. 13:690–702 [PubMed: 26489467]

238. Milles S, Mercadante D, Aramburu IV, Jensen MR, Banterle N, et al. 2015 Plasticity of an ultrafast interaction between nucleoporins and nuclear transport receptors. Cell 163:734–45 [PubMed: 26456112]

239. Hough LE, Dutta K, Sparks S, Temel DB, Kamal A, et al. 2015 The molecular mechanism of nuclear transport revealed by atomic-scale measurements. eLife 4:e10027

240. Liu SM, Stewart M. 2005 Structural basis for the high-affinity binding of nucleoporin Nup1p to the Saccharomyces cerevisiae importin-β homologue, Kap95p. J. Mol. Biol. 349:515–25 [PubMed: 15878174]

241. Bayliss R, Leung SW, Baker RP, Quimby BB, Corbett AH, Stewart M. 2002 Structural basis for the interaction between NTF2 and nucleoporin FxFG repeats. EMBO J. 21:2843–53 [PubMed: 12065398]

242. Bayliss R, Ribbeck K, Akin D, Kent HM, Feldherr CM, et al. 1999 Interaction between NTF2 and xFxFG-containing nucleoporins is required to mediate nuclear import of RanGDP. J. Mol. Biol. 293:579–93 [PubMed: 10543952]

243. Grant RP, Neuhaus D, Stewart M. 2003 Structural basis for the interaction between the Tap/NXF1 UBA domain and FG nucleoporins at 1 Å resolution. J. Mol. Biol. 326:849–58 [PubMed: 12581645]

244. Fribourg S, Braun IC, Izaurralde E, Conti E. 2001 Structural basis for the recognition of a nucleoporin FG repeat by the NTF2-like domain of the TAP/p15 mRNA nuclear export factor. Mol. Cell 8:645–56 [PubMed: 11583626]

245. Kobayashi J, Matsuura Y. 2013 Structural basis for cell-cycle-dependent nuclear import mediated by the karyopherin Kap121p. J. Mol. Biol. 425:1852–68 [PubMed: 23541588]

246. Kralt A, Jagalur NB, van den Boom V, Lokareddy RK, Steen A, et al. 2015 Conservation of inner nuclear membrane targeting sequences in mammalian Pom121 and yeast Heh2 membrane proteins. Mol. Biol. Cell 26:3301–12 [PubMed: 26179916]

247. Ibarra A, Hetzer MW. 2015 Nuclear pore proteins and the control of genome functions. Genes Dev. 29:337–49 [PubMed: 25691464]

248. Matsuura Y, Lange A, Harreman MT, Corbett AH, Stewart M. 2003 Structural basis for Nup2p function in cargo release and karyopherin recycling in nuclear import. EMBO J. 22:5358–69 [PubMed: 14532109]

249. Yaseen NR, Blobel G. 1999 Two distinct classes of Ran-binding sites on the nucleoporin Nup-358. PNAS 96:5516–21 [PubMed: 10318915]

250. Schrader N, Koerner C, Koessmeier K, Bangert JA, Wittinghofer A, et al. 2008 The crystal structure of the Ran-Nup153ZnF2 complex: a general Ran docking site at the nuclear pore complex. Structure 16:1116–25 [PubMed: 18611384]

251. Mahajan R, Delphin C, Guan T, Gerace L, Melchior F. 1997 A small ubiquitin-related polypeptide involved in targeting RanGAP1 to nuclear pore complex protein RanBP2. Cell 88:97–107 [PubMed: 9019411]

252. Werner A, Flotho A, Melchior F. 2012 The RanBP2/RanGAP1*SUMO1/Ubc9 complex is a multisubunit SUMO E3 ligase. Mol. Cell 46:287–98 [PubMed: 22464730]

253. Matunis MJ, Wu J, Blobel G. 1998 SUMO-1 modification and its role in targeting the Ran GTPase-activating protein, RanGAP1, to the nuclear pore complex. J. Cell Biol. 140:499–509 [PubMed: 9456312]

254. Rodríguez-Navarro S, Hurt E. 2011 Linking gene regulation to mRNA production and export. Curr. Opin. Cell Biol. 23:302–9 [PubMed: 21227675]

255. Pascual-Garcia P, Capelson M. 2014 Nuclear pores as versatile platforms for gene regulation. Curr. Opin. Genet. Dev. 25:110–17 [PubMed: 24632227]

256. Fischer T, Sträßer K, Rácz A, Rodríguez-Navarro S, Oppizzi M, et al. 2002 The mRNA export machinery requires the novel Sac3p–Thp1p complex to dock at the nucleoplasmic entrance of the nuclear pores. EMBO J. 21:5843–52 [PubMed: 12411502]

257. Fischer T, Rodríguez-Navarro S, Pereira G, Rácz A, Schiebel E, Hurt E. 2004 Yeast centrin Cdc31 is linked to the nuclear mRNA export machinery. Nat. Cell Biol. 6:840–48 [PubMed: 15311284]

258. Jani D, Valkov E, Stewart M. 2014 Structural basis for binding the TREX2 complex to nuclear pores, GAL1 localisation and mRNA export. Nucleic Acids Res. 42:6686–97 [PubMed: 24705649]

259. Jani D, Lutz S, Hurt E, Laskey RA, Stewart M, Wickramasinghe VO. 2012 Functional and structural characterization of the mammalian TREX-2 complex that links transcription with nuclear messenger RNA export. Nucleic Acids Res. 40:4562–73 [PubMed: 22307388]

260. Umlauf D, Bonnet J, Waharte F, Fournier M, Stierle M, et al. 2013 The human TREX-2 complex is stably associated with the nuclear pore basket. J. Cell Sci. 126:2656–67 [PubMed: 23591820]

261. Xu S, Powers MA. 2009 Nuclear pore proteins and cancer. Semin. Cell Dev. Biol. 20:620–30 [PubMed: 19577736]

262. Freibaum BD, Lu Y, Lopez-Gonzalez R, Kim NC, Almeida S, et al. 2015 GGGGCC repeat expansion in C9orf72 compromises nucleocytoplasmic transport. Nature 525:129–33 [PubMed: 26308899]

263. Joviêić A, Mertens J, Boeynaems S, Bogaert E, Chai N, et al. 2015 Modifiers of C9orf72 dipeptide repeat toxicity connect nucleocytoplasmic transport defects to FTD/ALS. Nat. Neurosci. 18:1226–29 [PubMed: 26308983]

264. Zhang K, Donnelly CJ, Haeusler AR, Grima JC, Machamer JB, et al. 2015 The C9orf72 repeat expansion disrupts nucleocytoplasmic transport. Nature 525:56–61 [PubMed: 26308891]

265. Grima JC, Daigle JG, Arbez N, Cunningham KC, Zhang K, et al. 2017 Mutant Huntingtin disrupts the nuclear pore complex. Neuron 94:93–107.e6 [PubMed: 28384479]

266. Toyama BH, Savas JN, Park SK, Harris MS, Ingolia NT, et al. 2013 Identification of long-lived proteins reveals exceptional stability of essential cellular structures. Cell 154:971–82 [PubMed: 23993091]

267. Tullio-Pelet A, Salomon R, Hadj-Rabia S, Mugnier C, de Laet MH, et al. 2000 Mutant WD-repeat protein in triple-A syndrome. Nat. Genet. 26:332–35 [PubMed: 11062474]

268. Handschug K, Sperling S, Yoon SJ, Hennig S, Clark AJ, Huebner A. 2001 Triple A syndrome is caused by mutations in AAAS, a new WD-repeat protein gene. Hum. Mol. Genet. 10:283–90 [PubMed: 11159947]

269. Basel-Vanagaite L, Muncher L, Straussberg R, Pasmanik-Chor M, Yahav M, et al. 2006 Mutated nup62 causes autosomal recessive infantile bilateral striatal necrosis. Ann. Neurol. 60:214–22 [PubMed: 16786527]

270. Neilson DE, Adams MD, Orr CM, Schelling DK, Eiben RM, et al. 2009 Infection-triggered familial or recurrent cases of acute necrotizing encephalopathy caused by mutations in a component of the nuclear pore, RANBP2. Am. J. Hum. Genet. 84:44–51 [PubMed: 19118815]

271. Miyake N, Tsukaguchi H, Koshimizu E, Shono A, Matsunaga S, et al. 2015 Biallelic mutations in nuclear pore complex subunit NUP107 cause early-childhood-onset steroid-resistant nephrotic syndrome. Am. J. Hum. Genet. 97:555–66 [PubMed: 26411495]

272. Kaneb HM, Folkmann AW, Belzil VV, Jao LE, Leblond CS, et al. 2015 Deleterious mutations in the essential mRNA metabolism factor, hGle1, in amyotrophic lateral sclerosis. Hum. Mol. Genet. 24:1363–73 [PubMed: 25343993]

273. Zhang X, Chen S, Yoo S, Chakrabarti S, Zhang T, et al. 2008 Mutation in nuclear pore component NUP155 leads to atrial fibrillation and early sudden cardiac death. Cell 135:1017–27 [PubMed: 19070573]

274. Folkmann AW, Dawson TR, Wente SR. 2014 Insights into mRNA export-linked molecular mechanisms of human disease through a Gle1 structure–function analysis. Adv. Biol. Regul. 54:74–91 [PubMed: 24275432]

275. Park E, Ahn YH, Kang HG, Miyake N, Tsukaguchi H, Cheong HI. 2017 NUP107 mutations in children with steroid-resistant nephrotic syndrome. Nephrol. Dial. Transplant. 32:1013–17 [PubMed: 27190346]

276. Braun DA, Sadowski CE, Kohl S, Lovric S, Astrinidis SA, et al. 2016 Mutations in nuclear pore genes NUP93, NUP205 and XPO5 cause steroid-resistant nephrotic syndrome. Nat. Genet. 48:457–65 [PubMed: 26878725]

277. Park M, Dean M, Cooper CS, Schmidt M, O'Brien SJ, et al. 1986 Mechanism of met oncogene activation. Cell 45:895–904 [PubMed: 2423252]

278. Pal K, Bandyopadhyay A, Zhou XE, Xu Q, Marciano DP, et al. 2017 Structural basis of TPR-mediated oligomerization and activation of oncogenic fusion kinases. Structure 25:867–77.e3 [PubMed: 28528776]

279. Singer S, Zhao R, Barsotti AM, Ouwehand A, Fazollahi M, et al. 2012 Nuclear pore component Nup98 is a potential tumor suppressor and regulates posttranscriptional expression of select p53 target genes. Mol. Cell 48:799–810 [PubMed: 23102701]

280. Cohen S, Au S, Panté N. 2011 How viruses access the nucleus. Biochim. Biophys. Acta Mol. Cell Res. 1813:1634–45

281. Le Sage V, Mouland AJ. 2013 Viral subversion of the nuclear pore complex. Viruses 5:2019–42 [PubMed: 23959328]

282. Yarbrough ML, Mata MA, Sakthivel R, Fontoura BM. 2014 Viral subversion of nucleocytoplasmic trafficking. Traffic 15:127–40 [PubMed: 24289861]

283. von Kobbe C, van Deursen JM, Rodrigues JP, Sitterlin D, Bachi A, et al. 2000 Vesicular stomatitis virus matrix protein inhibits host cell gene expression by targeting the nucleoporin Nup98. Mol. Cell 6:1243–52 [PubMed: 11106761]

284. Faria PA, Chakraborty P, Levay A, Barber GN, Ezelle HJ, et al. 2005 VSV disrupts the Rae1/mrnp41 mRNA nuclear export pathway. Mol. Cell 17:93–102 [PubMed: 15629720]

285. Di Nunzio F, Danckaert A, Fricke T, Perez P, Fernandez J, et al. 2012 Human nucleoporins promote HIV-1 docking at the nuclear pore, nuclear import and integration. PLOS ONE 7:e46037

286. Arhel NJ, Souquere-Besse S, Munier S, Souque P, Guadagnini S, et al. 2007 HIV-1 DNA Flap formation promotes uncoating of the pre-integration complex at the nuclear pore. EMBO J. 26:3025–37 [PubMed: 17557080]

287. Schaller T, Ocwieja KE, Rasaiyaah J, Price AJ, Brady TL, et al. 2011 HIV-1 capsid-cyclophilin interactions determine nuclear import pathway, integration targeting and replication efficiency. PLOS Pathog. 7:e1002439

288. Bichel K, Price AJ, Schaller T, Towers GJ, Freund SM, James LC. 2013 HIV-1 capsid undergoes coupled binding and isomerization by the nuclear pore protein NUP358. Retrovirology 10:81 [PubMed: 23902822]

289. Matreyek KA, Yücel SS, Li X, Engelman A. 2013 Nucleoporin NUP153 phenylalanine-glycine motifs engage a common binding pocket within the HIV-1 capsid protein to mediate lentiviral infectivity. PLOS Pathog. 9:e1003693

290. Price AJ, Jacques DA, McEwan WA, Fletcher AJ, Essig S, et al. 2014 Host cofactors and pharmacologic ligands share an essential interface in HIV-1 capsid that is lost upon disassembly. PLOS Pathog. 10:e1004459

291. Schmitz A, Schwarz A, Foss M, Zhou L, Rabe B, et al. 2010 Nucleoporin 153 arrests the nuclear import of hepatitis B virus capsids in the nuclear basket. PLOS Pathog. 6:e1000741

292. Bono F, Cook AG, Grünwald M, Ebert J, Conti E. 2010 Nuclear import mechanism of the EJC component Mago-Y14 revealed by structural studies of importin 13. Mol. Cell 37:211–22 [PubMed: 20122403]

293. Monecke T, Güttler T, Neumann P, Dickmanns A, Görlich D, Ficner R. 2009 Crystal structure of the nuclear export receptor CRM1 in complex with Snurportin1 and RanGTP. Science 324:1087–91 [PubMed: 19389996]

294. Murata K, Mitsuoka K, Hirai T, Walz T, Agre P, et al. 2000 Structural determinants of water permeation through aquaporin-1. Nature 407:599–605 [PubMed: 11034202]

295. van den Berg B, Black PN, Clemons WM Jr., Rapoport TA. 2004 Crystal structure of the long-chain fatty acid transporter FadL. Science 304:1506–9 [PubMed: 15178802]

296. Wu S, Tutuncuoglu B, Yan K, Brown H, Zhang Y, et al. 2016 Diverse roles of assembly factors revealed by structures of late nuclear pre-60S ribosomes. Nature 534:133–37 [PubMed: 27251291]

297. Pumroy RA, Nardozzi JD, Hart DJ, Root MJ, Cingolani G. 2012 Nucleoporin Nup50 stabilizes closed conformation of armadillo repeat 10 in importin α5. J. Biol. Chem. 287:2022–31 [PubMed: 22130666]

SUMMARY POINTS

1. The crystal structures of nearly all symmetric core nucleoporins have been determined at atomic resolution, revealing that nucleoporins possess structural similarities to both membrane-bending coats and soluble transport factors.

2. Cryo–electron tomography (cryo-ET) reconstructions of the human, yeast, and algal nuclear pore complexes (NPCs) have been acquired to resolutions at which individual nucleoporins can be resolved.

3. The combination of crystal structures and cryo-ET reconstructions, as well as other sources of restraints, including biochemical reconstitution, cross-linking mass spectrometry, and computational modeling, have yielded near-atomic composite structures of the human, yeast, and algal NPCs. These advances bridged the resolution gap between the high- and low-resolution structural techniques and established the stoichiometry and positioning of nucleoporins within intact NPCs.

4. The powerful combination of bottom-up and top-down approaches toward determining the structure of the NPC offers a paradigm for uncovering the architectures of other complex biological machines to near-atomic resolution.

5. The NPC consists of a defined spoke architecture with a concentric cylindrical organization of subunits.

6. Considering the massive size of the NPC, the symmetric core makes only relatively few contacts with the nuclear envelope pore membrane. These membrane contacts are spatially clustered and are mediated by amphipathic lipid packing sensor (ALPS)–containing β-propeller domains or amphipathic helices.

7. The channel nucleoporins, Nup62, Nup54, and Nup58, are positioned so that their FG repeats project evenly from the midpoint of the central transport channel. Their recruitment to the NPC by Nup93 depends on recognition of a stable, specific conformation of an equimolar complex formed by the three channel nucleoporins.

8. The symmetric core of the NPC forms a relatively rigid scaffold that provides binding sites for the asymmetric nucleoporins intercalated in the nuclear and cytoplasmic coat nucleoporin complex (CNC) rings.

9. Overall, the NPC architecture is evolutionarily conserved, most notably in the head-to-tail arrangement of the CNCs and the architecture of the inner ring. Notable differences include the absence of a second CNC ring on one or both sides of the nuclear envelope that has been observed thus far with a concurrent absence of Nup155 bridges.

10. Structural and biochemical characterization of the cytoplasmic filament nucleoporins has identified the major interaction hubs and provided snapshots

of the DDX19 catalytic cycle in the termination of messenger RNA (mRNA) export.

FUTURE ISSUES

1. An atomic-resolution model of the entire NPC will require continued progress in improving the resolution of cryo-ET reconstructions to allow flexible fitting of crystal structures, which will also reveal how nucleoporin conformations change in the context of the intact NPC.

2. A complete inventory of high-resolution crystal structures of nucleoporin–nucleoporin interactions is needed to complete the composite structure of the symmetric core. Notable examples are the many critical interactions between the unstructured linker nucleoporins and the structured nucleoporin domains in the inner ring.

3. Further biochemical, structural, and functional analyses are needed to determine the roles of the pore membrane proteins (POMs) in NPC structure, function, and assembly.

4. Further reconstitution experiments are necessary to determine the molecular architectures of the cytoplasmic filaments and the nuclear basket, to learn how they are anchored to the NPC symmetric core, how asymmetry between the nuclear and cytoplasmic faces is established and maintained, and how they contribute to mRNA export and the regulation of gene expression.

5. Structures of nucleoporins and NPCs from many divergent species are needed to provide insight into the evolutionary history of the NPC.

6. The combination of perturbation studies and cryo-ET creates the possibility of trapping transport or assembly intermediates to acquire movies of the NPC in motion during various nucleocytoplasmic transport events.

7. The complete in vitro reconstitution of the entire NPC from recombinant proteins will enable quantitative measures of nucleocytoplasmic transport in vitro and allow for a comprehensive interrogation of individual nucleoporin function.

8. What are the different molecular determinants that control NPC assembly during interphase or after mitosis? An accounting of the energy balance sheet for membrane bending is needed to determine the driving forces for membrane bending and the stabilization of nuclear envelope pores.

9. The consequences of altered NPC composition or structure due to cell-specific differences need to be established.

10. The mechanistic basis of nucleoporin diseases and the action of viral virulence factors that target the NPC need to be elucidated.

11. Once the near-atomic architecture of the entire intact human NPC is completed, the nucleoporin nomenclature should be revised such that the

nucleoporin names reflect their location and function in the intact NPC rather than their molecular masses, which differ across species.
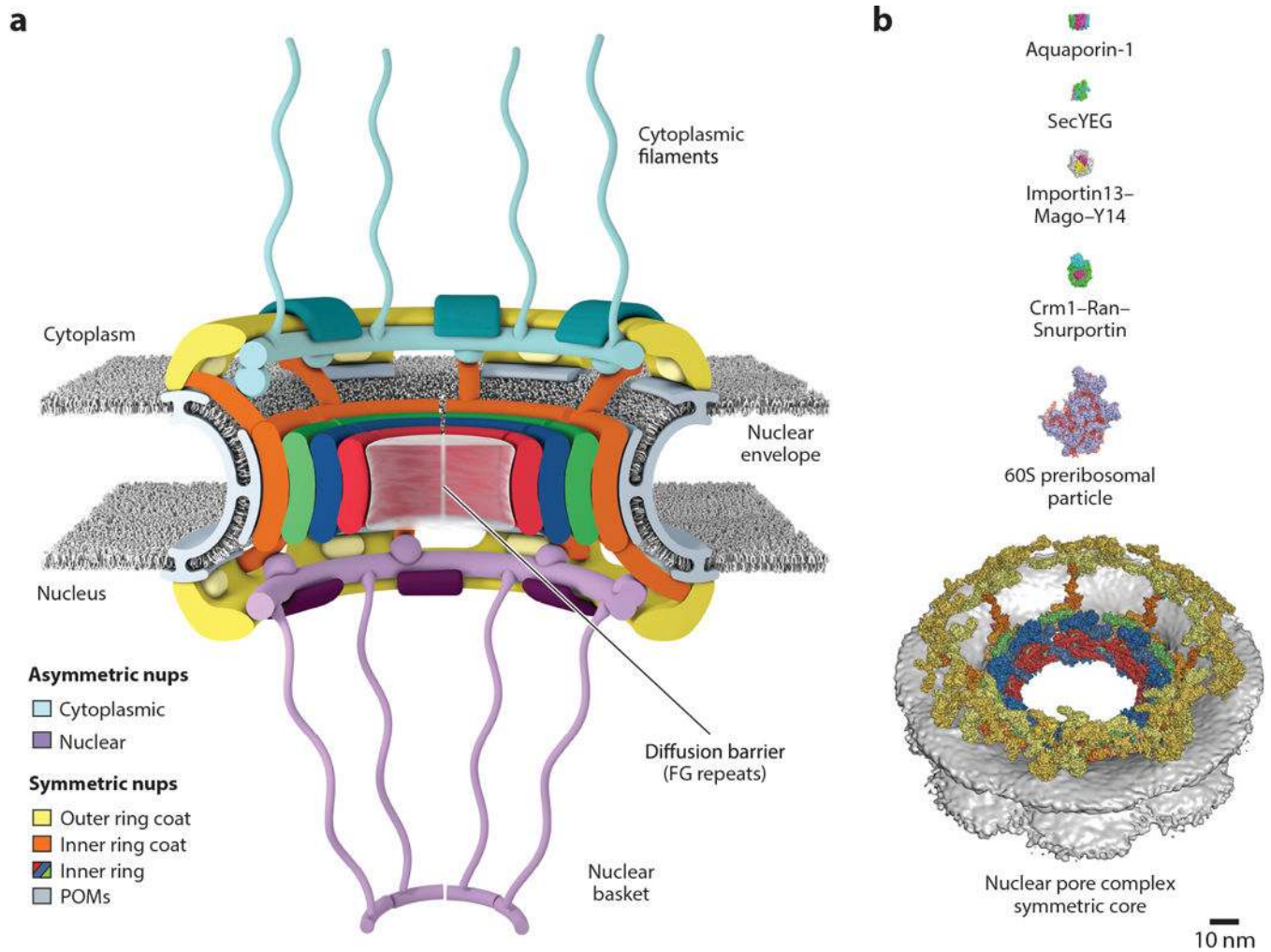
Figure 1.

Overview of the NPC. (*a*) Schematic representation of the NPC architecture. A cutaway view depicting half of an NPC is shown. (*b*) Comparison of sizes of the NPC with other membrane transporters and example nucleocytoplasmic transport cargoes. Surface representations of human Aquaporin-1 (PDB 1FQY), bacterial SecYEG (PDB 1RHZ), *Drosophila melanogaster* Importin13–Mago–Y14 (PDB 2X1G), mammalian Crm1–Ran(GTP)–Snurportin (PDB 3GJX), and a *Saccharomyces cerevisiae* 60S preribosomal particle (PDB 3JCT) are shown to scale with the human NPC symmetric core (41, 292–296). Abbreviations: NPC, nuclear pore complex; PDB, Protein Data Bank; POMs, pore membrane proteins.
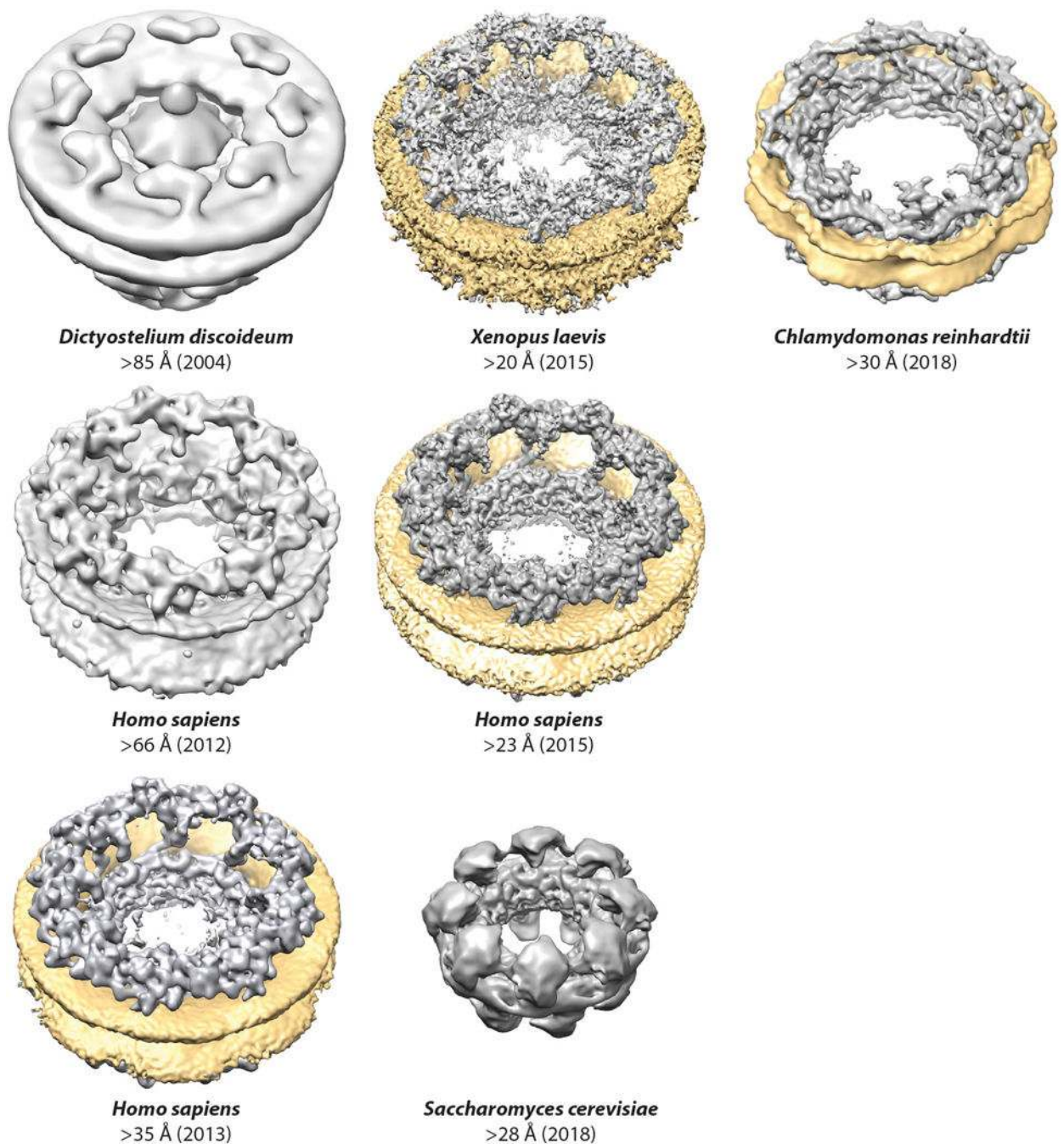
Figure 2.
Progress in cryo-ET reconstructions of the NPC. Surface representations of cryo-ET reconstructions are shown to scale for *Dictyostelium discoideum* (EMD 1097), *Homo sapiens* (2012, EMD 5411; 2013, EMD 2444; 2015, EMD 3103), *Chlamydomonas reinhardtii* (EMD 4355), *Xenopus laevis* (EMDs 3005–3008), and *Saccharomyces cerevisiae* (EMD 7321) (31–33, 35, 36, 38–40). When possible, the nuclear envelope was colored yellow. For the *D. discoideum* reconstruction and first *H. sapiens* reconstruction, the nuclear envelope is present but not colored. For the *S. cerevisiae* reconstruction, the NPCs were

purified and the nuclear envelope is not present. Abbreviations: cryo-ET, cryo–electron tomography; EMD, Electron Microscopy Databank; NPC, nuclear pore complex.

Symmetric nucleoporins

	Saccharomyces cerevisiae		Chaetomium thermophilum	Homo sapiens	
Coat nucleoporin complex	Nup120	(16)	Nup120	Nup160	(32)
	Nup85	(16)	Nup85	Nup75	(32)
	Seh1	(16)	-	Seh1	(32)
	Nup145C	(16)	Nup145C	Nup96	(32)
	Sec13	(16)	Sec13	Sec13	(32)
	Nup84	(16)	Nup84	Nup107	(32)
	Nup133	(16)	Nup133	Nup133	(32)
	-		-	Nup43	(32)
	-		Nup37	Nup37	(32)
	-		ELYS	ELYS†	(16)
Inner ring nups	Nup192	(16)	Nup192	Nup205‡	(32)
	Nup188	(16)	Nup188	Nup188‡	(16)
	Nic96	(32)	Nic96	Nup93	(48)
	Nup157	(16)	Nup170	Nup155	(48)
	Nup170	(16)			
	Nup53	(16)	Nup53	Nup53	(32)
	Nup59	(16)			
	Nup57	(32)	Nup57	Nup54	(32)
	Nup49	(32)	Nup49	Nup58	(32)
	Nsp1*	(48)	Nsp1*	Nup62*	(48)
	Nup100*	(16)	Nup145N*	Nup98*	(48)
	Nup116*	(16)			
	Nup145N*	(16)			
POMs	Ndc1	(16)	Ndc1	NDC1	(32)
	-		-	POM210	(32)
	-		-	POM121	(16)
	POM152	(16)	POM152	-	
	POM34	(16)	POM34	-	
	POM33		POM33	-	

Asymmetric nucleoporins

	Saccharomyces cerevisiae		Chaetomium thermophilum	Homo sapiens	
Cytoplasmic filament nups	Gle2	(16)	Gle2	Rae1	(48)
	Nup42	(8)	Nup42	Nup42	(8)
	Nup82	(16)	Nup82	Nup88	(16)
	Nup159	(16)	Nup159	Nup214	(16)
	Dbp5		Dbp5	DDX19	
	Gle1	(8)	Gle1	Gle1	(8)
	-		-	Nup358	(32)
	Dyn2	(16)	-	-	
Nuclear basket	Nup1	(8)	-	Nup153	(32)
	Nup2		Nup152 Nup56	Nup50	(16)
	Mlp1	(8)	Mlp1	Tpr	(32)
	Mlp2	(8)			
	Nup60	(16)	-	-	
	-		-	ALADIN	(32)

Figure 3.

Nomenclature for nucleoporins in *Saccharomyces cerevisiae*, *Chaetomium thermophilum*, and *Homo sapiens*, grouped by subcomplex. Asterisks (*) indicate that Nup98 and Nup62 and their homologs are also found in the cytoplasmic filaments or nuclear basket. The single dagger (†) indicates that ELYS is only a member of the nuclear coat nucleoporin complex in humans, rather than being symmetrically distributed. Its distribution in fungi remains uncertain. The double dagger (‡) indicates that Nup205/Nup188 molecules are also localized in the outer rings in humans. Stoichiometries of the nucleoporins in intact NPCs are indicated in parentheses next to the *S. cerevisiae* and *H. sapiens* nucleoporins (40, 50, 52).

Abbreviations: NPC, nuclear pore complex; nups, nucleoporin proteins; POMs, pore membrane proteins.
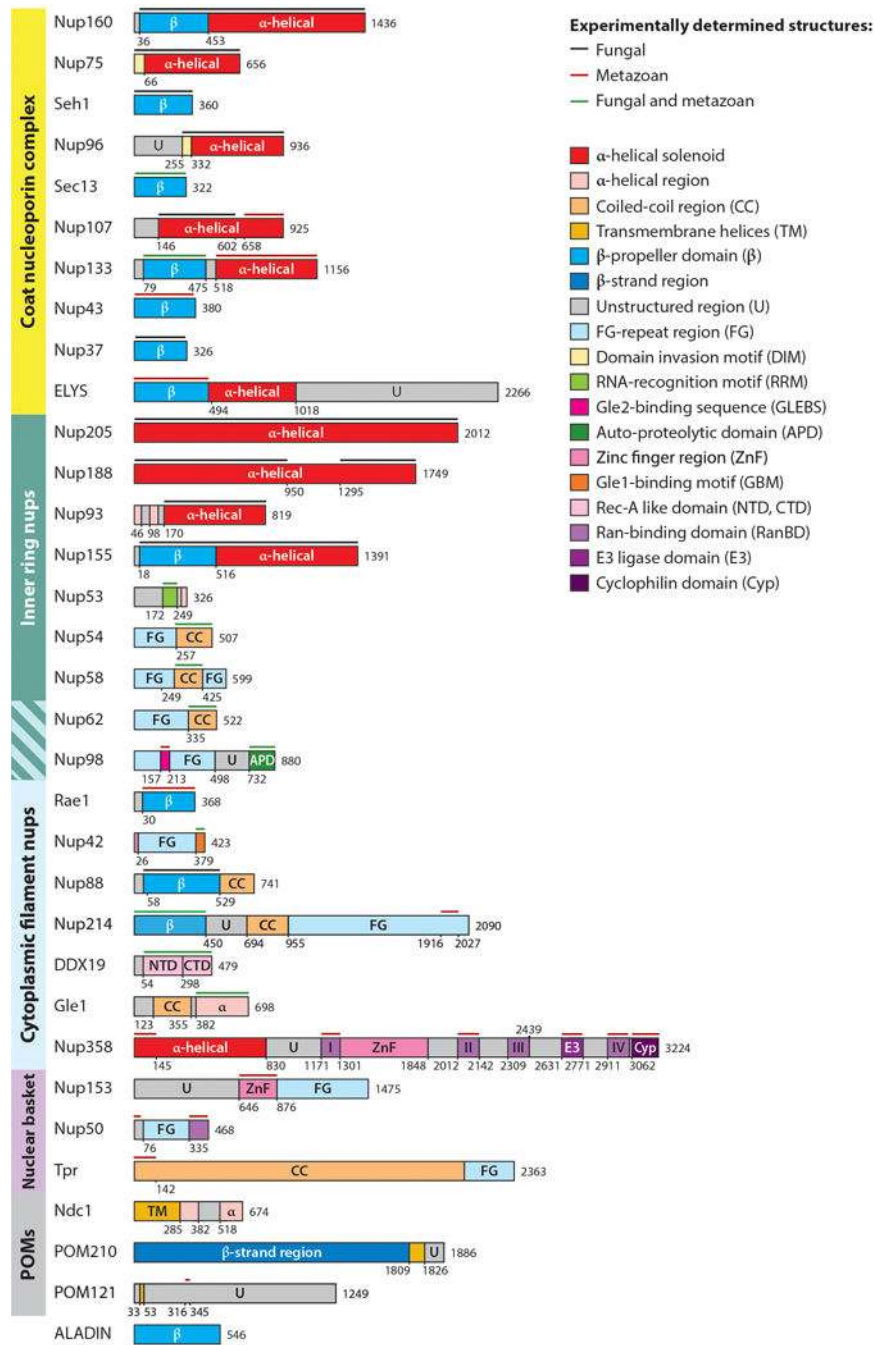
Figure 4.
Domain architectures of human nucleoporins and summary of structural characterization of individual nucleoporins. Bars above domain architectures indicate regions of the nucleoporins for which high-resolution structures are available, colored by the species from which the structures were determined. Abbreviations: nups, nucleoporin proteins; POMs, pore membrane proteins; NTD, N-terminal domain; CTD, C-terminal domain.
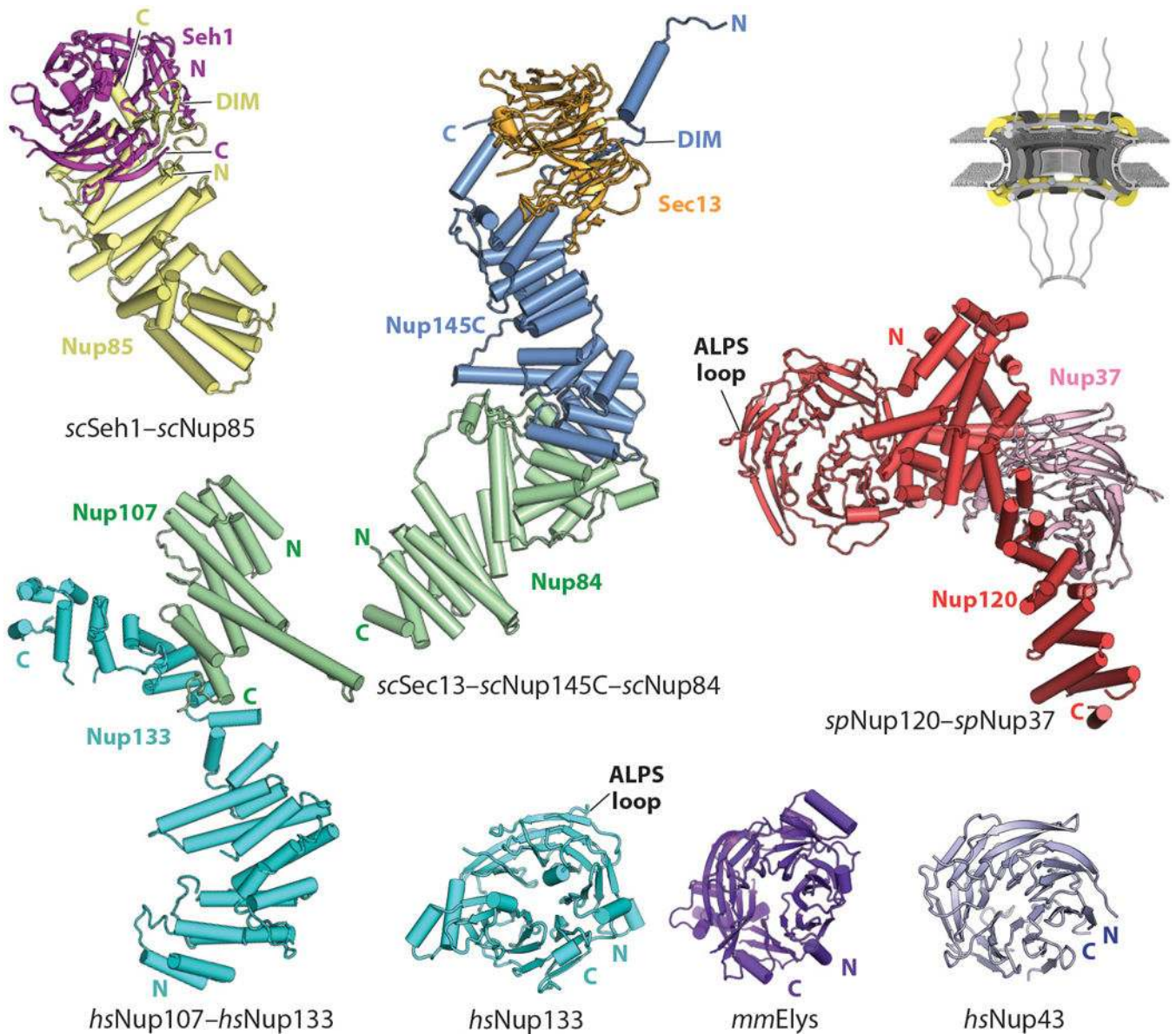
Figure 5.
Structures of nucleoporins in the CNC. A schematic of the NPC is shown in the top right corner, with the region of the NPC in which these nucleoporins are found colored in yellow. Crystal structures of *sc*Seh1–*sc*Nup85 (PDB 3F3F), *sc*Sec13–*sc*Nup145C–*sc*Nup84 (PDB 3IKO), Nup107–Nup133 (PDB 3I4R), *sp*Nup120–*sp*Nup37 (PDB 4FHN), Nup133 (PDB 1XKS), *mm*ELYS (PDB 4I0O), and Nup43 (PDB 4I79) are shown in ribbon representation (64, 68, 70, 71, 73, 97). Abbreviations: ALPS, amphipathic lipid packing sensor; CNC, coat nucleoporin complex; DIM, domain invasion motif; NPC, nuclear pore complex; PDB, Protein Data Bank.
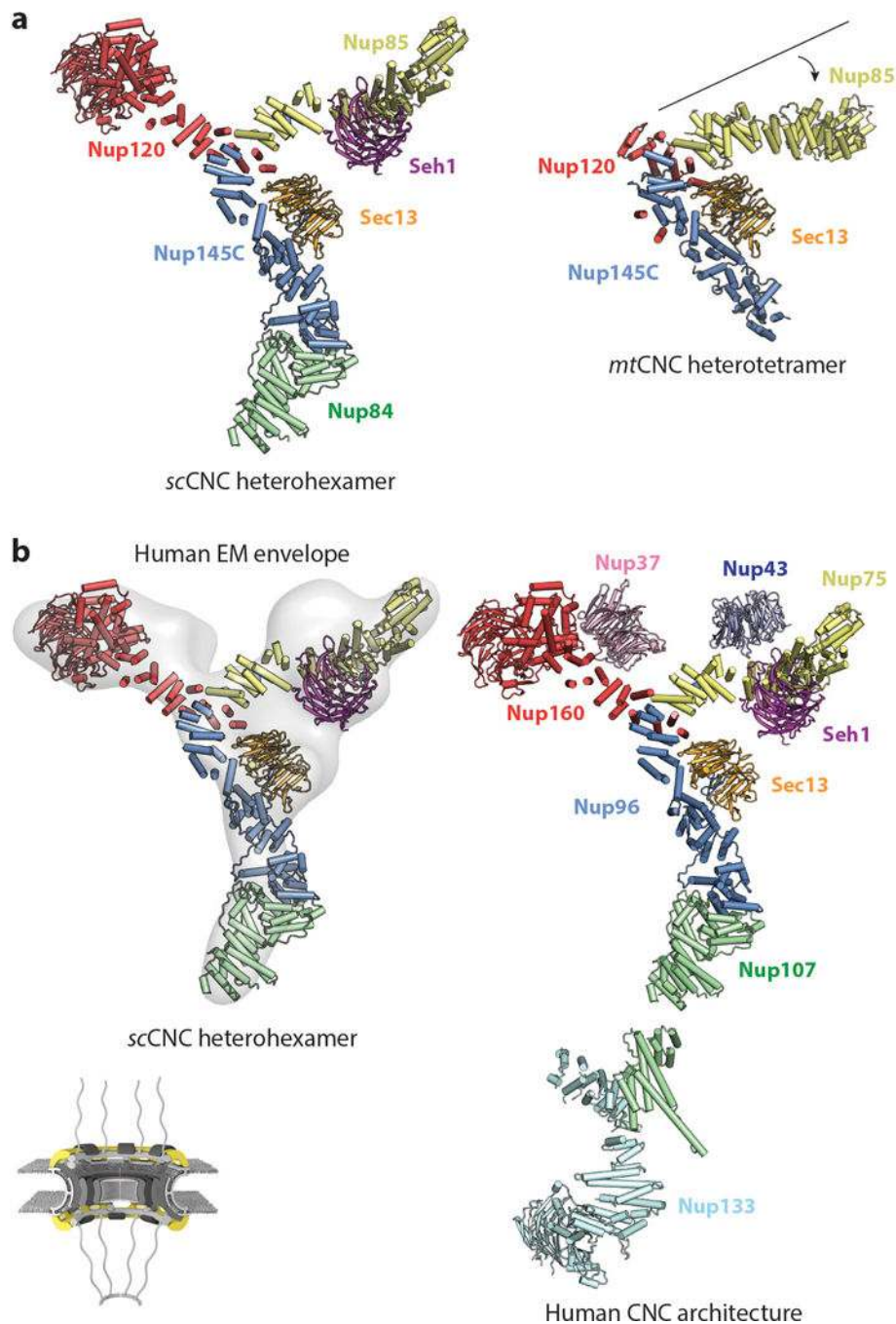
Figure 6.
Architecture of the CNC. A schematic of the NPC is shown in the bottom left corner highlighting, with the region of the NPC in which these nucleoporins are found colored in yellow. Crystal structures of the (*a*) *sc*Sec13–*sc*Nup145C–*sc*Nup84–*sc*Seh1–*sc*Nup85–*sc*Nup120 heterohexamer (PDB 4XMM) and *mt*Sec13–*mt*Nup145C–*mt*Nup85–*mt*Nup120 heterotetramer (PDB 4YCZ) are shown in the same orientation and coloring (75, 76). A crystallization chaperone antibody is omitted from the *sc*CNC heterohexamer for clarity. Note the different angle that the Nup85 arm forms in the two structures. (*b*) A negative-stain

electron tomography reconstruction of the human CNC (EMD 2443) is shown with the crystal structure of the *sc*CNC heterohexamer fitted into it (38, 76). The arrangement of all subunits within the human CNC is shown in a composite structure obtained through fitting of individual CNC component structures into a cryo–electron tomographic reconstruction of the intact human NPC. Abbreviations: CNC, coat nucleoporin complex; EMD, Electron Microscopy Databank; NPC, nuclear pore complex; PDB, Protein Data Bank.
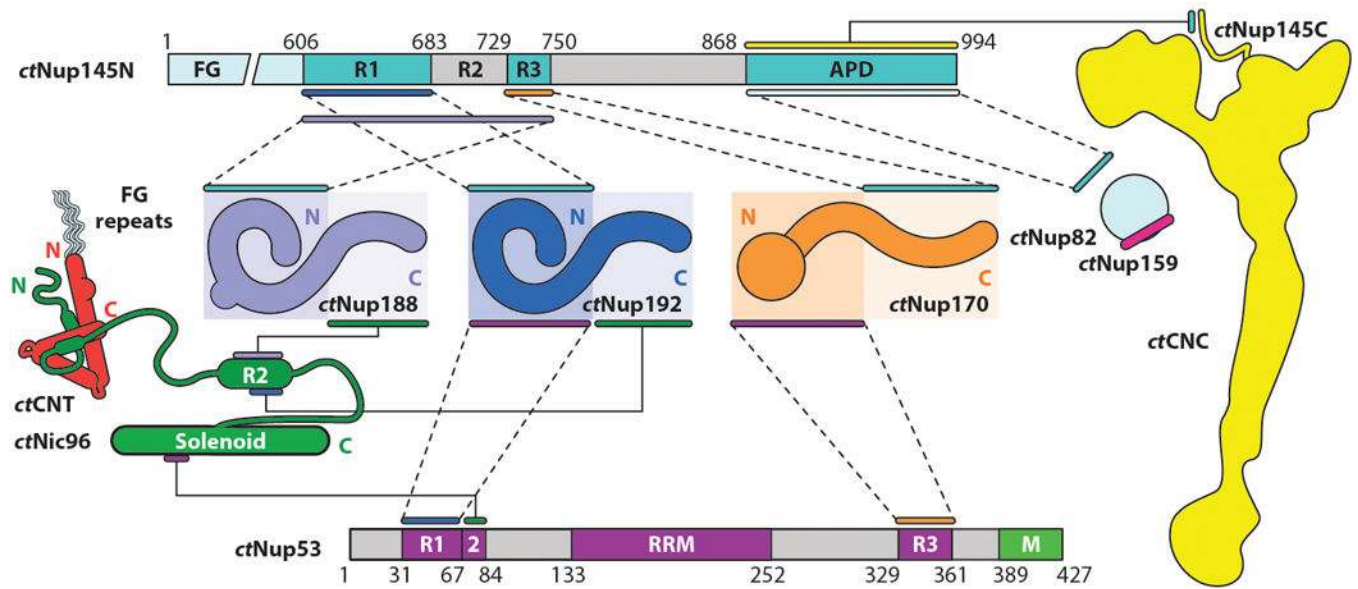
Figure 7.

Biochemical interaction map for nucleoporins from the thermophilic fungus *Chaetomium thermophilum*. Lines or pairs of dashed lines connecting two nucleoporins indicate interactions mapped to the respective regions of those nucleoporins. The *ct*CNT and *ct*CNC, which are formed through large hydrophobic interfaces, are depicted as diagrams representing the experimentally observed shapes of the complexes rather than the individual nucleoporins. The *ct*Nup82–*ct*Nup159 and *ct*CNT–*ct*Nic96 interactions are represented by diagrams of the interactions, rather than lines connecting the nucleoporins, as they have been characterized via X-ray crystallography. Figure adapted from Reference 41 with permission. Abbreviations: APD, autoproteolytic domain; CNC, coat nucleoporin complex; CNT, channel nucleoporin heterotrimer; RRM, RNA-recognition motif.
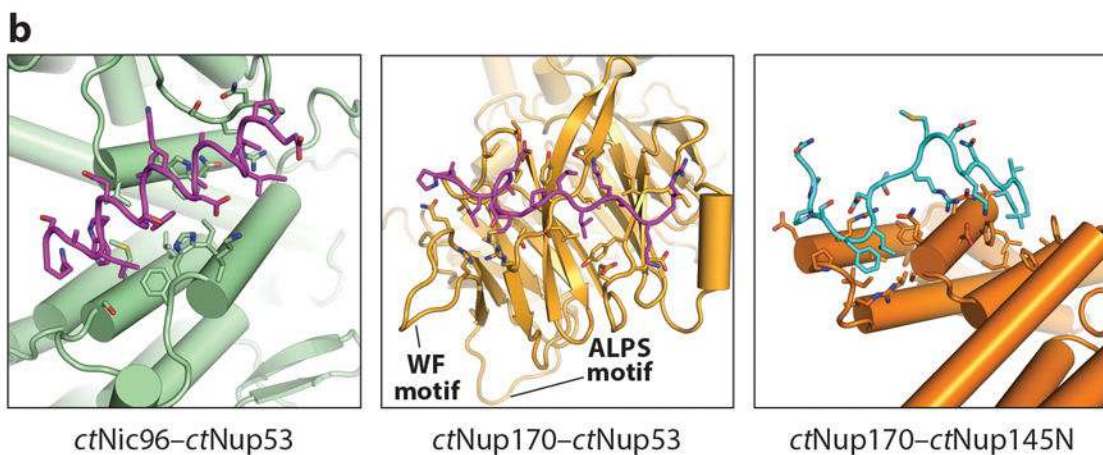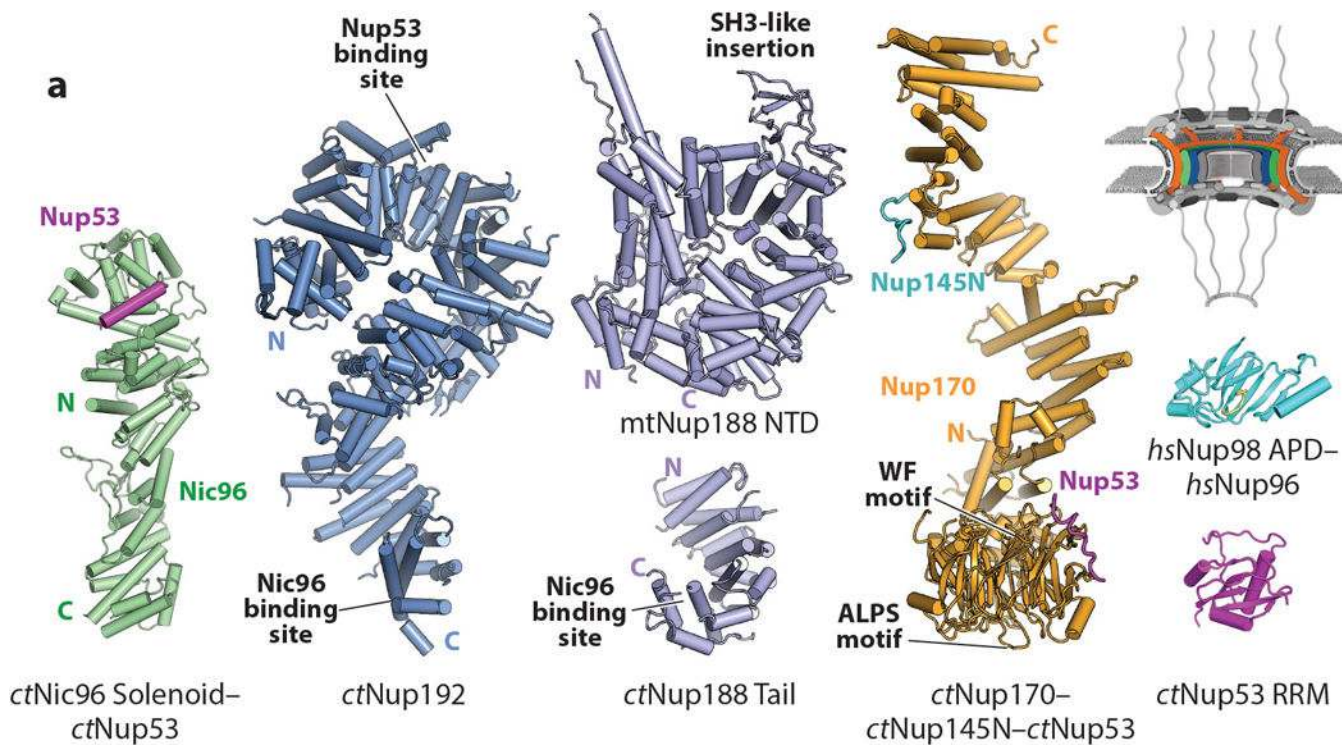
Figure 8.
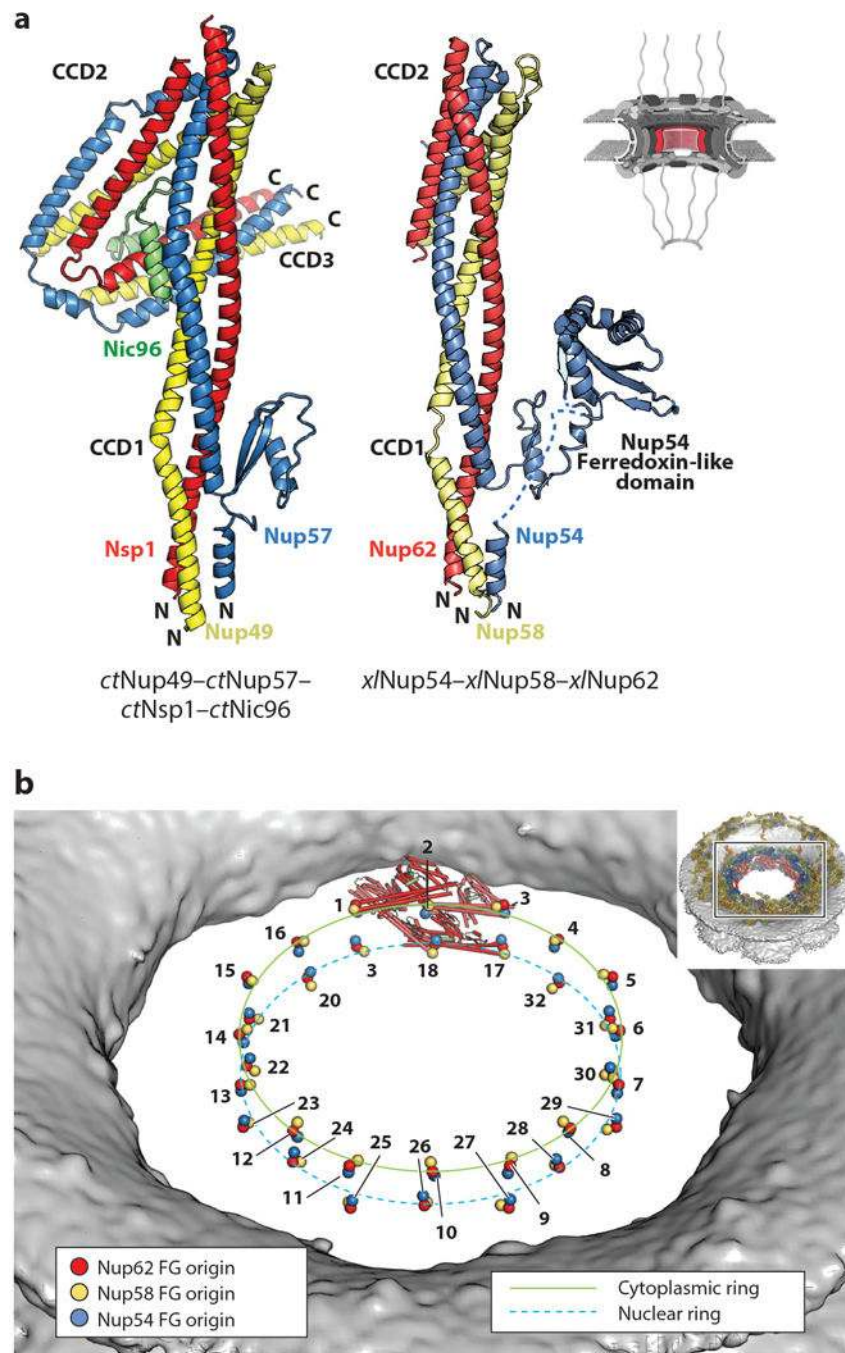Structures of nucleoporins in the IRCs. A schematic of the NPC is shown in the top right corner, with the region of the NPC in which these nucleoporins are found colored in orange, green, and blue. (*a*) A crystal structure of *ct*Nic96–*ct*Nup53 (PDB 5HB3), composite model of *ct*Nup192 (derived from PDBs 4KNH, 5HB4, and 5CWV), model of fungal Nup188 (derived from PDB 4KF7 and 5CWU), composite model of *ct*Nup170 (derived from PDBs 5HAX, 5HB0, and 5HB1), crystal structure of Nup98 bound to the N terminus of Nup96 (PDB 1KO6), and crystal structure of *ct*Nup53 (PDB 5HB7) are shown in ribbon representation (41, 102). (*b*) Zoomed views of the *ct*Nic96–*ct*Nup53, *ct*Nup170–*ct*Nup53, and *ct*Nup170–*ct*Nup145N interactions. Figure adapted from Reference 41 with permission.

Abbreviations: IRCs, inner ring complexes; NPC, nuclear pore complex; PDB, Protein Data Bank; RRM, RNA-recognition motif.

Figure 9.
Structure of the CNT. A schematic of the NPC is shown in the top right corner, with the region of the NPC in which these nucleoporins are found colored in red. (*a*) Crystal structures of the *ct*Nup49–*ct*Nup57–*ct*Nsp1–*ct*Nic96 complex (PDB 5CWS) and a model of *xl*Nup54–*xl*Nup58–*xl*Nup62 (combining PDBs 5C2U and 5C3L) are shown in ribbon representation in the same orientation and coloring (98, 113). Crystallization chaperone antibody (*ct*CNT–*ct*Nic96) and nanobody (*xl*CNT) were omitted from both structures for clarity. In the *xl*Nup54–*xl*Nup58–*xl*Nup62 complex, CCD3 was omitted for crystallization.

The Nup54 ferredoxin-like domain is not present in fungi. (*b*) Positioning of the CNTs in the human NPC maps the origins from which their N-terminal FG repeats project into the central transport channel to form the diffusion barrier (colored spheres). The CNTs from a single spoke are shown in ribbon representation. The FG origins form two stacked rings at the very center of the central transport channel. The inset shows the entire NPC with a box, indicating the orientation of the zoomed view. Abbreviations: CCD, coiled-coil domain; CNT, channel nucleoporin heterotrimer; NPC, nuclear pore complex; PDB, Protein Data Bank.
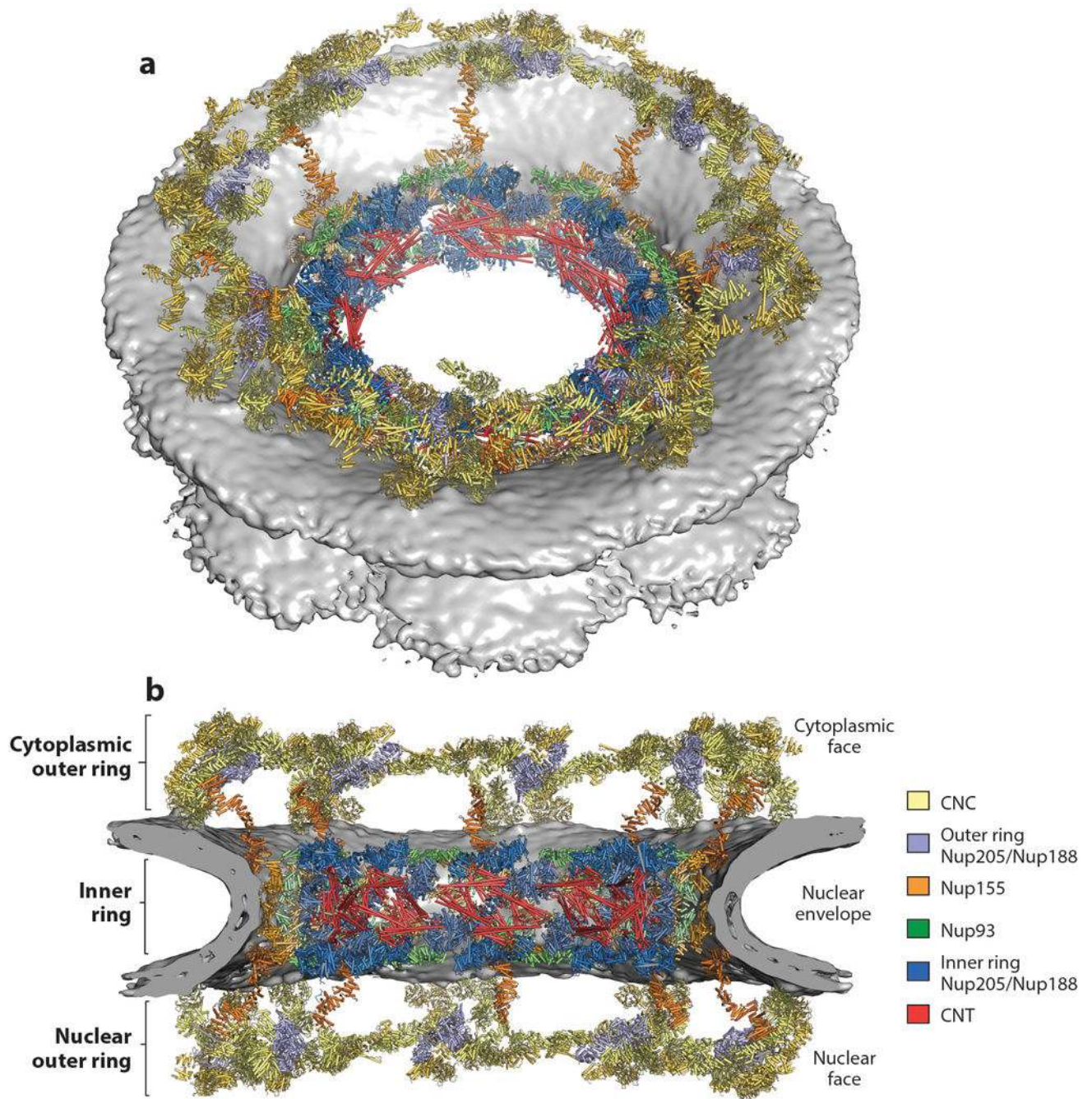
Figure 10.
Composite structure of the human NPC symmetric core. (*a*) A view of the entire NPC from the cytoplasmic side with docked crystal structures shown in ribbon representation. The gray surface represents the nuclear envelope. (*b*) A cutaway of the NPC viewed from the plane of the nuclear envelope with docked crystal structures shown in ribbon representation. Because Nup188 and Nup205 possess very similar overall shapes and cannot be distinguished at current resolutions, the assignment of the six positions per spoke is tentative. Figure adapted

from Reference 41 with permission. Abbreviations: CNC, coat nucleoporin complex; CNT, channel nucleoporin heterotrimer; NPC, nuclear pore complex.
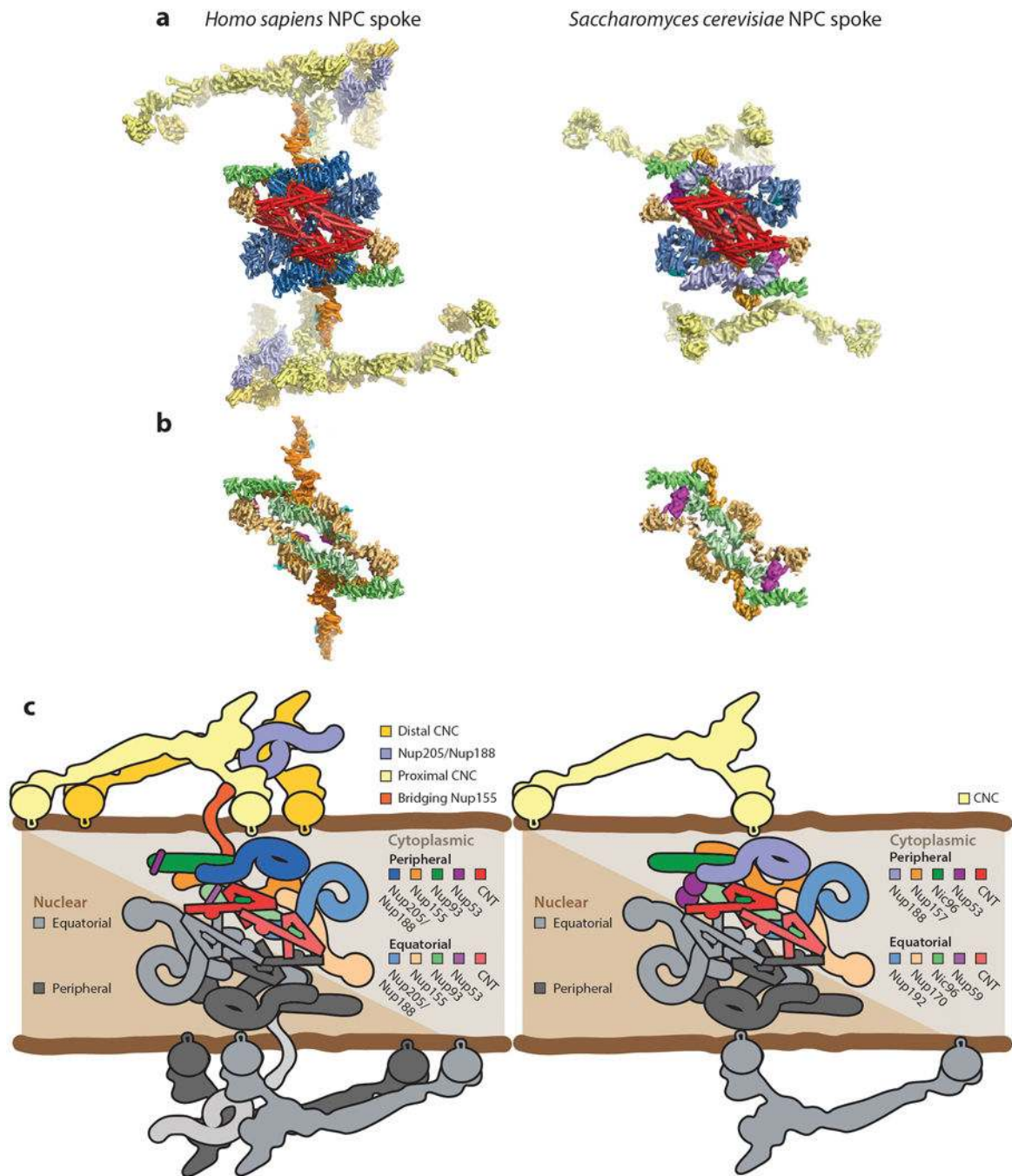
Figure 11.

Arrangement of subunits within an NPC spoke. (*a*) The arrangement of subunits in one spoke from the human NPC symmetric core (*left*) and the arrangement of subunits from one spoke in the *Saccharomyces cerevisiae* NPC symmetric core (*right*) are shown from the same view in a surface view. (*b*) The same views as in panel *a*, but with the Nup205/Nup192, Nup188, CNC, and CNT molecules removed to show the organization of molecules in the inner ring coat. (*c*) Schematics of the arrangement of subunits in the spokes. The precise orientation of the CNC in the *S. cerevisiae* NPC is ambiguous owing to the low

resolution of the outer rings in the currently available reconstruction. Abbreviations: CNC, coat nucleoporin complex; CNT, channel nucleoporin heterotrimer; NPC, nuclear pore complex.
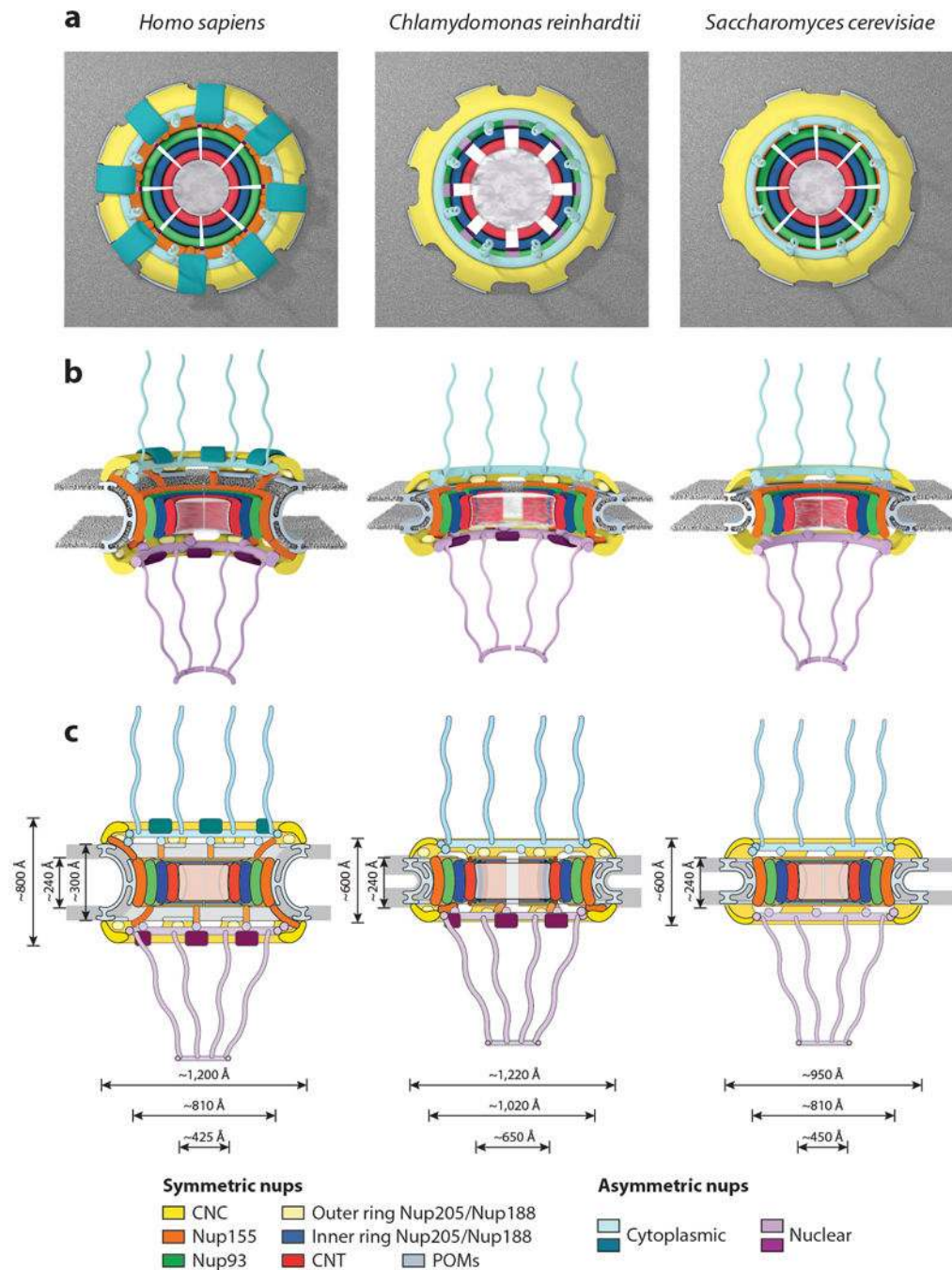
Figure 12.
Conservation of NPC architecture. Schematics of the human, *Chlamydomonas reinhardtii*, and *Saccharomyces cerevisiae* NPC architectures are shown, depicting overall differences observed among the three species in the top view (*a*), side view (*b*), and two-dimensional (*c*) schematics. Notably, the *S. cerevisiae* NPC is shorter in height than the human NPC, is embedded in a thinner nuclear envelope, but has approximately the same size transport channel and inner ring complex. The *C. reinhardtii* NPC has a dilated inner ring and is embedded in a thinner nuclear envelope compared with the human NPC but has the same

outer diameter. Abbreviations: CNC, coat nucleoporin complex; CNT, channel nucleoporin heterotrimer; NPC, nuclear pore complex; nups, nucleoporin proteins; POMs, pore membrane proteins.
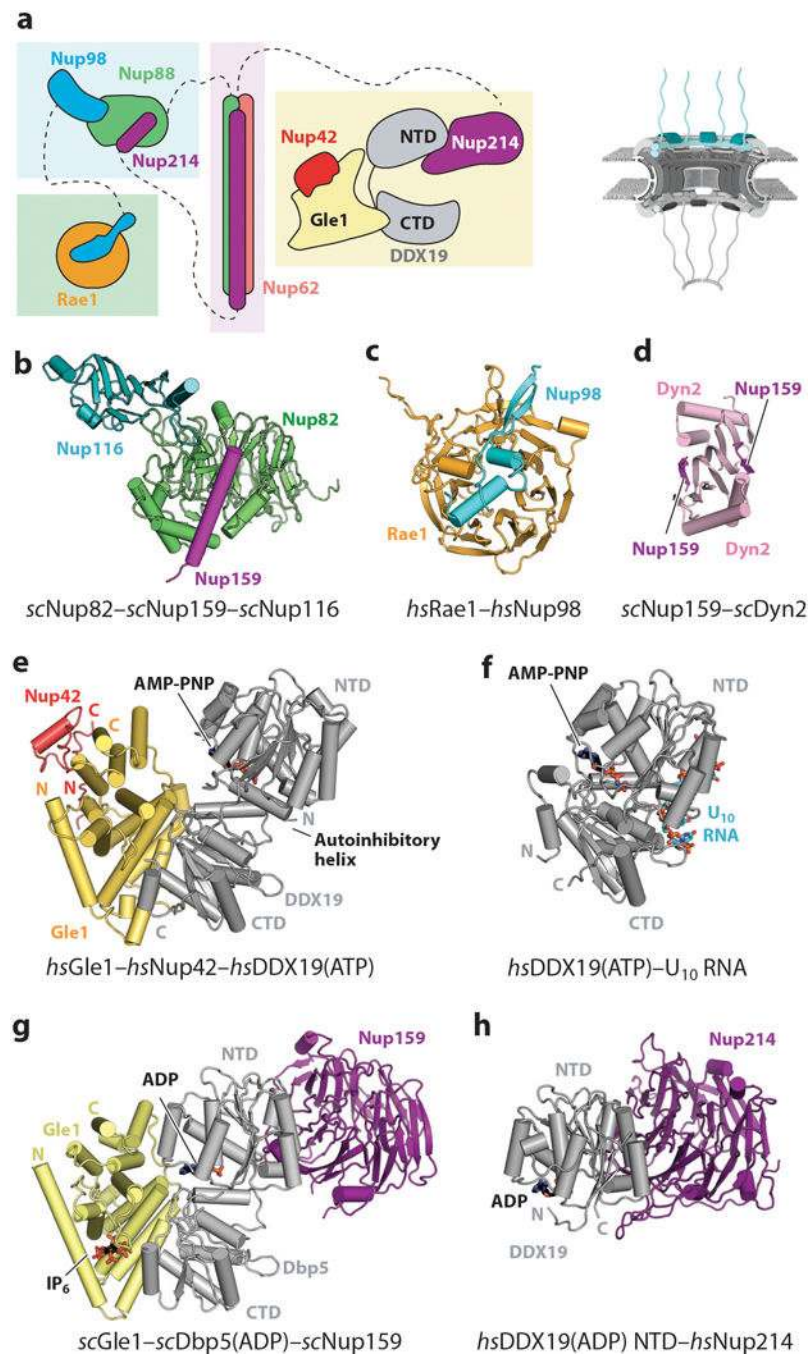
Figure 13.

Structures of cytoplasmic filament nucleoporins. A schematic of the NPC is shown in the top right corner, with the region of the NPC in which these nucleoporins are found colored in cyan. (*a*) Schematic representation of the cytoplasmic filament interaction hubs. FG repeats and other regions are omitted for clarity. Dashed lines indicate nucleoporins that are connected to different interaction hubs via flexible linkers. (*b*) Crystal structure of the *sc*Nup82–*sc*Nup159–*sc*Nup116 complex (PDB 3PBP) shown in ribbon representation (126). (*c*) Crystal structure of the Rae1–Nup98 complex (PDB 3MMY) shown in ribbon

representation (171). (*d*) Crystal structure of the *sc*Nup159–*sc*Dyn2 complex (PDB 4DS1) shown in ribbon representation (175). (*e*) Crystal structure of the Gle1–Nup42–DDX19 complex (PDB 6B4J) shown in ribbon representation (177). Gle1 binds to DDX19 and Nup42 on opposite surfaces of the protein. (*f*) Crystal structure of the DDX19–U$_{10}$ RNA complex (PDB 3G0H) shown in the same orientation as the Gle1–Nup42–DDX19 complex (205). DDX19 binds RNA and nucleotide on opposite surfaces of the protein. (*g*) Crystal structure of the *sc*Gle1–*sc*Dbp5–*sc*Nup159 complex (PDB 3RRM) shown in ribbon representation in the same orientation and coloring as the Gle1–Nup42–DDX19 complex (174). (*h*) Crystal structure of the DDX19–Nup214 complex (PDB 3FMP) shown in the same orientation as the *sc*Gle1–*sc*Dbp5–*sc*Nup159 complex (169). Abbreviations: AMP-PNP, Adenylyl-imidodiphosphate; CTD, C-terminal domain; NPC, nuclear pore complex; NTD, N-terminal domain; PDB, Protein Data Bank
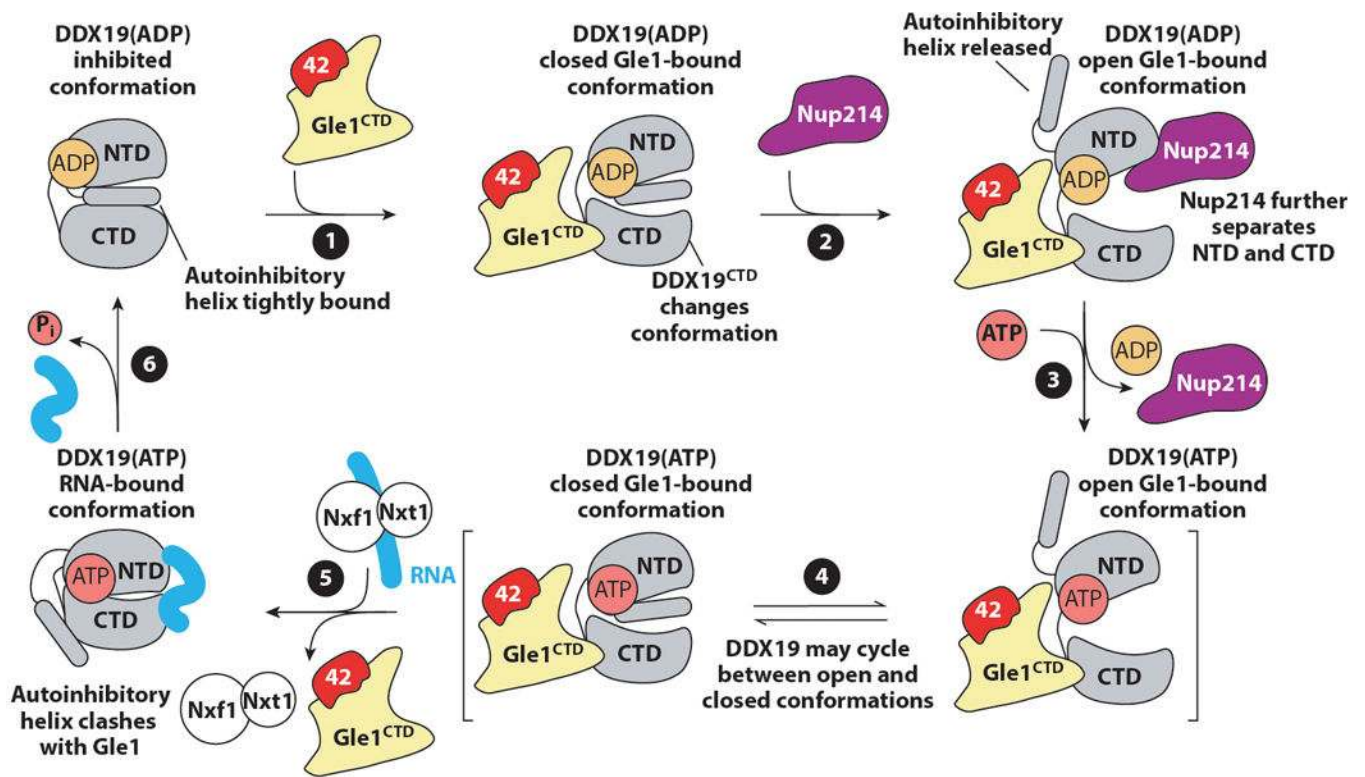
Figure 14.
A schematic representation of the proposed regulatory cycle of the activation of DDX19 by the NPC. DDX19 resides in an autoinhibited conformation. Gle1 binding to the DDX19 CTD results in conformational rearrangements in the CTD that destabilize the autoinhibited conformation (1). Nup214 binding may promote a more open conformation of DDX19 and complete release from autoinhibition (2). Nucleotide exchange may be promoted while DDX19 is in a more open conformation (3). DDX19 is able to adopt the autoinhibited conformation in both ATP- and ADP-bound states and may cycle between the autoinhibited and closed conformations (4). Upon binding RNA, DDX19 adopts a closed, catalytically active state and structural rearrangements are incompatible with Gle1 binding (5). ATP hydrolysis causes release of bound RNA and recycling of DDX19 to the beginning of the cycle (6). Figure adapted from Reference 177. Abbreviations: 42, Nup42; CTD, C-terminal domain; NPC, nuclear pore complex; NTD, N-terminal domain; ATP, adenosine triphosphate; ADP, adenosine diphosphate.
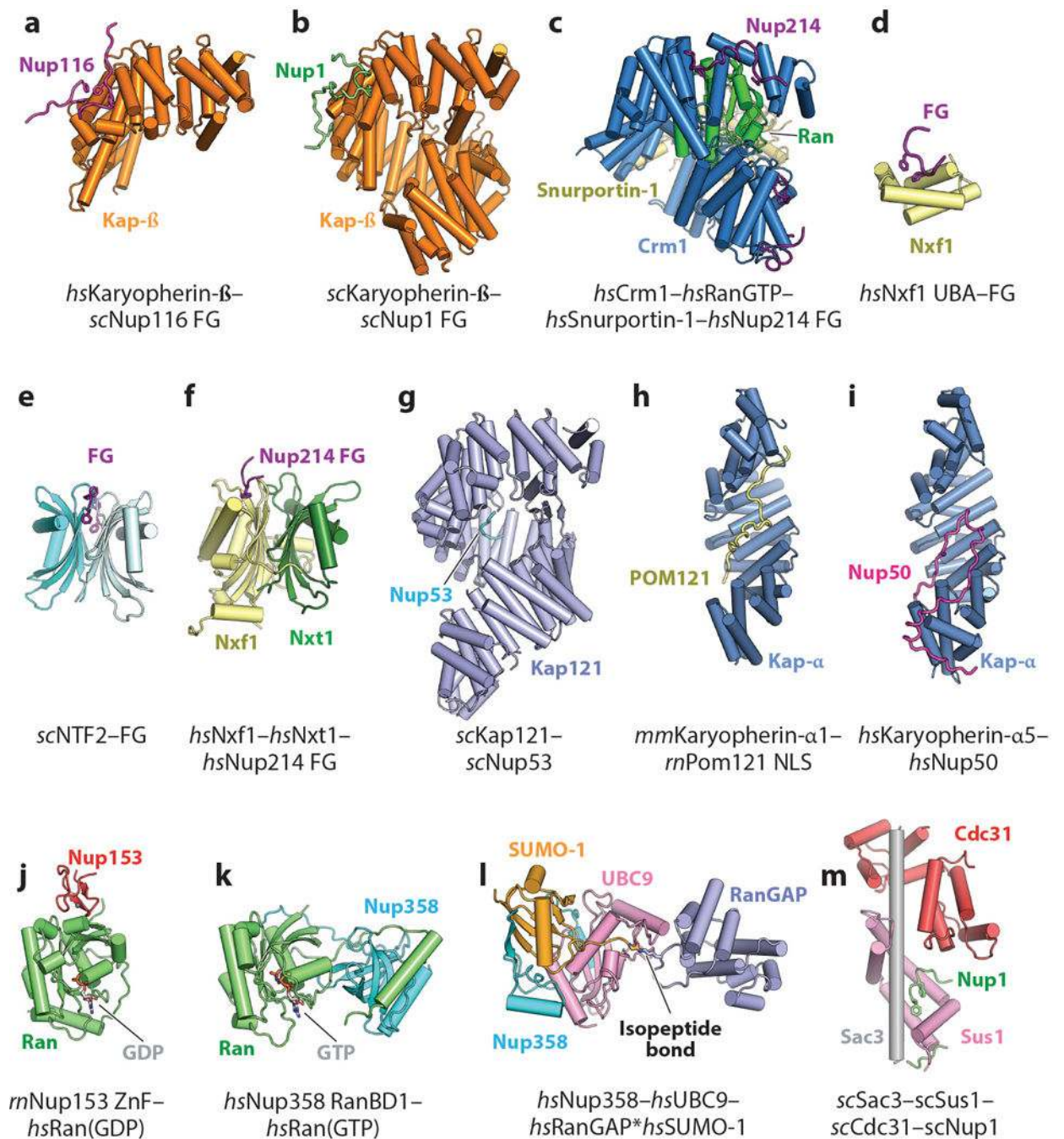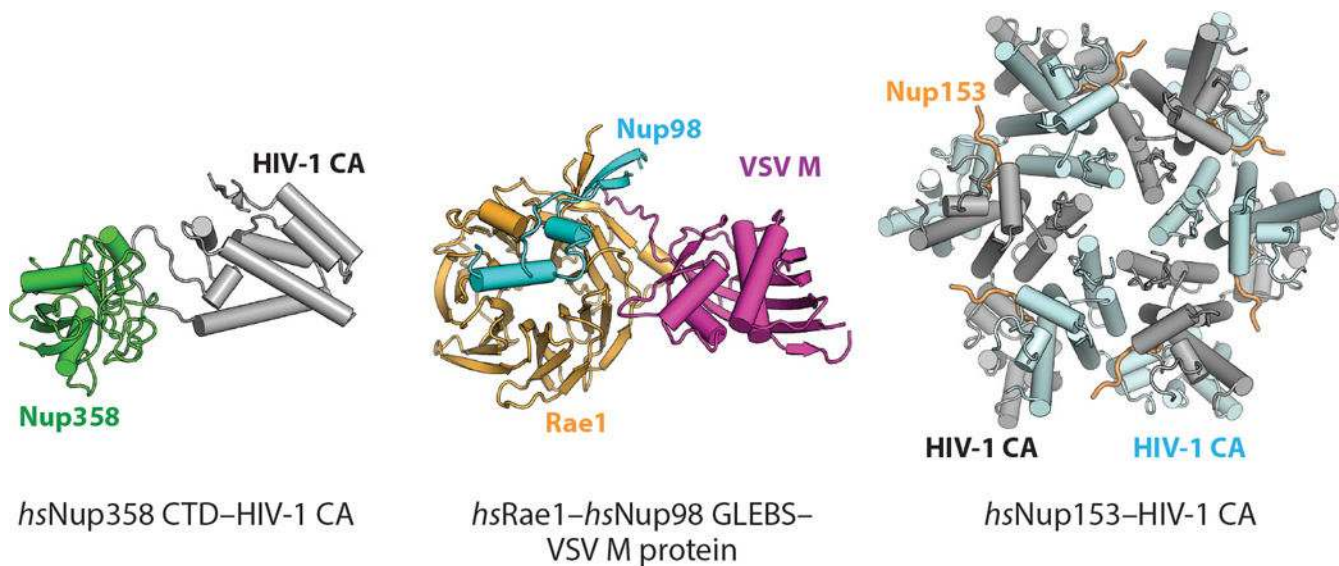
Figure 15.

Structures of the interactions between the NPC and nucleocytoplasmic transport machinery.
(*a*) Crystal structure of Karyopherin-β bound to an FG repeat from *sc*Nup116 (PDB 1O6P)
(233). (*b*) Crystal structure of *sc*Karyopherin-β bound to an FG repeat from *sc*Nup1 (PDB
5OWU) (240). (*c*) Crm1–Ran(GTP)–Snurportin-1 complex bound to several FG repeats
from Nup214 (PDB 5DIS) (237). (*d*) Crystal structure of the Nxf1 UBA domain bound to
the synthetic FG peptide (PDB 1OAI) (243). (*e*) Crystal structure of *sc*NTF2 bound to a
synthetic FG peptide (PDB 1GYB) (241). (*f*) Crystal structure of the Nxf1–Nxt1 complex

bound to a FG repeat from Nup214 (PDB 1JN5) (244). (*g*) Crystal structure of *sc*Kap121 bound to an NLS-like peptide from *sc*Nup53 (PDB 3W3Y) (245). (*h*) Crystal structure of *mm*Karyopherin-α1 bound to the NLS from *rn*Pom121 (PDB 4YI0) (246). (*i*) Crystal structure Karyopherin-α5 bound to the NLS-like sequence from Nup50 (PDB 3TJ3) (297). (*j*) Crystal structure of the *rn*Nup153 ZnF domain bound to Ran(GDP) (PDB 3GJ3) (224). (*k*) Crystal structure of the Nup358 RanBD1 bound to Ran(GTP) (PDB 1RRP) (214). (*l*) Crystal structure of the Nup358–UBC9–RanGAP*SUMO-1 complex (PDB 1Z5S) (215). (*m*) Crystal structure of the *sc*Sac3–*sc*Sus1–*sc*Cdc31 TREX-2 complex bound to an FG-like sequence from *sc*Nup1 (PDB 4MBE) (258). Abbreviations: NLS, nuclear localization signal; NPC, nuclear pore complex; PDB, Protein Data Bank; RanBD, Ran-binding domain; UBA, ubiquitin-associated; ZnF, zinc finger.

Figure 16.
Structures of interactions between the NPC and viral factors. Crystal structures of the Nup358–HIV-1 CA protein complex (PDB 4LQW), Rae1–Nup98 GLEBS–VSV M protein complex (PDB 4OWR), and Nup153–HIV-1 CA protein complex (PDB 4U0C) are shown in ribbon representation (176, 288, 290). Abbreviations: CA, capsid protein; CTD, C-terminal Domain; GLEBS, Gle2-binding sequence; NPC, nuclear pore complex; PDB, Protein Data Bank; VSV, vesicular stomatitis virus.